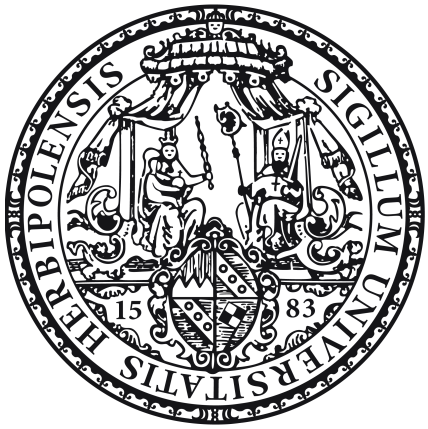

‘Signal-close-to-noise’ calcium activity reflects neuronal excitability

‘Signal-close-to-noise’ Kalziumaktivität als Ausdruck neuronaler Erregbarkeit

Doctoral thesis for a medical doctoral degree
at the Graduate School of Life Sciences,
Julius-Maximilians-Universität Würzburg,
Section Neuroscience

submitted by

Julian Hugo

from

Hamburg

Würzburg **2022**

Submitted on: ……..……..

Office stamp

Members of the Thesis Committee

Chairperson: **Prof. Dr. rer. nat. Uwe Gbureck**

Primary Supervisor: **PD Dr. rer. nat. Robert Blum**

Supervisor (Second): **Prof. Dr. med. Heike Rittner**

Supervisor (Third): **Prof. Dr. rer. nat. Carmen Villmann**

Supervisor (Fourth): **Dr. med. Beatrice Oehler**

Date of Public Defence: ……

Date of Receipt of Certificates: …….

Table of Contents

1 Introduction

1.1 Current state of research

1.1.1 Pain and nociception

Pain is one of the most common reasons for ambulatory medical consultations in Germany (Grobe et al., 2021). While the sensation of pain has a protective function and is necessary for survival (Basbaum and Jessell, 2013) chronic pain conditions are a significant burden to patients and constitute a major share of the *years lived with disability* globally (Vos et al., 2017). Formally, the International Association for the Study of Pain (IASP) defines pain as "an unpleasant sensory and emotional experience associated with, or resembling that associated with, actual or potential tissue damage", which is "always a personal experience" (Loeser et al., 2011). A state of pain is *chronic* if it lasts or recurs for more than three months (Treede et al., 2019). Nociceptive pain "arises from actual or threatened damage to non-neural tissue" (e.g., wounds and rheumatoid arthritis) and has to be distinguished from neuropathic pain, which is characterized by a lesion of the somatosensory nervous system (e.g., diabetic neuropathy and postherpetic neuralgia; Loeser et al., 2011).

In contrast to the highly subjective sensation of pain, nociception is the "neural process of encoding noxious stimuli" (Loeser et al., 2011). Molecular pain research investigates nociception, to gain insight into the underlying mechanisms of pain. Nociception does not, however, necessarily imply pain sensation (Loeser et al., 2011).

The ascending nociceptive pathway transmits noxious stimuli to the central nervous system. The somata of the primary nociceptive neurons (nociceptors) are located in the trigeminal or dorsal root ganglia (DRG). Nociceptors are pseudo-unipolar neurons, which are characterized by a single neurite arising from the soma that splits into a peripheral and a central axonal branch. The peripheral terminal innervates the target tissue (skin, muscle, and viscera) typically as free nerve endings. The central terminal forms synapses with the secondary sensory neuron and interneurons in laminae I, II, and V of the dorsal horn of the spinal cord (Basbaum and Jessell, 2013; Woolf and Ma, 2007). Glutamate is the primary excitatory neurotransmitter of the synapses connecting primary and secondary nociceptive neurons. Neuropeptides such as substance P and calcitonin gene-related peptide (CGRP) function as co-transmitters (Basbaum et al., 2009). From the dorsal horn, the secondary neuron projects to structures of the central nervous system such as the thalamus, reticular formation, mesencephalon, and hypothalamus, where stimuli are relayed to the somatosensory cortex (Basbaum and Jessell, 2013).

Anatomically, primary nociceptive neurons can be subdivided into two classes: firstly, thinly myelinated medium diameter Aδ fibers conduct action potentials at 5–30 m/s and are responsible for acute, well-localized fast pain. Secondly, unmyelinated small diameter C fibers conduct at 0.4–1.4 m/s and convey slow, poorly-localized pain (Basbaum et al., 2009; Dubin and Patapoutian, 2010). Nociceptors can be responsive to thermal (heat and cold), mechanical (intense pressure), chemical stimuli, or polymodal (multiple stimulus modalities; Basbaum et al., 2009; Basbaum and Jessell, 2013). The heterogeneity of nociceptors can be characterized by the differential expression of specific membrane proteins (e.g., transient receptor potential (TRP) channels). C fibers are subdivided into peptidergic (expressing Substance P and CGRP) and nonpeptidergic fibers (Basbaum et al., 2009). More recently, detailed characterizations of sensory neurons by RNA sequencing identified eleven fundamentally distinct types of DRG neurons with a high variance in gene expression among single cells. These clusters of sensory neurons are following earlier classifications based on size and histochemical markers, but they allow a better-defined view on the variance of the transcriptome in single cells within the categories (Usoskin et al., 2015).

Noxious thermal, mechanical, or chemical stimuli are transduced into electrical information by receptors (e.g., TRP channels). Initially, the activation of transduction molecules leads to membrane depolarization and the formation of a generator potential (receptor potential). If this depolarization surpasses a threshold, voltage-gated sodium channels (VGSC, details in section 1.1.5) generate an action potential and enable the transmission of signals to the central terminal (Basbaum et al., 2009; Waxman and Zamponi, 2014).

Ion channels of the TRP family are an important group of proteins that transduce sensory stimuli into generator potentials (Julius, 2013). Of this heterogeneous group, the subgroups transient receptor potential vanilloid (TRPV) and transient receptor potential ankyrin (TRPA) are of special interest for transduction of noxious thermal, mechanical or chemical stimuli (Julius, 2013). TRPV1 is activated by noxious heat (> 43 °C) and capsaicin, the pungent ingredient of chilies, and is expressed primarily on small-diameter DRG neurons (Caterina et al., 1997; Basbaum et al., 2009). TRPA1 is expressed on a subset of TRPV1-positive C fibers (Story et al., 2003). Stimulators of TRPA1 are a heterogeneous group of exogeneous (e.g., mustard oil (AITC) and acrolein) and endogenous mediators (e.g., reactive oxygen species (ROS), 4-hydroxy-2-nonenal (4-HNE), and protons). TRPA1 was shown to play a key role in peripheral sensitization during inflammation (Bautista et al., 2013).

1.1.2 Inflammation and pain

Acute inflammation is an innate physiological immune response towards infections or injuries that enables recovery after tissue damage. The primary goal is to maintain tissue homeostasis by pathogen elimination or tissue repair (Medzhitov, 2010; Rathinam and Chan, 2018). While a physiological inflammatory response is beneficial to control tissue damage, dysregulated inflammation is harmful (Medzhitov, 2010), and can cause damage itself (e.g., septic shock; Ward, 2010).

Cellular responses towards tissue damage are heterogeneous depending on the site and trigger. However, a generic inflammatory pathway can be identified, which includes an organized transport of plasma components and leukocytes to the site of tissue damage (Medzhitov, 2010). Tissue-resident macrophages act as sensors of tissue damage (e.g., via Toll-like receptors (TLRs) in infections) and release mediators such as cytokines, chemokines, and prostaglandins (Medzhitov, 2010). These mediators activate vascular endothelial cells that open tight junctions to allow the extravasation of plasma and proteins, release mediators to attract neutrophils, and facilitate their paracellular migration (Ward, 2010; Kolaczkowska and Kubes, 2013). Furthermore, released inflammatory mediators, including histamine, bradykinin, prostaglandins, and cytokines, act on free nerve endings to promote pain (Ji et al., 2014). Antidromic activation of nociceptors leads to the release of Substance P and CGRP from their peripheral terminals, promoting vasodilatation and plasma extravasation (neurogenic inflammation; Basbaum et al., 2009).

Traditionally, five cardinal symptoms characterize the clinical presentation of inflammation (Medzhitov, 2010): *rubor* (redness), *calor* (heat), *dolor* (pain), *tumor* (swelling), and *functio laesa* (loss of function). While redness and heat are directly related to vasodilatation, swelling to plasma extravasation, and loss of function to a combination of the prior symptoms, the mechanisms inducing pain are complex (Ward, 2010). Nociceptive pain accompanying inflammation clinically presents as “increased pain from a stimulus that normally provokes pain” (hyperalgesia) and “pain due to a stimulus that does not normally provoke pain” (allodynia; Loeser et al., 2011).

Acute inflammatory pain results from direct stimulation of nociceptors, e.g., protons can directly activate TRPV1 and acid-sensing ion channels (Basbaum et al., 2009). Persistent pain even after the resolution of acute inflammation, is propagated by peripheral and central sensitization mechanisms (Ji et al., 2014; Gold and Gebhart, 2010; Woolf and Salter, 2000).

Peripheral sensitization is the "increased responsiveness and reduced threshold of nociceptive neurons in the periphery" (Loeser et al., 2011) and is considered as a form of neural plasticity, i.e., the capability of neurons to alter their function. This type of plasticity is activity-dependent, meaning the excitability of nociceptors increases with repeated stimuli (Woolf and Salter, 2000). Sensitized neurons show spontaneous activity, lower thresholds for diverse stimuli, and increased responses to suprathreshold stimuli (Bennett et al., 2019). Peripheral sensitization can be due to mechanisms such as the altered expression of transduction molecules, phosphorylation, or receptor trafficking to new activity hot spots. Signal mediators are manifold and include, among many others, G protein-coupled receptors (GPCR e.g., prostaglandin receptors) and their corresponding ligands, neurotrophins, and cytokines (Gold and Gebhart, 2010; Ji et al., 2014).

The most common pharmaceuticals to tackle inflammatory pain are nonsteroidal anti-inflammatory drugs (NSAIDs), which block the prostaglandin synthesis by inhibiting cyclooxygenase (COX) isoforms (COX-1 and COX-2; Grosser et al., 2017). NSAIDs mediate antipyretic, analgesic, and antiphlogistic effects. Examples are diclofenac, ibuprofen and acetylsalicylic acid (Aspirin). NSAIDs are an established symptomatic treatment of inflammatory conditions such as rheumatoid arthritis and other pain conditions (Grosser et al., 2017). However, long-duration NSAID therapy is associated with an elevated risk of multiple adverse effects such as gastrointestinal ulcers and bleeding or renal failure, especially in presence of comorbidities (Grosser et al., 2017). Because adverse reactions are mainly attributable to the tissue-unselective COX inhibition, the investigation of specific targets on nociceptors might provide new approaches for pharmacological treatments (Gangadharan and Kuner, 2013).

1.1.3 Inflammatory mediators involved in peripheral sensitization

The molecular mechanisms of inflammatory mediators are diverse. However, their combined effect on metabotropic and ionotropic receptors eventually leads to a decreased threshold of nociceptor activation (Gangadharan and Kuner, 2013).

1.1.3.1 Prostaglandins

COX enzymes synthesize prostaglandins from arachidonic acid. COX-1 is expressed constitutively, while the expression of COX-2 is increased in inflammation, which strongly increases prostaglandin formation (Chen et al., 2013). There are several different prostaglandins of which prostaglandin E_2 (PGE_2) contributes most to nociceptor sensitization by activation of prostaglandin E-receptors (EP_1 and EP_4; Lin et al., 2006; Kawabata, 2011). Via protein kinase

A (PKA)- and protein kinase C (PKC)-dependent pathways, prostaglandin signaling leads to sensitization of TRPV1 (Moriyama et al., 2005) and activates the excitability mediator $Na_V1.9$ (voltage-gated sodium channel 1.9; Amaya et al., 2006; Petho and Reeh, 2012). The inhibition of nociceptor sensitization by blocking PGE_2 synthesis is considered the basis of the effectiveness of NSAIDs (Grosser et al., 2017).

1.1.3.2 Histamine

In inflammation, mast cells release histamine which activates histamine receptors (H_1, H_2, H_3, and H_4; Thangam et al., 2018). Studies have shown the antinociceptive effect of H_4 receptor antagonists, which suggests a direct involvement of histamine in nociception (Hsieh et al., 2010). Substance P and CGRP stimulate mast cells to release histamine, while histamine mediates the release of Substance P and CGRP from nociceptive terminals. This signaling circuit is involved in maintaining neurogenic inflammation (Rosa and Fantozzi, 2013).

1.1.3.3 Bradykinin

Bradykinin is produced as a byproduct in the coagulation pathway. This oligopeptide is derived from high-molecular-weight kininogen by kallikrein-dependent hydrolysis (Ward, 2010; Wang et al., 2006) and acts on B_1 (upregulated in inflammation) and B_2 receptors expressed on nociceptors (Yaksh, 2010). Both receptors are GPCR and induce $G\alpha_i$- and $G\alpha_q$-pathways to activate phospholipase A_2 (PLA_2), PKC, and PKA pathways (Wang et al., 2006). Downstream effects are increased prostaglandin synthesis, lowered thresholds of VGSC, and sensitization of ionotropic receptors such as TRPA1 and TRPV1 (Wang et al., 2006; Wang et al., 2008; Petho and Reeh, 2012).

1.1.3.4 Reactive oxygen species

ROS are highly reactive metabolites of oxygen, including superoxide anions (O_2^-), hydroxyl radicals, hydrogen peroxide (H_2O_2), and hypochlorous acid (Mittal et al., 2014). Low concentrations of ROS have signaling functions, while high concentrations cause DNA damage and cell death (Binder et al., 2016). Persistent ROS production has been shown to contribute to the development of chronic inflammatory diseases (Binder et al., 2016). The enzymatic production of ROS by endothelial cells, neutrophils, and macrophages is most important under inflammatory conditions (Hackel et al., 2013): NADPH oxidases oxidize molecular oxygen to O_2^-, which is then transformed to low reactive H_2O_2. This process can occur spontaneously, due to the high reactivity of H_2O_2, or is promoted by superoxide dismutase. Myeloperoxidase, an enzyme mostly expressed in neutrophils, produces the highly reactive hypochlorous acid from H_2O_2 (Mittal et al., 2014). Neutrophils produce ROS to eliminate pathogens (Kolaczkowska

and Kubes, 2013). Under physiological circumstances antioxidant enzymes (superoxide dismutase, catalase, and glutathione peroxidase) eliminate ROS. If a balance between ROS formation and protective antioxidant capacity cannot be maintained, a metabolic state called *oxidative stress* is induced (Mittal et al., 2014; Binder et al., 2016).

Oxidative stress has been found to contribute to multiple mechanisms in inflammation: 1) upregulation of cellular adhesion molecules on endothelial cells, which results in increased recruitment of neutrophils (Patel et al., 1991); 2) disassembly of tight junctions between endothelial cells (Rao, 2008), leading to increased plasma extravasation; 3) pronociceptive properties by activation and sensitization of TRPV1 (Keeble et al., 2009; Ibi et al., 2008); 4) oxidization of phospholipids (lipid peroxidation) of the lipid bilayer membrane of cells to form highly reactive oxidized phospholipids (OxPL; Binder et al., 2016).

1.1.4 Oxidized phospholipids in inflammatory pain

Phospholipids are essential components of mammalian cell membranes and circulating lipoproteins. The most abundant type of PLs are phosphoglycerides, which are characterized by a glycerol backbone linked to a hydrophobic tail of two fatty acid chains and a hydrophobic head. Phosphatidylcholine is the most frequent phosphoglyceride found in cell membranes (Lodish et al., 2016), of which 1-palmitoyl-2-arachidonoyl-*sn*-glycerol-3-phosphatidylcholine (PAPC) is a naturally occurring representative.

Due to their abundance, lipids are a prime target of lipid peroxidation by ROS in oxidative stress (Binder et al., 2016). Polyunsaturated fatty acids are particularly prone to free-radical oxidation due to the presence of carbon double bonds (Freigang, 2016; Bochkov et al., 2010). Non-enzymatic oxidation of PLs is a stochastic process, that includes multiple mechanisms (fragmentation, cyclization, and further oxidation) and yields a variety of oxidation products (Bochkov et al., 2010; Catala, 2009). In the case of PAPC, the heterogeneous mixture of its oxidation products (OxPAPC) is composed of 1-palmitoyl-2-(5-oxovaleroyl)-*sn*-glycero-3-phosphocholine (POVPC), 1-palmitoyl-2-glutaryl-*sn*-glycero-3-phosphocholine (PGPC), 1-palmitoyl-2-(5,6)-epoxyisoprostaneE2-*sn*-glycero-3-phosphocholine (PEIPC), 1-palmitoyl-2-(5,6-epoxyisoprostaneA2)-sn-glycero-3-phosphocholine (PECPC) and other components (Bretscher et al., 2015). During the oxidation process reactive by-products such as aldehydes (e.g., 4-HNE) are released (Catala, 2009).

OxPL have been identified *in vivo* in several inflammatory disorders (Freigang, 2016), such as atherosclerosis (Lee et al., 2012), acute respiratory distress syndrome (Imai et al., 2008), and

Alzheimer's dementia (Usui et al., 2009). OxPL have been identified on apoptotic cells, microvesicles, and oxidized low-density lipoproteins (Binder et al., 2016).

1.1.4.1 Pro- and anti-inflammatory effects of OxPL

The effects of OxPL in inflammation are diverse: investigations showed that OxPL are not only involved in the initiation and amplification of inflammation but also in its resolution (Bochkov et al., 2010; Bochkov et al., 2017; Oskolkova and Bochkov, 2020). As an explanation for the heterogeneous effects of OxPL, the diverse composition of OxPL mixtures and the concentration level of OxPL has been suggested (Bochkov et al., 2010; Freigang, 2016; Oskolkova et al., 2010). OxPL are known to act on toll-like receptors, scavenge receptors, and soluble pattern recognition receptors (e.g., C-reactive protein and antibodies; Freigang, 2016; Bochkov et al., 2017).

Pro-inflammatory signaling of OxPL has been elucidated most thoroughly in atherosclerosis (Zhong et al., 2019; Lee et al., 2012), where OxPL promote monocyte adhesion to the endothelium and pro-inflammatory cytokine release (van der Valk et al., 2016), foam cell formation and plaque generation (Que et al., 2018). One key mechanism contributing to the anti-inflammatory effects of OxPAPC is the inhibition of lipopolysaccharide (LPS)-induced signaling to increase E-selectin expression, Nuclear factor kappa-light-chain-enhancer of activated B cells (NFκB) upregulation, and tumor necrosis factor release (Oskolkova et al., 2010).

Moreover, OxPL elicit effects by interfering with the cell membrane. It has been shown that OxPL increase membrane rigidity (Borst et al., 2000) and impair or alter the function of membrane proteins (Catala, 2009). The diversity of OxPAPC-mediated effects might also be explained by the observed variety of cellular destinations of individual components: PGPC, for example, is preferentially stored in lysosome membranes, while POVPC remains in the plasma membrane (Moumtzi et al., 2007).

1.1.4.2 OxPL in inflammatory pain

Recently, the involvement of OxPAPC in inflammatory nociception has been established (Oehler et al., 2021; Figure 1-1). It was shown that OxPAPC is produced in inflamed tissue and activates heterologous expressed TRPA1 and TRPV1 channels in human embryonic kidney 293 cells as well as in murine DRG neurons *in vitro* (Oehler et al., 2017; Liu et al., 2016). Furthermore, injection of OxPAPC into rodent hind paws revealed the development of persistent mechanical (Liu et al., 2016) and thermal hyperalgesia and release of CGRP (Oehler et al., 2017). Interestingly, OxPAPC induces long-lasting hyperalgesia, often over hours, which

suggests an involvement in proalgesic cascades and peripheral sensitization (Oehler et al., 2017). Importantly, the components of OxPAPC are unstable and highly reactive under *in vivo* conditions. This suggests that these proalgesic substances are transient mediators in inflammation (Stemmer and Hermetter, 2012; Domingues et al., 2013). Oehler et al. showed that at least 15 min after injection of exogenous OxPAPC in hind paws of the rat, OxPAPC components are not detectable in the inflamed tissue (Oehler et al., 2017). However, metabolites from OxPAPC degradation such as lysophosphatidylcholine, PGPC, 4-HNE, and 15d-PGJ_2 are enriched in inflamed tissue and show high biological activity (Oehler et al., 2017; Oehler et al., 2021).

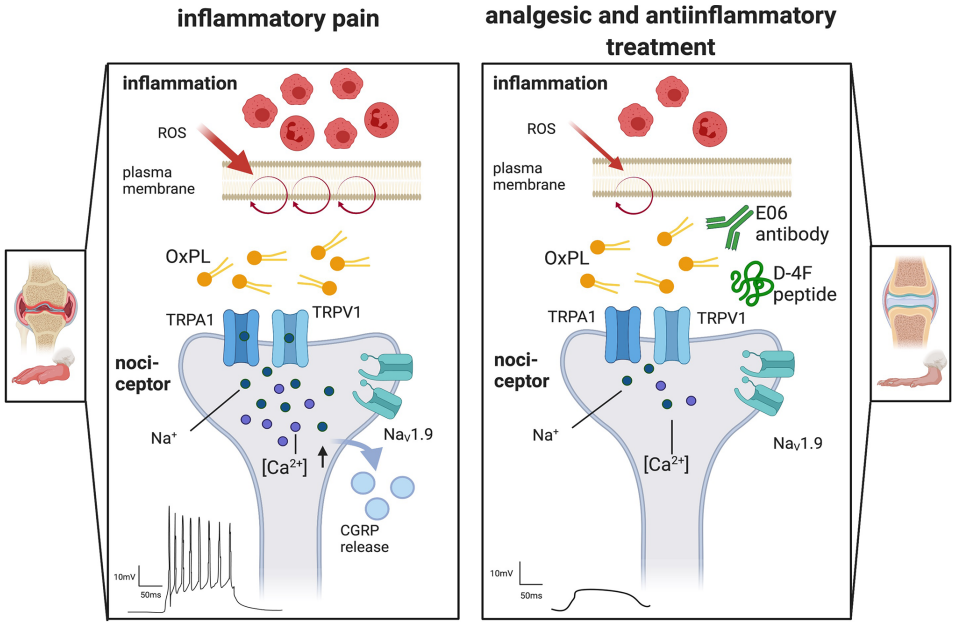

Figure 1-1: **Proalgesic mechanisms of OxPL in inflammatory pain and therapeutic options**. Left panel: In inflammation immune cells release ROS, which oxidize phospholipids. OxPL have been shown to activate TRPA1 and TRPV1, leading to downstream activation of VGSC and subsequent nociception. Right panel: Treatment with the D-4F peptide or E06 antibodies can attenuate nociception. CGRP, calcitonin gene-related peptide; Nav1.9, voltage-gated sodium channel 1.9; OxPL, oxidized phospholipids; ROS, reactive oxygen species; TRPA1, transient receptor potential ankyrin 1; TRPV1, transient receptor potential vanilloid 1, VGSC, voltage-gated sodium channel. Published under Creative Commons Attribution License (CC BY; Oehler et al., 2021)

PGPC, a rather stable oxidation end product of the OxPL degradation pathways, was shown to activate TRPA1 non-electrophilically. PGPC can induce repetitive action potential firing of cultured murine nociceptors (Martin et al., 2018). Additionally, $Na_V1.9$ has been identified as being responsible for the potentiation of PGPC-induced action potential firing frequencies and calcium spikes under inflammatory conditions (Martin et al., 2018).

Studies further investigated possible strategies to block OxPAPC-induced nociception and pain. Indeed, the apolipoprotein A-I mimetic peptide D-4F successfully attenuated OxPAPC-

invoked calcium influx *in vitro* and hyperalgesia *in vivo* (Oehler et al., 2017). This was also observed when E06, a monoclonal antibody against OxPL, was used *in vitro* (Oehler et al., 2017) and *in vivo* (Mohammadi et al., 2018; Oehler et al., 2021; Figure 1-1).

While acute actions of OxPL as acute mediators of nociceptor excitation are well described, it remains unclear whether this group of substances is also mediating nociceptor sensitization.

1.1.5 Voltage-gated sodium channels

Action potentials (AP) in neurons are the basis of signal transmission and neurotransmitter release in sensory neurons. VGSCs facilitate the influx of sodium ions across the plasma membrane to depolarize the membrane potential (Koester and Siegelbaum, 2013), hereby amplifying generator potentials induced by transduction channels (e.g., TRP channels) and trigger APs (Bennett et al., 2019). VGSCs have been found to regulate the excitability and frequency of AP firing in nociceptors (Dib-Hajj et al., 2010).

The relevance of three VGSCs ($Na_V1.7$, $Na_V1.8$, and $Na_V1.9$) in human pain signaling has been validated by the discovery of multiple genetic mutations of the corresponding genes in patients with pain disorders (Dib-Hajj and Waxman, 2019; Baker and Nassar, 2020; Goodwin and McMahon, 2021). Interestingly, mutations of $Na_V1.9$ (encoded by SCN11A) could be linked to childhood painful disorders (Huang et al., 2019; Leipold et al., 2015; Leng et al., 2017; Okuda et al., 2016), painful peripheral neuropathy (Han et al., 2015; Huang et al., 2014), but also congenital insensitivity to pain (Huang et al., 2017; Leipold et al., 2013; Woods et al., 2015). Patients also showed intestinal dysmotility (Huang et al., 2019; Leipold et al., 2013; Woods et al., 2015) and delayed motor development (Huang et al., 2019).

Nine coding genes (SCN1A - SCN5A, SCN8A - SCN11A) code for the pore-forming α subunits of the different VGSCs, which are associated with modulatory β subunits. The α subunit consists of four homologous domains each made of six transmembrane segments. The S4 segments contain positively charged amino acids and function as a voltage sensor. The S5/S6 segments form the pore domain, which acts as a selectivity filter for sodium ions (Bennett et al., 2019). VGSCs have three voltage-dependent activity states: *open* (active, for < 1 ms during depolarization), *inactive* (following depolarization, not activatable), and *closed* (in hyperpolarized states, activatable; Bennett et al., 2019). VGSC can be categorized based on their tetrodotoxin (TTX) sensitivity: $Na_V1.1$, $Na_V1.2$, $Na_V1.3$, $Na_V1.4$, $Na_V1.6$, and $Na_V1.7$ are TTX-sensitive and $Na_V1.5$, $Na_V1.8$ and $Na_V1.9$ are insensitive to TTX (Bennett et al., 2019).

1.1.5.1 Voltage-gated sodium channel 1.9 ($Na_V1.9$)

Among VGSCs $Na_V1.9$ has unique properties, as it is active close to the resting membrane potential. The channel is preferentially expressed on small-sized (< 30 μm) DRG (Amaya et al., 2000), trigeminal and myenteric neurons (Rugiero et al., 2003) and has also been identified on motoneurons (Subramanian et al., 2012). On DRG neurons, $Na_V1.9$ is localized in soma, axons, peripheral and central terminals (Dib-Hajj et al., 2015). Interestingly, the expression on specific cellular populations relates to the clinical phenotype (pain, intestinal dysmotility, and delayed motor development) presented in patients with $Na_V1.9$ mutations (Huang et al., 2019; Leipold et al., 2013; Woods et al., 2015).

Biophysically, $Na_V1.9$ has unique gating properties that emphasize its importance in AP formation. Nav1.9 opens at more hyperpolarized membrane potentials than other VGSCs (-60 to -70 mV), which is close to the resting membrane potential of DRG neurons and shows ultra-slow inactivation leading to a persistent sodium current (Cummins et al., 1999). In effect, the range of voltages in which $Na_V1.9$ is active is large (i.e., large window current). This implies a wide range of voltages in which $Na_V1.9$ may open spontaneously or persistently (Dib-Hajj et al., 2015). Due to its properties, it has been proposed that $Na_V1.9$ does not contribute to the AP upstroke itself but rather acts as a threshold channel prolonging and potentiating subthreshold stimuli (Dib-Hajj et al., 2015; Bennett et al., 2019).

1.1.5.2 $Na_V1.9$ in inflammatory conditions

As mentioned earlier, inflammation leads to altered neuronal functioning via peripheral sensitization. Several studies have established a link between $Na_V1.9$ activity and neural excitability in inflammation (Cheng et al., 2021). When DRG neurons were incubated with guanosine-5'-triphosphate (GTP) or its non-hydrolyzable analog Guanosine 5'-O-[gamma-thio]-triphosphate (GTPγS), $Na_V1.9$ currents, spontaneous and stimulated firing frequencies increased, while AP thresholds decreased (Figure 1-2). This experiment confirmed that Nav1.9 activity is stimulated by GPCR signaling (Baker et al., 2003; Ostman et al., 2008). Exposition to PGE_2 for 1 h led to a GPCR-mediated increase in $Na_V1.9$ currents (Rush and Waxman, 2004). This sensitizing effect could not be observed when DRG neurons were exposed to single inflammatory mediators (PGE_2, bradykinin, histamine, adenosine-5'-triphosphate (ATP), and norepinephrine) for a short time. $Na_V1.9$ current and AP firing did, however, increase when these inflammatory mediators were applied together in a mixture (Maingret et al., 2008). Similar effects were shown due to acute interleukin-1-β (IL-1-β) exposition (Binshtok et al., 2008). $Na_V1.9$ was shown to potentiate the excitatory effect of PGPC on murine DRG neurons

under inflammatory conditions only (Martin et al., 2018). The underlying mechanism is based on a brief increase in the resting membrane potential by inflammatory mediators, which has been shown to be reduced in $Na_V1.9$ knockout (KO) mice (Martin et al., 2018). Lowered cholesterol content of cell membranes due to inflammation also led to enhanced excitation mediated by $Na_V1.9$ (Amsalem et al., 2018). *In vivo*, heat and mechanical hypersensitivity induced by inflammatory mediators or inflammation models was decreased or absent in $Na_V1.9$ KO mice compared wildtype (WT) mice (Amaya et al., 2006; Lolignier et al., 2011; Priest et al., 2005). Single-fiber recordings of C fibers prepared from $Na_V1.9$ KO mice showed reduced axonal sensitivity to heat and mechanical stimuli (Hoffmann et al., 2017).

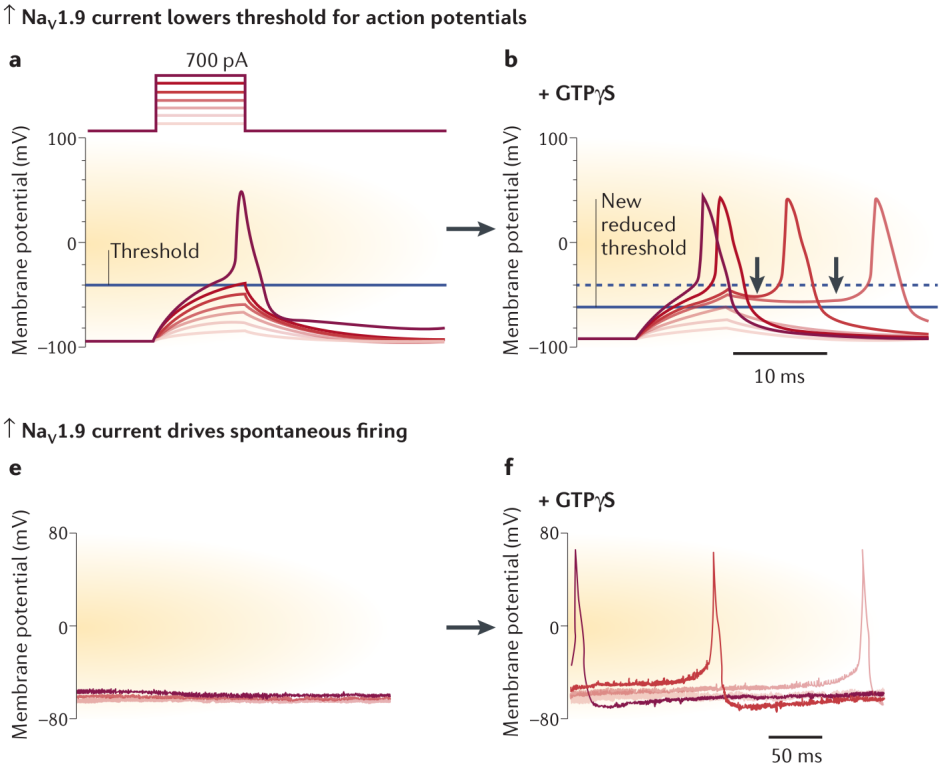

Figure 1-2: **Na$_V$1.9 increases the excitability of DRG neurons**. (**a**) Stimulus currents injected into small-diameter DRG neurons depolarize the membrane potential and evoke AP firing if the membrane potential surpasses a threshold. (**b**) Treatment with GTPγS reduces the current threshold for AP firing of DRG neurons. (**e**) Current clamp recording of unstimulated DRG neurons showing no spontaneous firing. (**f**) GTPγS leads to an increase in Na$_V$1.9 currents, which drive spontaneous firing. AP, action potential; DRG, dorsal root ganglion; GTPγS, Guanosine 5'-O-[gamma-thio]-triphosphate; Na$_V$1.9, voltage-gated sodium channel 1.9. Adapted from Dib-Hajj et al., 2015. With kind permission of Springer Nature.

The threshold for AP generation is considered to determine the electrical excitability of neurons, which largely depends on VGSCs and other voltage-gated ion channels (Koester and Siegelbaum, 2013). Plasticity, in the context of neuronal excitability, is the persistent alteration of the intrinsic electrical properties of neurons mediated by expression patterns or biophysical properties of ion channels (Debanne, 2009). In the context of $Na_V1.9$ mutations, shifts of

excitability of neurons to both hyper- and hypoexcitable states were observed in electrophysiological experiments (Huang et al., 2017; Leipold et al., 2013).

1.1.6 Neuronal calcium activity

Spontaneous calcium activity in the central sensory system has been studied extensively, while fewer insights are available on peripheral sensory neurons (Imaizumi et al., 2018). Previous experiments with DRG neurons have focused on the analysis of spontaneous APs in single-nerve fiber recordings. Here, increased spontaneous AP formation in spinal cord injury (SCI) models (Bedi et al., 2010) and complete Freund's adjuvant-induced inflammation (Djouhri et al., 2006) were reported. Human DRG neurons from neuropathy patients showed increased spontaneous AP rates in whole-cell patch clamp (North et al., 2019). Ongoing activity in C-fibers after SCI was associated with prolonged depolarization of the resting membrane potential, lowered AP threshold, and an increase in large depolarizing spontaneous fluctuations of the membrane potential (Odem et al., 2018). Increased depolarizing spontaneous fluctuations were also shown to be related to the sensitizing effect of serotonin (Lopez et al., 2020).

Calcium signaling is an evolutionarily conserved mechanism, that facilitates a multitude of intracellular signaling processes, including initiation of transcription, cytoskeleton interaction, recruitment of membrane proteins into the plasma membrane, programmed cell death, and cell-to-cell signaling (Clapham, 2007). In neuronal signaling, calcium ions are involved in synaptic transmission, the induction of activity-dependent synaptic plasticity, and neural development (Brini et al., 2014). The wide range of signaling is facilitated by the distinct spatial and temporal organization of calcium signals (Berridge et al., 2003). Spatial compartmentalization is particularly apparent in neuronal axons (Berridge et al., 2003). Two distinct temporal kinetics of spontaneous calcium activity have been described in developing neurons: waves, that last approximately 30 s at a rate of 1 h^{-1}, occur locally, and contribute to growth cone migration. Spikes are shorter (10 s), occur 1-10 times per hour, and are propagated along the neuron (Spitzer et al., 2000; Spitzer, 2006). Spikes contribute to neurotransmitter synthesis and trigger differential gene transcription (Berridge et al., 2003).

On the molecular level, the initiation of spontaneous excitation can be attributed to ligand-dependent, non-synaptic transmitter signaling (Gu and Spitzer, 1995), or to cell-autonomous excitation by ion channels active at subthreshold membrane potentials. Studies in motoneurons have established a link between spontaneous calcium signals and $Na_V1.9$, which acts as an upstream trigger of calcium activity regulating axonal growth without affecting neuron survival (Subramanian et al., 2012; Wetzel et al., 2013).

1.1.6.1 'Signal-close-to-noise' calcium activity

Albeit much is known about calcium as a signaling mediator and neuronal excitant in general, the signaling impact of calcium signals that are homeostatic or regulate subthreshold neuronal excitability remains unclear.

Prada et al. define such signal-close-to-noise calcium activity as subthreshold non-spike-like signals, close to measurement noise carrying biologically relevant information (Prada et al., 2018). Multiple computational tools investigating calcium signaling have been developed based on signal processing strategies such as denoising and demixing (Pnevmatikakis et al., 2016) or thresholding (Romano et al., 2017). These tools, however, do not reliably detect homeostatic, signal-close-to-noise calcium activity (Prada et al., 2018). To reliably analyze these signals Prada et al. developed Neural Activity Cubic (NA^3) an open-source tool, which identifies (subthreshold) calcium activity events and neuronal activity states (Prada et al., 2018). Transients are identified by a hard-coded algorithm based on continuous wavelet transform (CWT, wavelet ridge walking), while neural activity states are quantified by calculating the signal variance in a sliding window (Figure 1-3, Prada et al., 2018). At present, NA^3 is the only verified tool for calcium activity quantification that is able to detect signal-close-to-noise activity events.

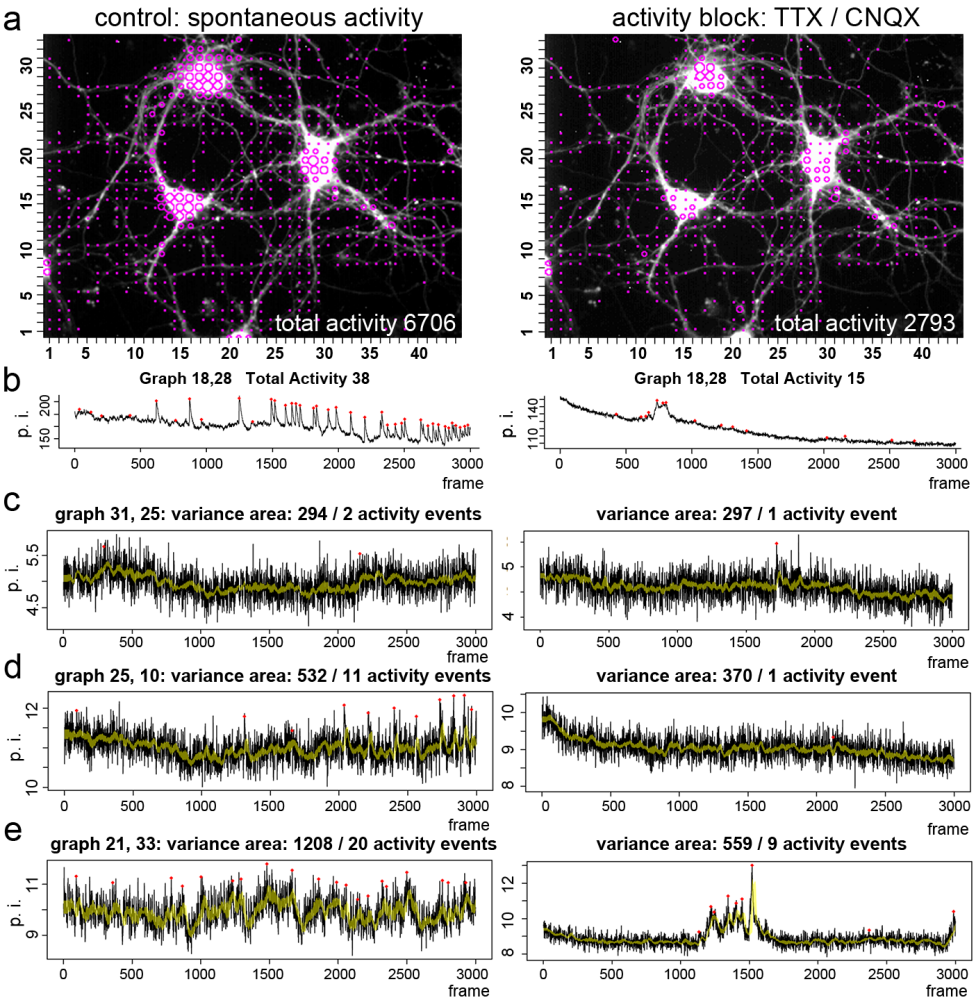

Figure 1-3: **Computation of activity events and variance area by NA[3] to determine the neuronal activity state**. Analysis of hippocampal neurons before (left column) and after activity block (right column). (a) Activity map. (b) Calcium imaging trace in spiking area. Spikes are reduced by activity block. (c-e) Calcium imaging traces of non-spiking areas. (c) A region in which activity block does not affect activity count and variance area. (d, e) Decreased activity counts and variance area after activity block. Activities detected are marked with red dots, the yellow band indicates the trace variance area in a sliding window (30 frames). CNQX, 6-cyano-7-nitroquinoxaline-2,3-dione; NA[3], Neural Activity Cubic; TTX, tetrodotoxin. Published under Creative Commons Attribution License (CC BY; Prada et al., 2018)

1.2 Aim of the thesis

Genetic investigations of humans with pain disorders, *in vivo* and *in vitro* experiments of rodent DRG neurons have established a link between $Na_V1.9$, nociception, and peripheral sensitization (Dib-Hajj and Waxman, 2019; Martin et al., 2018). Furthermore, $Na_V1.9$ was shown to contribute to spontaneous calcium signaling (Subramanian et al., 2012; Wetzel et al., 2013). The novel inflammatory pain mediator OxPAPC has been found to significantly contribute to acute nociception and peripheral sensitization in rodents and is thought to contribute to the complex signaling cascades of other inflammatory mediators (Liu et al., 2016; Martin et al., 2018; Mohammadi et al., 2018; Oehler et al., 2017). The computational tool NA^3 has been validated to reliably determine neuronal signal-close-to-noise calcium activity and activity states, providing proxies for neuronal excitability (Prada et al., 2018).

This thesis aims to characterize spontaneous calcium activity in neuronal compartments as a proxy to investigate neuronal excitability. A focus was put on $Na_V1.9$, which is the most important mediator of nociceptor excitability and therefore is the best candidate that may function as an upstream trigger molecule for spontaneous calcium activity events. Subsequently, the effect of OxPAPC on the excitability of DRG neurons and its interplay with other inflammatory mediators was investigated. The following hypotheses summarize the scope of this thesis. They are visualized in Figure 1-4.

1. The number of 'signal-close-to-noise' calcium activity events and the variance of calcium signals reflect the excitability state of DRG neurons.
2. $Na_V1.9$-dependent excitability of DRG neurons is reflected in the number of spontaneous calcium activity events per time in neuronal compartments (Figure 1-4A).
3. Long-lasting (1 h) exposure to OxPAPC increases the excitability of cultured small-diameter DRG neurons (Figure 1-4A).
4. Long-lasting (30 min) exposure to OxPAPC sensitizes subgroups of DRG neurons for inflammatory mediators (bradykinin, histamine, and PGE_2; Figure 1-4B).

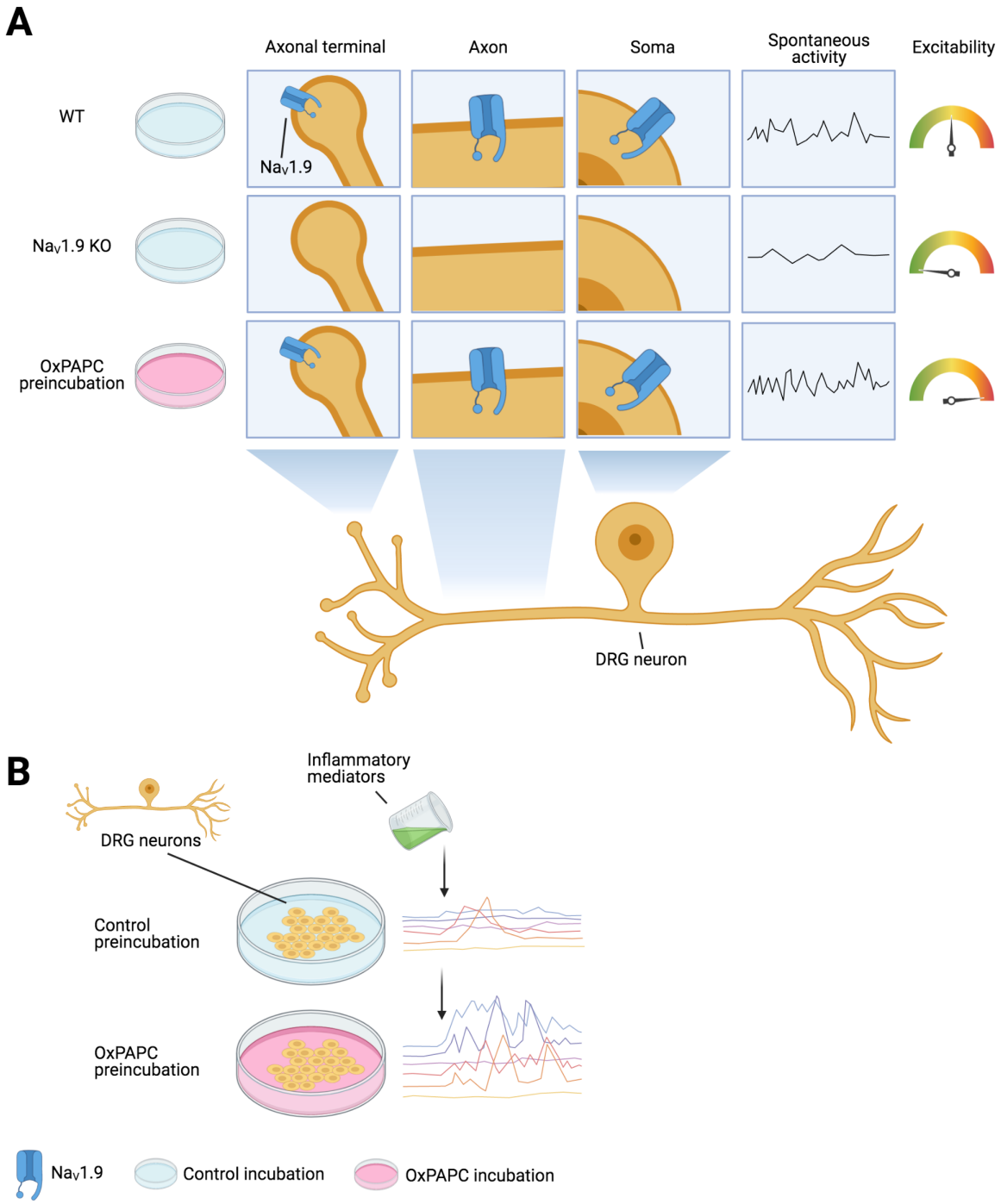

Figure 1-4: **Outline: Hypotheses of this study.** (**A**) Nav1.9-dependent excitability of DRG neurons is reflected in the number of spontaneous calcium activity events per time in neuronal compartments and long-lasting (1 h) exposure to OxPAPC increases the excitability of DRG neurons. (**B**) Long-lasting (30 min) exposition to OxPAPC sensitizes DRG neurons for inflammatory mediators (bradykinin, histamine, and PGE_2). DRG, dorsal root ganglion; KO, knockout; Nav1.9, voltage-gated sodium channel 1.9; OxPAPC, oxidized PAPC; WT, wildtype. Created with BioRender.com

2 Materials

2.1 Animals

For this thesis, WT C57BL/6J mice and $Na_V1.9$ KO (*Scn11a*$^{-/-}$, backcrossed with C57BL/6J for a minimum of nine generations; Ostman et al., 2008) were used. All animals were bred in the animal care facility of the Institute for Clinical Neurobiology at the University of Würzburg, Versbacherstraße 5, 97078 Würzburg, Germany. Animals were kept in a non-sterile environment, guaranteed free unlimited (*ad libitum*) access to water and food at 20 to 22 °C room temperature and 50 to 70 % humidity with a day-night-rhythm of 12 hours. The animals were subjected to regular examinations by the institutional animal welfare officer every three months. All experiments involving animals were performed in accordance with the European Union guidelines. The experiments were approved by the Institutional Animal Care and Utilization Committee and the responsible animal protection authority (Regierung von Unterfranken, Peterplatz 9, 97070 Würzburg, Germany).

For experiments involving only WT DRG neurons, six- to eight-week-old mice were used. In the experiments comparing $Na_V1.9$ KO to WT DRG neurons, age-matched 20 to 24-week-old mice were used.

Cultured rodent DRG neurons are well established to study the functions and plasticity of primary sensory neurons *in vitro*, as they have been found to have similar characteristics as sensory neurons *in vivo* (Malin et al., 2007).

2.2 Chemicals

Table 2-1: **Cell culture chemicals**

Name		Company	Catalogue No.
Ampuwa® sterile water	Aqua	Fresenius Kabi	0575621/00
Boric Acid		AppliChem	A2940
DMEM/F-12, GlutaMAX™ Supplement	DMEM/F12	Thermo Fisher Scientific	31331-028
Dulbecco's Modified Eagle Medium (1X), high glucose	DMEM	Thermo Fisher Scientific	11965-092
Dulbecco's Phosphate Buffered Saline	PBS	Sigma-Aldrich	D8537
Ethanol		Sigma-Aldrich	32205

Fetal Bovine Serum	FBS	Thermo Fisher Scientific	10270106
Hanks' Balanced Salt Solution	HBSS	Thermo Fisher Scientific	14170-088
Laminin-111 (murine)		Sigma-Aldrich	CC095-M
Liberase™ Thermolysin high (TH) Research Grade		Sigma-Aldrich	05401135001
Liberase™ Thermolysin medium (TM) Research Grade		Sigma-Aldrich	05401119001
Nerve Growth Factor-7S from murine submaxillary gland	NGF	Sigma-Aldrich	N0513
Penicillin Streptomycin	Pen Strep	Thermo Fisher Scientific	15070063
Poly-DL-ornithine hydrobromide	PORN	Sigma-Aldrich	P8638

Table 2-2: **Immunocytochemistry chemicals**

Name		**Company**	**Catalogue No.**
Aqua-Poly/Mount		Polysciences	18606
di-Sodium hydrogen phosphate dihydrate	Na_2HPO_4 * 2 H_2O	Merck	119753
Horse serum		Linaris	SHD3250KYA
Paraformaldehyde	PFA	Alpha Aesar	A11313
Potassium dihydrogen phosphate	KH_2PO_4	Merck	104873
Triton® X-100		Sigma-Aldrich	T8787
Tween20		AppliChem	A4974

Table 2-3: **Calcium imaging chemicals**

Name		**Company**	**Catalogue No.**
4-(2-hydroxyethyl)-1-piperazineethanesulfonic acid	HEPES	Carl Roth	HN77
Bradykinin acetate salt	BK	Sigma-Aldrich	B3259
Calcium chloride	$CaCl_2$	Merck	102378
Chloroform		Sigma-Aldrich	288306
D(+)-Glucose monohydrate	Glucose	Merck	108342

Dimethylsulfoxid	DMSO	AppliChem	A3672
Forskolin	FSK	alomone labs	F-500
Histamine		Sigma-Aldrich	H7125
Magnesium chloride hexahydrate	$MgCl_2$ * $6H_2O$	Merck	105833
Oregon Green™ 488 BAPTA 1-AM, cell permeant	OGB-1	Thermo Fisher Scientific	O6807
Oxidized PAPC	OxPAPC	Hycult Biotech	HC4035
Pluronic® F-127		Thermo Fisher Scientific	P6867
Potassium chloride	KCl	Merck	104936
Prostaglandin E_2	PGE_2	Sigma-Aldrich	P5640
Sodium chloride	NaCl	Sigma-Aldrich	31434
Sodium hydroxide (5N)	NaOH	Merck	109913

2.3 Antibodies and labelling toxins

Table 2-4: **Primary antibodies**

Epitope	Host	Company/Producer	Catalogue No.	Dilution
βIII-Tubulin	Mouse	Neuromics	MO15013	1:200
Microtubule-associated protein 2 (MAP2)	Mouse	Sigma-Aldrich	M1406	1:200
$Na_V1.9$ (T71n)	Rabbit	PD Dr. Robert Blum		1:500
Neurofilament protein L (NFL)	Chicken	abcam	ab24520	1:1000
TRPV1	Goat	Santa Cruz	sc-12498	1:400

Table 2-5: **Secondary antibodies**

Target	Host	Conjugate	Company	Catalogue No.	Dilution
Chicken	Donkey	Alexa Fluor® 488	Jackson	703-545-155	1:800
Chicken	Donkey	Cy™3	Jackson	703-165-155	1:800
Goat	Donkey	Alexa Fluor® 488	Jackson	705-545-147	1:800
Mouse	Donkey	Cy™5	Jackson	715-175-150	1:800
Rabbit	Donkey	Cy™3	Jackson	711-165-152	1:800
Rabbit	Donkey	Alexa Fluor® 488	Jackson	711-545-152	1:800

Table 2-6: **Labelling toxins**

Name	Target	Conjugate	Company	Catalogue No.	Dilution
Phalloidin	F-actin	Acti-Stain™ 555	Cytoskeleton, Inc.	PHDH1	1:100

2.4 Solutions

Table 2-7: **Cell culture solutions**

Solution	Composition	
Borate buffer	0.15 M	boric acid in sterile H_2O titrated to pH 8.3 using NaOH
DRG neuron culture medium	10 % 1 % 100 ng/ml	FBS Pen Strep NGF (freshly added on day of usage) in DMEM/F12 stored at 37 °C and 5 % CO_2
Laminin solution	0.25 µg/ml	Laminin-111 in HBSS stored at -20 °C (thawed only once)
PORN solution	10 mM	PORN in borate buffer
TH enzyme solution	0.12 mg/ml 1 mM	Liberase™ TH Research Grade EDTA in DMEM
TM enzyme solution	0.12 mg/ml 1 mM	Liberase™ TM Research Grade EDTA in DMEM

Table 2-8: **Immunocytochemistry solutions**

Solution	Composition	
4 % PFA solution	4% 10 %	PFA (ρ, mass concentration) PBS (10×) in Aqua titrated to pH 7.35 using NaOH
Permeabilization and blocking solution	10 % 0.3 % 0.1 %	horse serum Triton® X-100 Tween20 in PBS (1×)
Washing solution	0.1 % 0.1 %	Triton® X-100 Tween20 in PBS (1×)

Table 2-9: **Calcium imaging solutions**

Solution	Composition	
Calcium imaging buffer (CIB; Oehler et al., 2012)	135 mM 6 mM 1 mM 1 mM 10 mM 5.5 mM	NaCl KCl $MgCl_2$ $CaCl_2$ HEPES Glucose in sterile H_2O titrated to pH 7.4 using NaOH
FSK solution	10 µM	FSK in CIB
Inflammatory mediator mixture (IM, high concentration)	50 nM 1 µM 500 nM	Bradykinin Histamine PGE_2 in CIB
IM (low concentration)	5 nM 100 nM 50 nM	Bradykinin Histamine PGE_2 in CIB
KCl solution	90 mM	KCl in CIB
OGB-1 stock solution	200 mg/ml 4.5 mM	Pluronic OGB-1 in DMSO
OxPAPC solution	10 µM	OxPAPC in CIB or DRG medium prepared directly before use

2.5 Equipment

Table 2-10: **Disposable material**

Name	Manufacturer
Coverslips (10 mm)	Marienfeld
Coverslips Ø 50 mm	Marienfeld
Culture dish (4-well, circular)	Greiner bio-one
High vacuum grease	Dow Corning

Table 2-11: **Cell culture equipment**

Name	Manufacturer
Thermomixer comfort	Eppendorf
Centrifuge MiniSpin®	Eppendorf

Table 2-12: **Immunofluorescence equipment**

Name	Description	Manufacturer
FV1000-IX81	Inverted confocal laser scanning microscope	Olympus
UPLFLN 40x O NA 1.3	40×, numerical aperture (NA) 1.3 objective	Olympus
UPLSAPO 60x O NA 1.35	60×, NA 1.35 objective	Olympus

Table 2-13: **Calcium imaging equipment**

Name	Description	Manufacturer
Badcontroller V	Temperature controller	Luigs & Neumann
BX51WI	Fixed stage upright microscope	Olympus
Calcium imaging chamber		PD Dr. Robert Blum
LUMPlanFI/IR 40x/0.80 W	40×, NA 0.8 objective	Olympus
Minipuls 3	Peristaltic pump	Gilson
OM 806	Osmometer	Löser
pE excitation system (Serial No. 0565)	LED illumination system	CoolLED
Rolera-XR	Digital charge-coupled device (CCD) camera	QImaging
SM 7 control system		Luigs & Neumann
TC-344B	Dual automatic temperature controller	Warner Instruments
TH4-200	Halogen lamp power supply unit	Olympus
U-25ND6	Neutral density filter	Olympus
UMPlanFL N 10x/0.3	10×, NA 0.3 objective	Olympus

2.6 Software

Table 2-14: **Software**

Name	Version	Developer	Identifier
Fluoview FV10-ASW	4.2.2.9	Olympus	RRID:SCR_014215
ImageJ	2.0.0	National Institutes of Health (Schneider et al., 2012)	RRID:SCR_003070
Inkscape	0.92	The Inkscape Project	RRID:SCR_014479
Microsoft Excel	2010	Microsoft	RRID:SCR_016137

NA[3]	1.0	Prada et al. (Prada et al., 2018)	
OriginPro	2019b	OriginLab Corporation	RRID:SCR_014212
R	3.6.1	R Foundation for Statistical Computing Team, 2019	RRID:SCR_001905
RStudio	1.2.5019	RStudio, Inc.	RRID:SCR_000432
StreamPix	4.23.2	NorPix	RRID:SCR_015773

3 Methods

3.1 Coating of coverslips with PORN and laminin

Glass coverslips are negatively charged and therefore need to be coated with charge enhancers to allow the attachment of the negatively charged cellular membranes. Coverslips were coated with poly-DL-ornithine hydrobromide (PORN) and laminin-111. Laminin-111 acts as a strong stimulator for neurite growth in DRG neurons (Plantman et al., 2008).

10 mm coverslips were covered with ethanol, flamed, and then transferred into 4-well culture dishes. Next, coverslips were covered with 100 µl PORN solution (10mM) and incubated for 60 min at 37 °C. After incubation, coverslips were rinsed with water three times, dried, and stored at 4 °C. Laminin-111 coating was conducted on the same day as DRG preparation. Coverslips were covered with 100 µl laminin solution (100 ng/ml) and stored at room temperature for 60 min. The laminin solution was removed directly before plating the DRG suspension to avoid drying out.

3.2 Preparation of murine DRG neurons

DRG neurons were prepared as described in previous studies (Oehler et al., 2017; Malin et al., 2007). Mice were asphyxiated with CO_2 and killed by cervical dislocation. After removing the dorsal skin, the spinal column was dissected cranial of the sacrum and caudal of the skull. Now the spinal column was opened in the sagittal plane and covered with cooled DMEM for the course of the preparation. DRGs were collected from the intervertebral foramina of all levels of the spinal cord and carefully cleaned of attached nerve bundles and connective tissue. Isolated DRGs were stored in 2 ml DMEM on ice.

In the following protocol, centrifugation of cell suspensions was conducted at 3000 revolutions per minute for 3 min (MiniSpin®, Eppendorf). Settings used for incubation in the Thermomixer (Eppendorf) were 37°C, 900 revolutions per minute at an interval of 30 s (duration of alternating mixing and standstill phases).

After DRG preparation, the cell suspension was centrifuged and the supernatant was removed. The DRG tissue was incubated with 1.5 ml TH enzyme solution in the Thermomixer for 25 min. The suspension was centrifuged, and the supernatant discarded. The tissue was then incubated with 1.5 ml TM enzyme solution in the Thermomixer for 10 min. After centrifugation, the supernatant was discarded, and the remaining tissue was re-suspended in 1 ml DRG culture medium. The tissue was gently dissociated through careful repeated pipetting

(approximately 10 times) with a 1 ml pipet tip to form a homogenous suspension. The suspension was centrifuged again, the supernatant discarded and re-suspended in DRG culture medium. The cell suspension was plated on cover glasses pre-coated with PORN.

The amount of medium used for re-suspension and the amount of cell suspension plated on the cover glasses were adjusted depending on the cell concentration required for the respective experiment. For calcium imaging experiments measuring spontaneous activity in single neurons and immunocytochemistry, cells were plated at low density (approx. 3×10^3 cells per 10 mm coverslip). For calcium imaging experiments measuring the response of DRG soma to sensitizing agents, cells were plated at high density (approx. 8×10^3 cells per 10 mm coverslip). Plating densities were evaluated microscopically directly after cell plating.

The cover glasses were incubated for 45 min at 37 °C and 5% CO_2 to allow cell sedimentation and attachment. Finally, 2 ml DRG medium per 4-well dish was added. The cells were cultured for 20 to 22 h at 37 °C and 5% CO_2 before experiments were conducted.

3.3 Immunocytochemistry

Indirect (secondary) immunofluorescence was used for immunocytochemistry of DRG neurons. Hereby, epitopes located on the membrane and in intracellular compartments of cells are visualized. First, cells are fixed with the crosslinker PFA. To allow antibody diffusion to intracellular compartments, cells are incubated with a permeabilization solution containing detergents (e.g., Triton® X-100 and Tween20). Further, unspecific binding sites are blocked by incubation with a common protein (e.g., bovine serum albumin) or with serum (e.g., horse serum). In my experiments, permeabilization and blocking was performed at the same time using a single permeabilization and blocking solution.

Indirect immunofluorescence relies on the specific binding of a primary unlabeled antibody against the epitope of interest. Subsequently, the secondary fluorophore-labeled antibodies bind specifically to the primary antibody. The fluorescence signal intensity is amplified due to multiple binding of secondary antibodies to one primary antibody. The location of the epitope is identified by fluorescence microscopy.

3.3.1 Indirect immunofluorescence protocol

Primary and secondary antibodies were dissolved in permeabilization and blocking solution. The antibody loading was performed in a self-built dark semi-wet chamber to avoid drying out and bleaching of fluorescent dyes.

Cells cultured on 10 mm coverslips were fixed with 500 µl pre-warmed (37°C) 4% PFA solution for 15 min at room temperature. Then, they were incubated with 500 µl permeabilization and blocking solution for 1 h at room temperature. Next, primary antibodies were dissolved in the desired dilution in permeabilization and blocking solution and stored on ice. Cells were incubated in 75 µl primary antibody solution for 2.5 h at room temperature. Now, secondary antibodies were dissolved in the desired dilution in permeabilization and blocking solution, stored on ice, and protected from light. After removing the primary antibody solution, cells were washed four times using the washing solution and incubated with 75 µl secondary antibody solution at room temperature for 1.5 h. For the specific antibody concentrations used, refer to the primary and secondary antibody list in section 0. Next, cells were washed with washing solution three times and twice with PBS (1×). The coverslips were dipped in water and mounted upside-down on microscope slides using Aqua Polymount. Slides were stored at 4 °C protected from light.

3.3.2 F-actin labeling with phalloidin

The phallotoxin phalloidin was used to visualize filamentous actin (F-actin). Phalloidin specifically binds to F-actin complexes (Melak et al., 2017). Here, the fluorophore-labeled Acti-stain™ 555 was used. As phalloidin binds directly to F-actin, Acti-stain™ 555 was dissolved together with the secondary antibodies in permeabilization and blocking solution and incubated as described in 3.3.1.

3.3.3 Confocal imaging and image editing

Confocal images were acquired with an FV1000-IX81 inverted confocal laser scanning microscope (Olympus), a UPLSAPO 60× objective (oil, NA 1.35; Olympus) and a UPLFLN 40× objective (oil, NA 1.3; Olympus) using 473, 559, and 635 nm laser diodes and the FV10-ASW software (Olympus). Images were taken as 12-bit z-stacks and saved in Olympus .oib format. ImageJ was used to adjust the images in brightness and contrast and to flatten the z-stack using maximum intensity projection. The final figures were created using Inkscape.

3.4 OxPAPC solution preparation

OxPAPC was dissolved in chloroform to transfer desired amounts into glass tubes. The liquid chloroform was evaporated using a stream of nitrogen. OxPAPC was stored at -20 °C in glass tubes protected from light. For usage of OxPAPC in experiments, the lipid film was re-suspended thoroughly in the desired solvent (DMEM or CIB).

3.5 Calcium imaging

Calcium imaging is the standard technique used to assess intracellular changes in calcium concentration in neurons (Grienberger and Konnerth, 2012; Tsien, 1981). Calcium is an essential signaling ion in neuronal cells responsible for multiple functions such as activity-dependent synaptic plasticity, gene transcription, or neurotransmitter release (Grienberger and Konnerth, 2012).

In this thesis, the non-ratiometric single-wavelength calcium indicator Oregon Green BAPTA 1-AM (OGB-1) was used. The fluorophore used for detection is conjugated to two important functional groups: an acetoxymethyl (AM) ester and 1,2-bis(o-aminophenoxy)ethane-N,N,N′,N′-tetraacetic acid (BAPTA; Rudolf et al., 2003). The lipophilic properties of the AM ester allow the diffusion of the calcium indicator across the lipid bilayer membrane of cells. Cleavage of the AM ester by intracellular esterases removes the lipophilic functional group and, hereby, entraps the indicator molecule intracellularly. BAPTA is a calcium chelator, which binds two calcium ions. Calcium-binding induces a conformational change of the calcium indicator, resulting in up to a 14-fold increase of emitted fluorescence. OGB-1 is excited at a wavelength of 488 nm and emits fluorescence at 520 nm. High-affinity calcium indicators such as OGB-1 have a large signal-to-noise ratio, allowing the recording of signals-close-to-noise (Paredes et al., 2008; Johnson and Spence, 2010). The emitted calcium-induced fluorescence is recorded using photon detectors (e.g., CCD-cameras).

3.5.1 Calcium imaging protocol

In experiments comparing OxPAPC incubation with control conditions, DRG neurons plated on coverslips were incubated with 500 µl 10 µM OxPAPC for either 30 min, for recording the response to sensitizing agents, or 1 h, for recordings of spontaneous activity. 500 µl DMEM was used as control incubation for the same time periods. For recordings of spontaneous activity in WT and $Na_V1.9$ KO DRG neurons, spontaneous activity was compared between both genetic conditions. The different experimental setups and calcium imaging protocols are visualized in Figure 3-1.

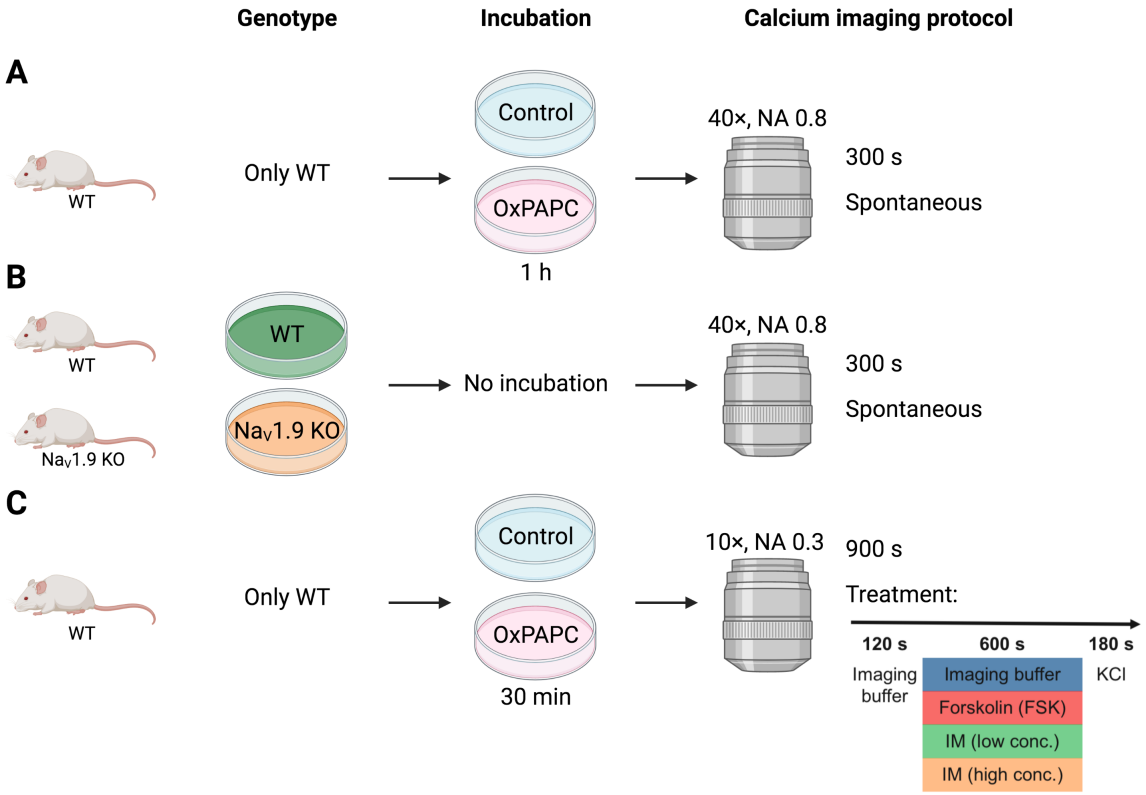

Figure 3-1: **Outline of different experimental setups and calcium imaging protocols**. For each experimental setup, the used genotype, incubation, and calcium imaging protocol is shown. (**A**) Murine WT DRG neurons were incubated in 10 µM OxPAPC for 1 h. Calcium imaging was performed at high spatial resolution for 300 s without stimulation. (**B**) Murine WT or Nav1.9 KO DRG neurons were recorded by calcium imaging at high spatial resolution for 300 s without incubation and stimulation. (**C**) Murine WT DRG neurons were incubated in 10 µM OxPAPC for 30 min. Calcium imaging was performed at low spatial resolution for 900 s. The neurons were treated with CIB, FSK, IM (low conc.), or IM (high conc.) for 600 s and finally exposed to KCl. High spatial resolution imaging was performed using a 40×, NA 0.8 objective, low spatial resolution imaging using a 10×, NA 0.3 objective. CIB, calcium imaging buffer; conc., concentration; IM, inflammatory mediator mixture; FSK, forskolin; KO, knockout; Nav1.9, voltage-gated sodium channel 1.9; NA, numerical aperture; OxPAPC, oxidized PAPC; WT, wildtype. Created with BioRender.com

For calcium indicator dye loading, coverslips were incubated with 500 µl CIB containing 0.5 µl OGB-1 stock solution (4.5 µM OGB-1) for 15 min at 37 °C and 5% CO2 and then placed in the perfusion chamber filled with 1.0 to 1.5 ml CIB. Buffers, agonists, and mediators were constantly perfused using a peristaltic pump (Minipuls 3, Gilson) and kept at 25°C using a flow-through temperature controller (TC-344B, Warner Instruments). A temperature controller (Bath controller V, Luigs & Neumann) kept the perfusion chamber at 25 °C throughout the experiments. Recordings were started approximately 5 min after the coverslip was placed in the perfusion chamber to allow the calcium indicator to reach a steady state. In all experiments, the recordings were acquired at a rate of 10 frames per second (fps), with an exposure time of 100 ms. Recordings were acquired using a fixed stage upright microscope (BX51WI, Olympus) and

a digital CCD camera (Rolera-XR, QImaging). Depending on the experimental setup different objective lenses were used. Measurements were recorded in 8-bit greyscale with StreamPix and saved in AVI (Audio Video Interleave) format.

To enable comparability between the experiments, LED intensity, surrounding light sources, binning settings (2×2), and natural density filters were kept constant.

3.5.1.1 Spontaneous activity

For recordings of spontaneous activity of DRG neurons, images were acquired for 300 s. Here a 40×, NA 0.8 objective (LUMPlanFI/IR 40x/0.80 W, Olympus) was used (Figure 3-1A, B). The image section was chosen so that the soma, axons, and axonal terminals of one DRG neuron were recorded in the same image series. For recordings, small size DRG neurons were selected. Each coverslip was used for four to five recordings of different DRG neurons. Throughout the experiment, CIB was perfused through the perfusion chamber at a constant rate of 3 ml/min.

3.5.1.2 Response to sensitizing agents

Measurements recording the activity of DRG neurons in response to treatment with forskolin (FSK), inflammatory mediator mixture (IM; high and low concentration), or CIB were recorded for 900 s using a 10×, NA 0.3 objective (UMPlanFL N 10x/0.3, Olympus). The image section was chosen to record a high number of DRG neuron somata. The perfusion chamber was perfused at a constant rate of 1.5 ml/min according to the following protocol: for 120 s, a baseline was recorded, while the chamber was perfused with CIB. After 120 s the respective sensitizing solution was perfused into the chamber for a total period of 600 s. At 720 s, 1 ml KCl solution (90 mM) was carefully pipetted directly into the perfusion chamber. Recordings were ended after 900 s (9000 images). The experimental schedule is summarized in Figure 3-1C and Table 3-1. After each experiment, the perfusion chamber and the conducting tubes were cleaned with CIB.

Table 3-1: S**chedule of calcium imaging experiments measuring response to sensitizing agents.**

Time	Duration	Phase	
0 s	120 s	Baseline period	Perfusion of CIB
120 s	600 s	Treatment period	Perfusion of sensitizing agents (FSK or IM) or control (CIB)
720 s	180 s	Assessment of neuronal viability	KCl solution pipetted into recording chamber
900 s	-	End of recording	

CIB, calcium imaging buffer; FSK, forskolin; IM, inflammatory mediators mixture.

3.6 Analysis of calcium imaging data

3.6.1 Labelling of regions of interest

Regions of interest (ROIs) were marked using the *ROI Manager* plugin in ImageJ. In single-cell recordings, ROIs were placed on axonal terminals, axons, and somata of individual DRG neurons. In experiments recording at low spatial resolution (experiments measuring the response to sensitizing agents), only somata were labeled with oval ROIs. ROIs were saved and used for manual and automated activity detection.

3.6.2 Extraction of calcium imaging data from AVI files

Recordings were imported into ImageJ for analysis. Mean pixel greyscale values (8 bit) per ROI over time were measured using the *ROI Manager* plugin. This data was either transferred to Excel for further processing or saved as comma-separated values (CSV) files for automated analysis by NA[3].

3.6.1 Identification of viable neurons in low spatial resolution calcium imaging

To identify neuronal cells with a reaction to the KCl stimulus (control stimulus as viability test), the change in mean fluorescence of ROIs in the KCl-exposed period from 720 to 900 s compared to the KCl-unexposed period from 600 to 710 s was calculated. If the ratio was above or equal to 1.1, cells were considered KCl-reaction positive. Only neurons reacting to the KCl stimulus were included in subsequent analyses.

3.6.2 Manual analysis

3.6.2.1 Background correction

In the analysis of both experimental setups, three ROIs were placed in each recording in regions without any neuronal structure to record the background signal. The mean background signal was then subtracted from the ROI signal for each frame individually, resulting in data corrected for background fluctuations.

3.6.2.2 Calculation of Δ F/F0

From background-corrected data, the change in fluorescence signal at frame *i* (F_i) relative to an inactive period in the same recording (F_0) was calculated.

$$\Delta F/F_0 = \frac{F_i - F_0}{F_0}$$

Here $\Delta F/F_0$ cannot be used to determine absolute values of the fluorescence signal as OGB-1 is a single-wavelength (non-ratiometric) calcium indicator (Paredes et al., 2008). As fluorescence intensity cannot be compared directly between measurements, the definition of a

threshold value for peak classification is not possible. Also, data recorded from single-wavelength calcium indicators cannot be used to calculate a ratio between Ca^{2+}-bound and Ca^{2+}-free states, which is possible with ratiometric dyes such as Fura-2 (Rudolf et al., 2003).

3.6.2.3 Spontaneous activity measurements

The data was pasted to OriginPro and line graphs were drawn for analysis. The graphs were analyzed heuristically for fluorescence peaks by manual counting. The same calcium imaging recordings were also analyzed using NA^3 for automated, unbiased activity detection as described in section 3.6.3.

3.6.3 Automated analysis

Manual calcium activity detection is based on heuristics of the individual researcher and heuristic annotation of regions-of-interests causes interobserver variability (Segebarth et al., 2020). Furthermore, biologically relevant spontaneous calcium activities are presumed to be encoded in signal-close-to-noise (Prada et al., 2018). NA^3 is an R-based open-source tool, which is experimentally verified to identify calcium activity events and neuronal activity states. Transients are identified by a continuous wavelet transform-based algorithm (wavelet ridge walking), while neural activity states are quantified by calculating the signal variance in a sliding window (Prada et al., 2018).

For the experiments reported in this thesis, NA^3 was modified to allow sequential batch processing of multiple calcium imaging recordings, implementing CSV file format as input file additionally to raw AVI recordings, and reporting analysis results in CSV file format. The modifications made the code independent of the Bio7 environment and additional Java code. The modified R source code is available on GitHub[1].

Assessment of calcium imaging recordings using NA^3 requires several parameters to be determined before analysis (Prada et al., 2018): signal average threshold (SAT), signal-to-noise ratio (SNR), and variance window. As the tool was used with predefined ROIs only, setting the window size was not necessary. Single-cell recordings were analyzed with SAT 1.3 and SNR 2.25. Low-resolution imaging of multiple neuronal somata was conducted at SAT 3.1 and SNR values 1.75 and 2.25.

3.6.3.1 Signal average threshold

Similarly, to the background correction described in section 3.6.2.1, the SAT was determined by measuring the background fluorescence of three background ROIs in ten

[1] https://github.com/j-hugo/ModifiedNA3

different calcium imaging recordings over time and calculating the mean. The SAT was determined for single-cell and multiple soma measurements separately.

3.6.3.2 Signal-to-noise ratio

To determine an SNR value, multiple cells showing high, low, or no activity were selected. These cells and traces from background ROIs (serving as negative controls) were analyzed at multiple SNR values (1.50, 1.75, 2.00, 2.25, 2.50, 3.00, and 3.50). The mean number of detected activity counts per category was plotted against the SNR values to visually select a suitable SNR value. This value was selected where the number of activities detected in background ROIs was minimal, while it was still possible to differentiate neurons labeled with *no activity* from the background with regards to activity counts (i.e., signal-close-to-noise).

3.6.3.3 Variance window

The variance window describes a sliding range of frames for which the variance is calculated. The total variance of a timespan is used to calculate the variance area. The variance window was set to 30 frames (3 s at 10 fps) in this study. The variance area was assessed for 30 s timespans of the whole measurement.

3.6.4 Processing of measurement data

If several ROIs were placed on axons or axonal terminals belonging to the same neuron, the mean number of activities detected in axons or axonal terminals of each neuron was calculated. The number of counted activities was divided by the recording time (calcium activity events per minute).

The variance area was calculated by summing the variance area of the 30 s timespans and division by the recording time. This applies to the baseline and treatment period.

3.6.4.1 ROI area

ROI areas were measured in ImageJ in pixel^2. This value was then converted to µm^2. The conversion factor for calcium imaging recordings using the 10×, NA 0.3 objective, and 2×2 binning settings is 1 pixel = 2.586 µm. For analysis, marked somata were grouped in three size categories (small: ≤ 313 µm^2, medium: ≤ 707 µm^2, and large: >707 µm^2), based on previous publications (Carlin et al., 2018; Suzuki et al., 2010).

3.6.4.2 Variance ratio and time series

For each DRG neuron, the measured variance area per time of the treatment period (150 - 690 s) was standardized by the variance area per time of the baseline period (0 - 120 s) to

calculate the *variance ratio*. To avoid artifacts, 30 s at the start and end of the treatment period were omitted.

$$variance\ ratio = \frac{VA_{treatment}}{VA_{baseline}}$$

For the time series analysis, the variance ratio was calculated for 30 s timeframes (standardized by baseline variance area).

To identify *responsive* neurons, variance ratios 1.5-fold interquartile range (IQR) above the upper quartile (Q_3) of the control data were classified as responsive (i.e., variance ratio > Q_3 + 1.5 × IQR). For *responsive* cells, the number of times the variance ratio was supra-threshold was counted.

3.7 Statistical analysis

R (R Core Team, 2019) and RStudio were used for statistical analysis.

Descriptive statistical analysis was performed to gain an overview of the measured data. This included *n*, mean, standard deviation, standard error of the mean, minimum, median, maximum, and IQR. To determine whether the data were normally distributed, histograms of the data were assessed and the Shapiro-Wilk test for normality was performed. The result of the normality testing determined the used hypothesis test. When at least one data series of the entire dataset contained not-normally distributed data, a non-parametric hypothesis test was applied.

Two independent non-parametric samples were compared using the Mann-Whitney U test. More than two independent non-parametric samples were compared using the Kruskal-Wallis test followed by Dunn's post hoc test with p-adjustment according to Holm.

Two independent normally distributed samples were compared using the Student's t-test. More than two independent normally distributed samples were compared using the one-way ANOVA followed by the Student's t-test with p-adjustment according to Holm.

Pearson's χ^2 test was chosen for pairwise comparison of proportions, followed by p-adjustment according to Holm, if more than two proportions were compared.

Statistical significance of hypothesis testing was assessed with a significance level of $\alpha = 0.05$. In all plots, statistical significance test results are presented as follows: ns: $p > 0.05$, *: $p < 0.05$. **: $p < 0.01$, ***: $p < 0.001$.

4 Results

4.1 Cultured DRG neurons express TRPV1 in growth cones and are pseudo-unipolar.

To perform calcium imaging measurements focused on specific sub-structures of DRG neurons, I investigated the characteristics of the cultured cells by immunocytochemistry.

Here, I stained DRG neurons with antibodies against neurofilament protein L (NFL) and microtubule-associated protein 2 (MAP2). Cultured neurons showed immunoreactivity against NFL in somata and neurites while MAP2 was preferentially found in somata (Figure 4-1). This is in line with the typical morphology of pseudo-unipolar neurons.

Furthermore, anti-TRPV1 immunoreactivity was detected in neurites and growth cones of the cultured neurons (Figure 4-2). Growth cones were identified by visualization of F-actin with the labeling toxin phalloidin.

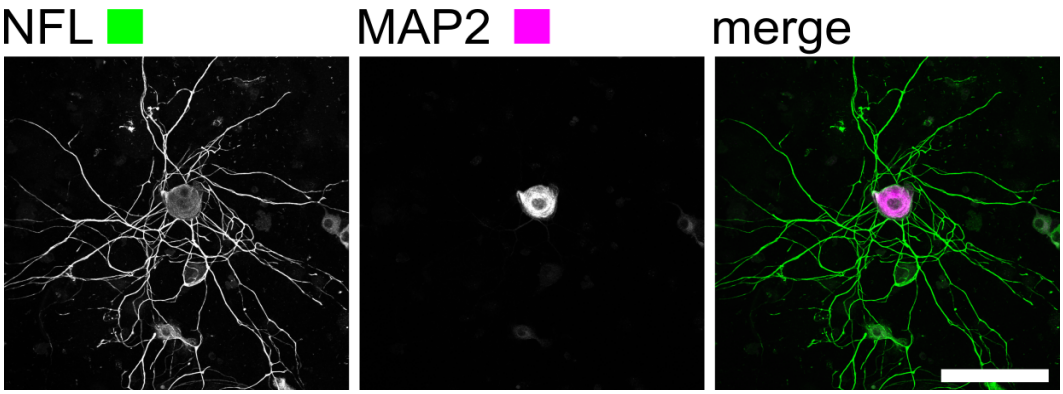

Figure 4-1: **Neurites of DRG neurons show immunoreactivity against NFL, somata against MAP2**. Representative immunofluorescence image of cultured murine WT DRG neurons stained with antibodies against NFL and MAP2. DRG somata and neurites showed consistent immunoreactivity against NFL (■). Notably, somata, but not the neurites, were immunoreactive for MAP2 (■). Scale bar: 100 µm. DRG, dorsal root ganglion; NFL, neurofilament protein L; MAP2, microtubule-associated protein 2; WT, wildtype.

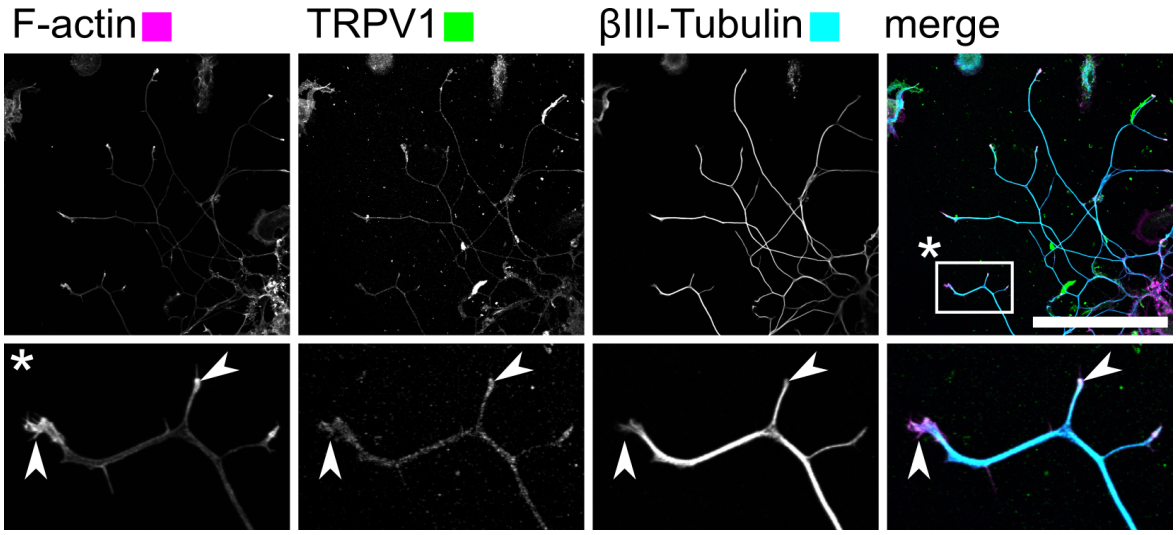

Figure 4-2: **TRPV1 co-localizes with F-actin in growth cones.** Representative immunocytochemistry image of murine WT DRG neurons against TRPV1 and βIII-Tubulin. Phalloidin was used to visualize F-actin. Anti-βIII-Tubulin-immunoreactivity (■) was observed in axonal neurites. F-actin (■) was stained most prominently in growth cones. Immunoreactivity against TRPV1 (■) was detected in neurites and growth cones. Scale bar: 100 µm. * is a magnification of the highlighted area. Arrowheads indicate exemplary growth cones. DRG, dorsal root ganglion; F-actin, filamentous actin; TRPV1, transient receptor potential vanilloid 1; WT, wildtype.

4.2 DRG neurons show spontaneous calcium activity events in somata, axons, and axonal terminals

To investigate spontaneous activity in DRG neurons, I conducted calcium imaging of single DRG neurons with high spatial and temporal resolution. For this, DRG neurons were loaded with the high-affinity calcium indicator OGB-1. Calcium imaging was performed at 10 fps for 5 min without stimulation to monitor spontaneous calcium activity events in DRG neurons. An image of an exemplary calcium imaging recording of a single DRG neuron is depicted in Figure 4-3A. The overlay in Figure 4-3B and Figure 4-3C visualizes soma, axons, and axonal terminals, the neuronal structures analyzed in this study.

The recorded DRG neurons exhibit a variety of spontaneous calcium activity events. Representative examples of spontaneous signals of WT DRG neurons are presented in Figure 4-4. The numbered ROIs on the left correspond to the traces on the right.

Some DRG neurons showed no calcium activity events at all during the recording time (Figure 4-4A). Some DRG neurons displayed synchronous activity events in neighboring neuronal areas (Figure 4-4B). In this recording, ROIs 4 and 5 and ROIs 6 and 7 respectively had similar timings of activity events with similar kinetics. DRG neurons also exhibited asynchronous activity events in neighboring areas (e.g., Figure 4-4C). Here, ROIs 8 and 9 and ROIs 10 and 11 showed differently shaped and timed activity events, even though located adjacent to each other. Also, different kinetics of the spontaneous calcium activity events could be observed. Some regions of DRG neurons exhibited spike-like signals (■ in ROIs 13 and 14), others showed transient-like signals (* in ROIs 6 and 8).

In summary, I observed spontaneous calcium activity events in axonal terminals, axons, and the somata of WT DRG neurons. These spontaneous signals appeared in different shapes.

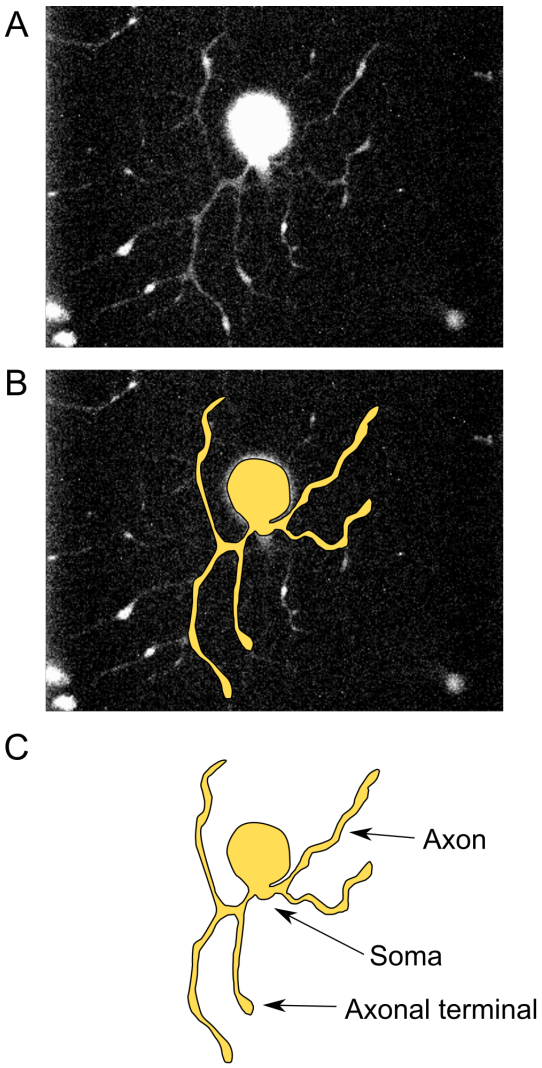

Figure 4-3: **Calcium imaging recordings with high spatial and temporal resolution allow the dedicated analysis of calcium activity events in different cellular structures.** Representative image of a single DRG neuron visualized by calcium imaging using OGB-1. Imaging was conducted at high spatial (40×, NA 0.8 objective) and temporal (10 fps) resolution. (**A**) An exemplary frame of a single DRG neuron calcium imaging recording. (**B**) Overlay visualizing parts of the DRG neuron imaged. (**C**) Overlay only, indicating the different structural compartments of DRG neurons analyzed in this study. DRG, dorsal root ganglion; fps, frames per second; NA, numerical aperture; OGB-1, Oregon Green 488 BAPTA 1-AM.

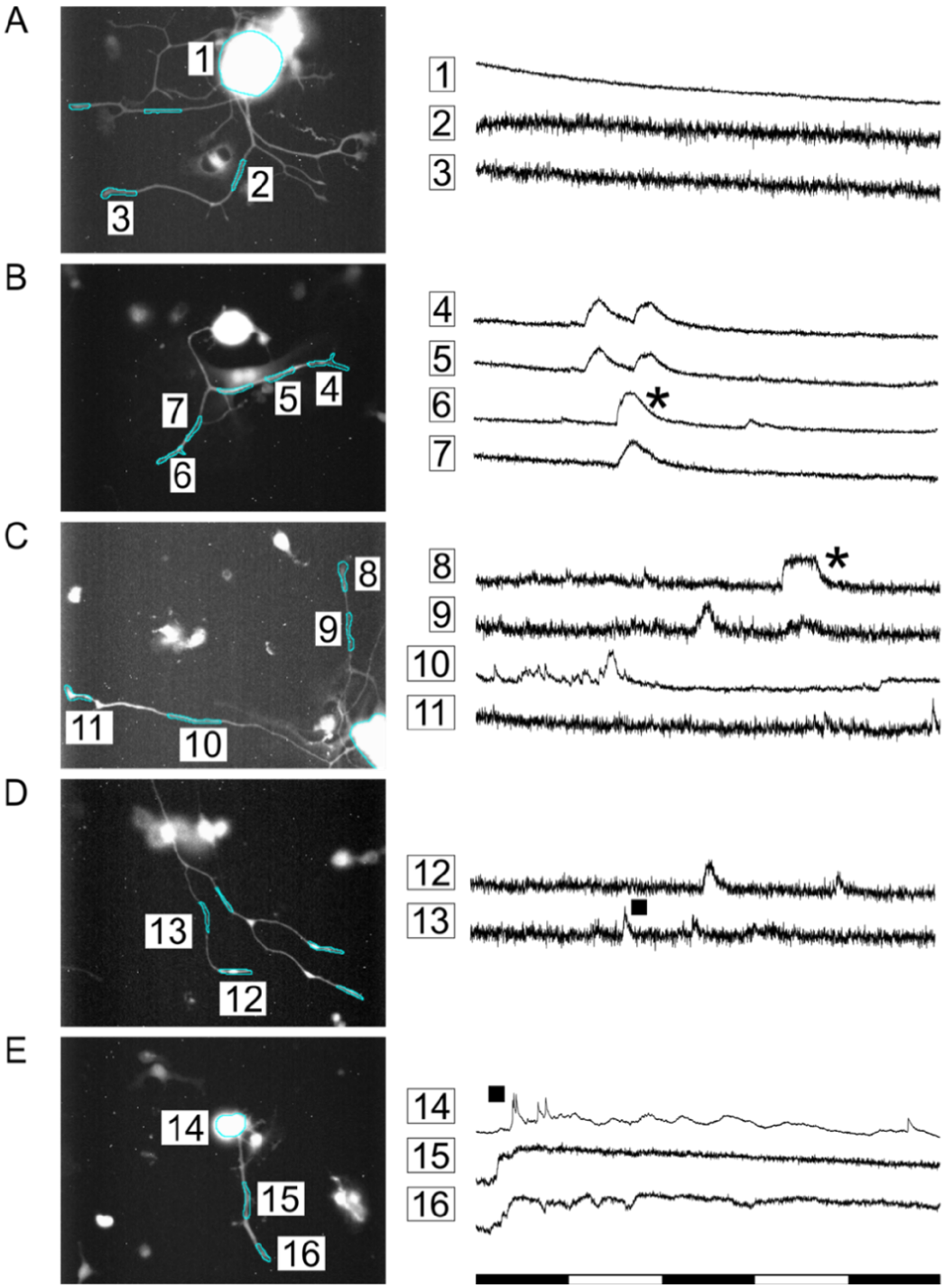

Figure 4-4: **DRG neurons show a variety of spontaneous calcium activity event patterns.** Calcium imaging of WT DRG neurons was conducted for 300 s without stimulation. The numbered ROIs on the left correspond to the shown calcium imaging traces on the right. Cyan labels (■) show ROIs where the calcium imaging traces were recorded. Calcium imaging traces were assessed visually for calcium activity event patterns. ■ show exemplary spike-like and * show exemplary transient-like calcium activities. Each section of the scale bar represents 60 s. DRG, dorsal root ganglion; ROI, region of interest; WT, wildtype.

4.3 Automated calcium trace analysis correlates with manual analysis but shows higher sensitivity to calcium events

Heuristic analysis of calcium imaging traces is typically used to quantify the number of calcium activity events in calcium imaging data. However, heuristic analysis of signal traces might be subjective, driven by unconscious annotation preferences or expectations of the experimenter. Therefore, I aimed to use the open-source tool Neural Activity^3 (Prada et al., 2018) as an alternative to manual counting. This tool uses a hard-coded algorithm based on CWT to detect calcium activity events from calcium imaging traces. NA^3 is the only calcium activity quantification tool biologically verified to detect non-spike-like signal-close-to-noise activity events (Prada et al., 2018).

Here, NA^3 was used to analyze calcium imaging recordings of 129 DRG neurons. Automated calcium activity detection with NA^3 was then compared with manual, heuristic calcium activity detection (Figure 4-5). An exemplary calcium imaging trace analysis, recorded from an axon of a DRG neuron, is shown in Figure 4-5A. Here, red vertical lines indicate the calcium activity events detected by NA^3 (settings: SAT 1.3, SNR 2.25). In this measurement, NA^3 detected 22 calcium events.

The distributions of calcium activity event counts in the manual and automated analysis were stratified by neuronal structure (axonal terminals, axons, and somata; in columns, Figure 4-5B). The analysis reveals that manual activity detection could only count very few signals in some of the neurons, while, in many cases, no activity events were heuristically detected. Interestingly, algorithm-based detection of activity events with NA^3 identified higher calcium activity event counts. This was true for all analyzed neuronal structures. This is also reflected in the median and IQR of the number of calcium activity events detected per minute of automated (median: 0.667; IQR: 0.300, 1.600) compared to manual detection (median: 0.000; IQR: 0.000, 0.400).

The scatterplot (Figure 4-5C) and Bland-Altman plot (Figure 4-5D) visualize the relationship between automated and manual activity detection for each of the analyzed calcium imaging traces. The scatterplot in Figure 4-5C plots automated (y-axis) against manual detection (x-axis). The Bland-Altman plot (Figure 4-5D) tests the agreement of two methods (Bland and Altman, 1999). This is done by plotting the difference between the two methods (automated – manual; y-axis) against the mean of the methods (x-axis) for each calcium imaging trace. In both visualizations, most data points lie above the line of equality (Figure 4-5C, D; grey dashed line in both plots), indicating a systematically higher number of activity

events detected by the automated method compared to manual counting. The scatterplot describes a positive correlation between automated and manual counts (Figure 4-5C, Spearman's $\rho = 0.68$). The Bland-Altman plot (Figure 4-5D) shows a positive association between the difference and mean of the methods compared. As the mean count of the two methods increases, the discrepancy between them increases as well, i.e., in more active calcium imaging traces, automated calcium activity event detection detects more events than manual detection (Spearman's $\rho = 0.91$).

In summary, manual and automated calcium activity event detection correlate positively. Automated detection of calcium events detected systematically more calcium activity events than manual analysis. Furthermore, the discrepancy in counts between both methods increased in calcium imaging traces with higher activity rates.

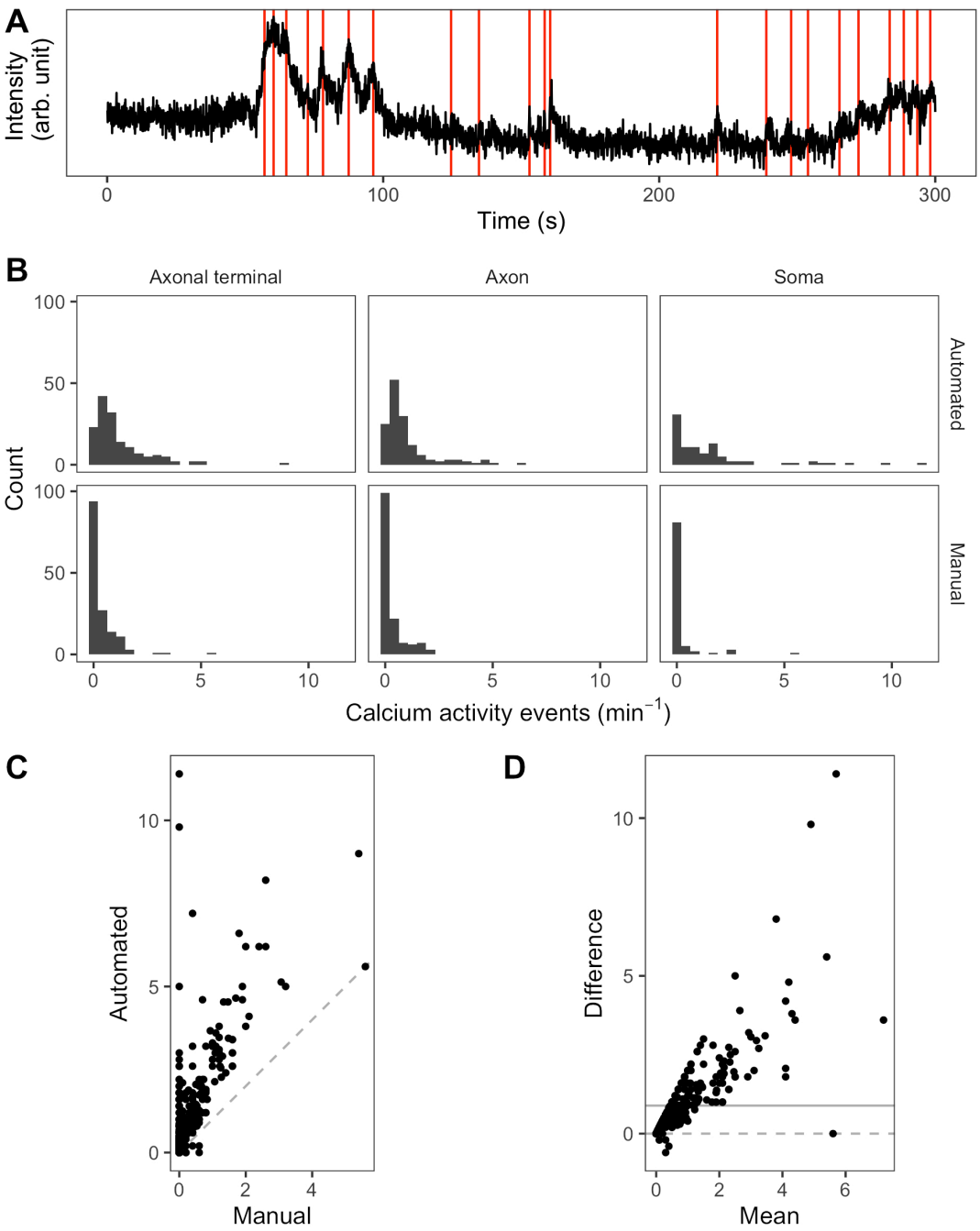

Figure 4-5: **Comparison of manual and automated calcium activity event counting methods.** Calcium imaging recordings were analyzed manually or automated using NA^3 (SAT: 1.3, SNR: 2.25). (**A**) An exemplary calcium imaging trace recorded from a WT DRG neuron axon. Activities detected by NA^3 are indicated by red vertical lines. (**B**) Histograms show the distribution of the detected calcium activity event counts per minute stratified by detection method by row (automated and manual) and DRG neuron structure by column (axonal terminal, axon, and soma). (**C** & **D**) Plots show the relationship between automated and manual calcium activity event detection. In both plots, one data point resembles an identical calcium imaging trace assessed with both methods. (**C**) Scatterplot of automated (y-axis) against manual detection (x-axis). The grey dashed line shows the line of equality (y = x). (**D**) Bland-Altman plot (Bland and Altman, 1999): the y-axis shows the difference between the two methods (automated - manual), the x-axis shows the mean count of both methods combined. As the data is not normally distributed, no limits of agreement are shown. The grey dashed line shows the line of equality (difference = 0), the grey solid line shows the mean of differences. n(all ROIs) = 389, n(Axonal terminals) = 152, n(Axons) = 144, n(Soma) = 93. Arb. unit, arbitrary units; DRG, dorsal root ganglion; NA^3, Neural Activity Cubic; ROI, region of interest; SAT, signal average threshold; SNR, signal-to-noise ratio; WT, wildtype.

4.4 $Na_V1.9$ triggers spontaneous calcium activity in axons and somata of cultured DRG neurons

It has been shown that $Na_V1.9$, a voltage-gated sodium channel and excitability mediator, can trigger spontaneous calcium activity in neurons (Ostman et al., 2008). To gain insight into the local expression of $Na_V1.9$, I performed immunocytochemistry on WT and $Na_V1.9$ KO murine DRG neurons.

WT DRG neurons showed immunoreactivity against $Na_V1.9$ in axonal terminals, axons, and somata, as previously described (Martin et al., 2018). $Na_V1.9$ protein was often co-localized with immunoreactivity against TRPV1, a pain-related ion channel (Figure 4-6A). In immunocytochemistry of $Na_V1.9$ KO DRG neurons, no immunoreactivity against $Na_V1.9$ was detected (Figure 4-6B), while exhibiting immunoreactivity against TRPV1. This experiment revealed co-expression of $Na_V1.9$ and TRPV1 in cultured murine sensory neurons, indicating that the corresponding cells belong to the nociceptor-like cell lineage.

Next, I conducted calcium imaging of 57 WT and 36 $Na_V1.9$ KO DRG neurons. To record spontaneous calcium activity, neurons were imaged for 5 minutes at 10 fps without stimulation. DRG neurons were prepared from three mice for both genotypes. ROIs were placed on axonal terminals, axons, and somata to allow a differentiated analysis of calcium activities in all three neuronal structures. Automated analysis of the calcium imaging traces was performed using NA^3 (settings: SAT 1.3, SNR 2.25).

First, I compared the activity counts from automated calcium activity event detection between neuronal structures in WT DRG neurons (data included in Figure 4-7). Here, no statistically significant difference between neuronal structures could be observed (statistical hypothesis testing by Kruskal-Wallis test, $p = 0.56$, hypothesis testing not visualized). Transients recorded from somata had a slightly higher median activity count per minute and larger IQR (median: 1.000; IQR: 0.200, 1.800) compared to axons (median: 0.600; IQR: 0.300, 1.067) and axonal terminals (median: 0.747; IQR: 0.330, 1.608).

Second, I compared the activity counts between WT and $Na_V1.9$ KO DRG neurons (Figure 4-7). The median count of calcium activity events per minute was higher in WT compared to KO neurons in all neuronal structures. WT DRG neurons showed a significantly higher count of spontaneous activity events in axons (WT: 0.800 min^{-1}, KO: 0.400 min^{-1}, $p = 0.002$) and somata (WT: 1.400 min^{-1}, KO: 0.400 min^{-1}, $p = 0.042$). WT neurons also showed a higher count of spontaneous activity events in axonal terminals (WT: 0.867 min^{-1}, KO: 0.600 min^{-1}, p =

0.085), however, this difference was not statistically significant. Statistical hypothesis testing was performed by Mann-Whitney U test.

In summary, immunocytochemistry revealed $Na_V1.9$- and TRPV1-positive WT sensory neurons in the cell culture. Automated activity detection of single-cell calcium imaging of these cells showed a significantly lower calcium activity event count in axons and somata of $Na_V1.9$ KO DRG neurons. The experiment shows that spontaneous calcium events, measured by calcium imaging and analyzed by NA^3 are of biological origin and are triggered by the excitability mediator $Na_V1.9$. This indicates that imaging signal-close-to-noise calcium activity in somata can be a representative measure for the activity status of cultured nociceptors.

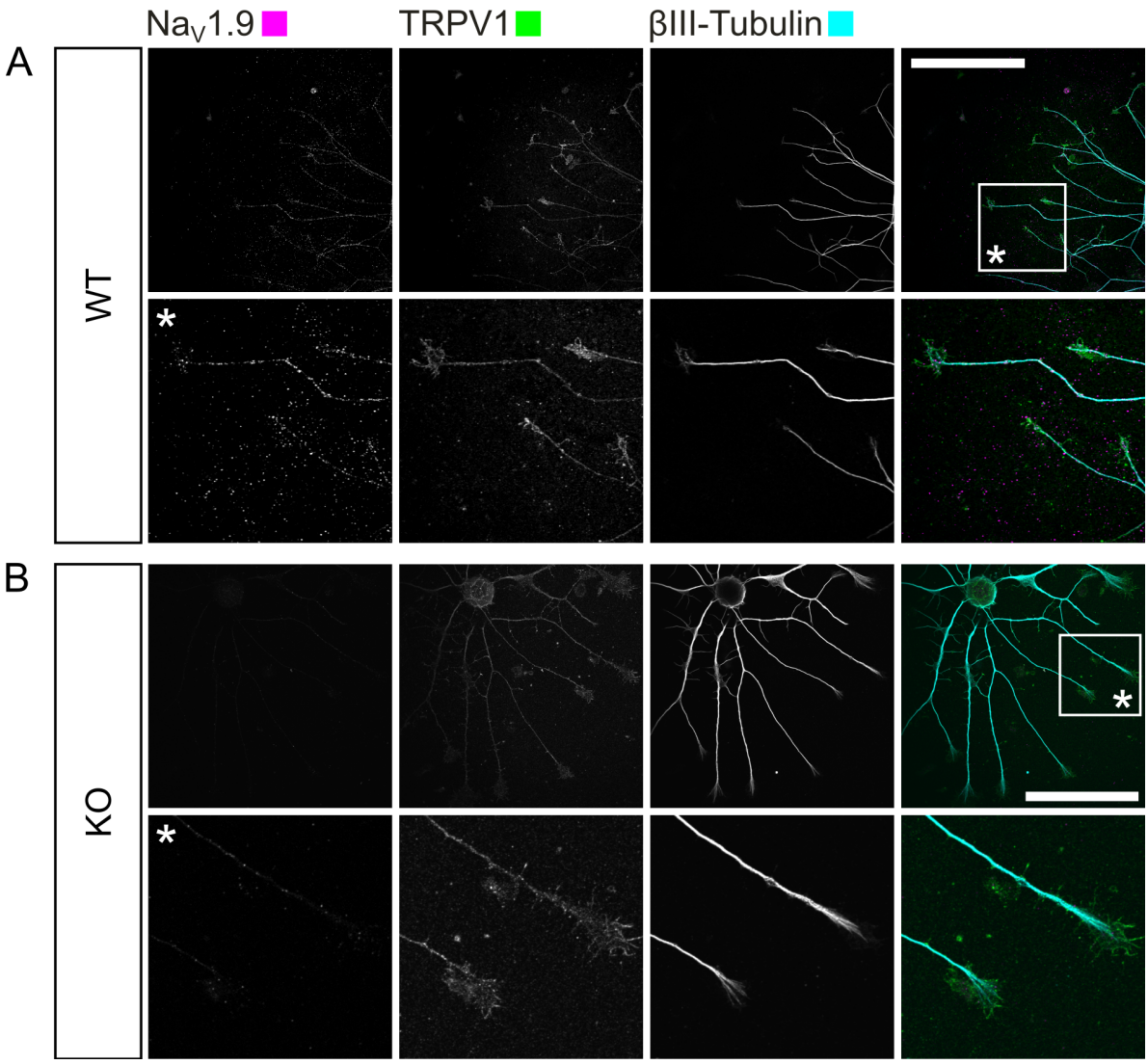

Figure 4-6: **Na$_V$1.9 and TRPV1 co-localize in axons and growth cones in WT DRG neurons.** Representative image of immunofluorescence staining of murine WT and Na$_V$1.9 KO DRG neurons against Na$_V$1.9, TRPV1, and βIII-Tubulin. (**A**) WT DRG neurons showed immunoreactivity against Na$_V$1.9 (■) and TRPV1 (■) in axons and growth cones while (**B**) Na$_V$1.9 KO DRG neurons showed no immunoreactivity against Na$_V$1.9 in somata, axons and growth cones. Neurites were identified by immunoreactivity against βIII-Tubulin (■). ∗ are magnifications of the highlighted areas above. Scale bars: 100 µm. DRG, dorsal root ganglion; KO, knockout; Na$_V$1.9, voltage-gated sodium channel 1.9; TRPV1, transient receptor potential vanilloid 1; WT, wildtype.

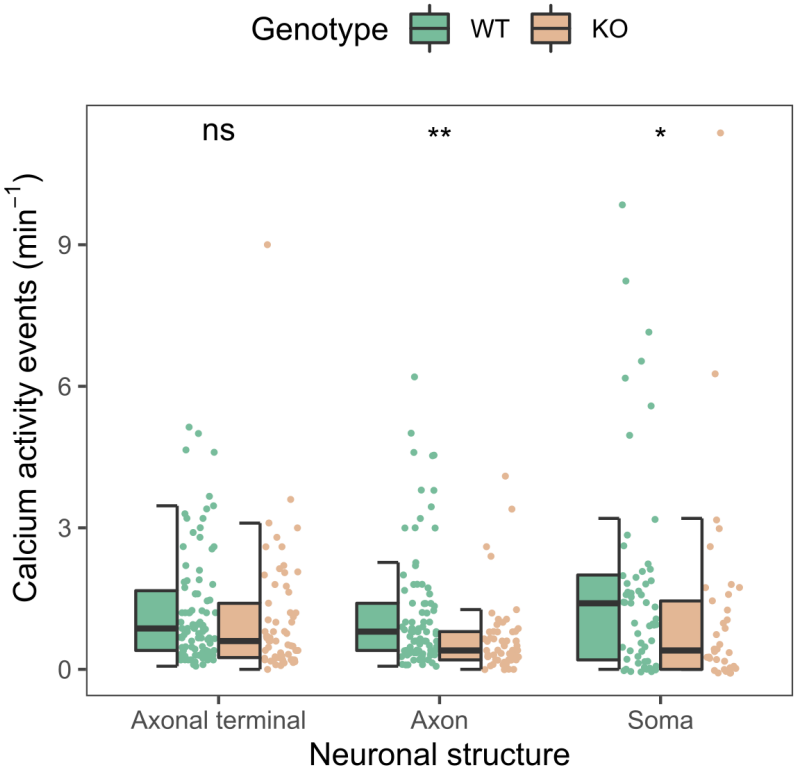

Figure 4-7: **WT DRG neurons show a significantly higher calcium activity event count per time in axons and somata compared to Nav1.9 KO DRG neurons.** Calcium imaging recordings of WT (■) and Nav1.9 KO (■) DRG neurons were analyzed for spontaneous calcium activity events by NA^3 (SAT: 1.3, SNR: 2.25). Boxplots show the number of spontaneous calcium activity events detected per minute. The bold line indicates the median, the box indicates the IQR, and whiskers show the lowest/highest value within the 1.5-fold IQR. Original data points are shown as dots. n(Axonal terminal, WT) = 91, n(Axonal terminal, KO) = 61, n(Axon, WT) = 87, n(Axon, KO) = 57, n(Soma, WT) = 57, n(Soma, KO) = 36. Hypothesis testing by pairwise Mann-Whitney U test. ns: $p > 0.05$, *: $p < 0.05$, **: $p < 0.01$. DRG, dorsal root ganglion; IQR, interquartile range; KO, knockout; NA^3, Neural Activity Cubic; Nav1.9, voltage-gated sodium channel 1.9; SAT, signal average threshold; SNR, signal-to-noise ratio; WT, wildtype.

4.5 The number of spontaneous calcium activity events per time in WT DRG neurons is not increased by pre-incubation with OxPAPC

My experiments with $Na_V1.9$ KO neurons indicate that signal-close-to-noise calcium activity can be used to test the influence of putative inflammatory mediators on neuronal excitability. This opens the possibility to investigate whether oxidized phospholipids such as OxPAPC are excitability mediators or not. To answer this question DRG neurons were exposed to OxPAPC before conducting calcium imaging.

First, I incubated WT DRG neurons with 10 µM OxPAPC or DMEM (control) for 1 hour. Then, calcium imaging recordings of spontaneous activity at the single-cell level were performed for 5 min. ROIs were placed on the different neuronal structures (axonal terminals, axons, and somata). Automated analysis of the resulting calcium imaging traces was performed using NA^3 (settings: SAT 1.3, SNR 2.25).

The medians and distribution of calcium activity event counts per minute of both incubation groups were similar in all analyzed structures (Figure 4-8). Statistical hypothesis testing by Mann-Whitney U test showed no significant difference in calcium activity event count distributions between OxPAPC and DMEM incubation in all neuronal structures.

In conclusion, incubation of DRG neurons with OxPAPC before calcium imaging did not influence the number of spontaneously triggered calcium activity events. This indicates that OxPAPC, which can acutely activate cultured sensory neurons, does not induce persistent calcium activity.

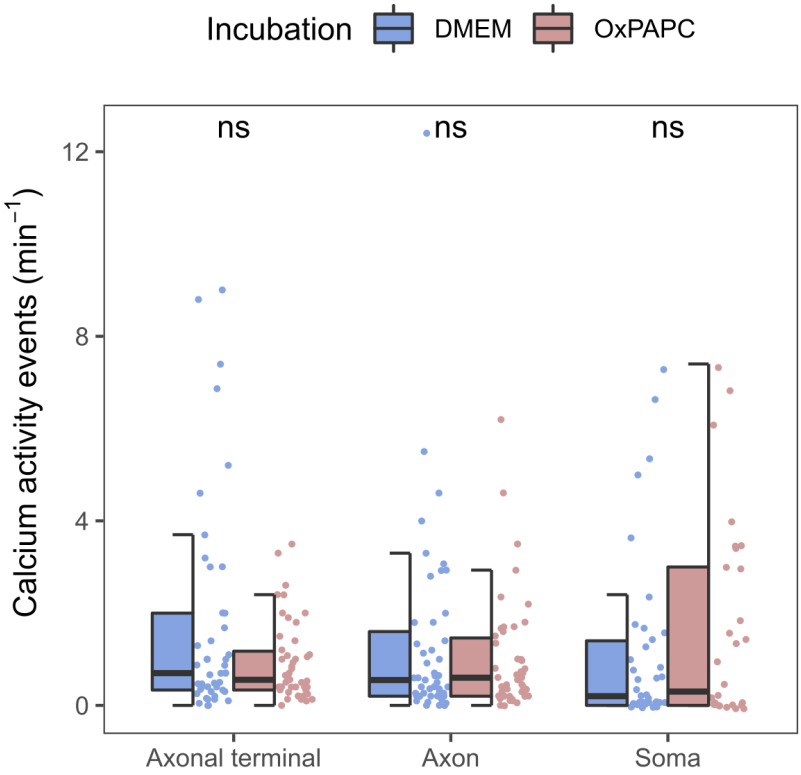

Figure 4-8: **OxPAPC incubation does not affect the excitability of DRG neurons.** Calcium imaging recordings of WT DRG neurons pre-incubated with DMEM (control, ■) or OxPAPC (10 µM, ■) for 1 h were analyzed for spontaneous calcium activity events by NA^3 (SAT: 1.3, SNR: 2.25). Boxplots show the number of spontaneous calcium activity events detected per minute. The bold line indicates the median, the box indicates the IQR, and whiskers show the lowest/highest value within the 1.5-fold IQR. n(Axonal terminal, DMEM) = 45, n(Axonal terminal, OxPAPC) = 46, n(Axon, DMEM) = 47, n(Axon, OxPAPC) = 46, n(Soma, DMEM) = 37, n(Soma, OxPAPC) = 30. Original data points are shown as dots. Hypothesis testing by pairwise Mann-Whitney U test. ns: $p > 0.05$., DMEM, Dulbecco's Modified Eagle Medium; DRG, dorsal root ganglion; IQR, interquartile range; NA^3, Neural Activity Cubic; OxPAPC, oxidized PAPC; SAT, signal average threshold; SNR, signal-to-noise ratio; WT, wildtype.

4.6 Calcium imaging traces from DRG neuronal somata show different activity patterns in response to inflammatory mediators

Next, I investigated whether DRG neurons incubated with OxPAPC show altered responsiveness to inflammatory mediators. To be able to analyze a higher number of DRG neurons, I restricted the analysis to neuronal somata and conducted calcium imaging at lower spatial resolution (10×, NA 0.3 objective).

ROIs were placed so that calcium imaging traces of individual DRG neuron somata could be analyzed (Figure 4-9A, B, C). Using the pixel area of the ROIs, I calculated the area of individual somata. The soma size of cultured DRG neurons can be used for categorizing sensory neuron subtypes. Figure 4-9D shows a density plot describing the distribution of the soma area (median ROI area = 461.50 μm^2, blue dashed line). Based on the classification ranges mentioned in section 3.6.4.1, ROIs were classified as small-, medium-, and large-sized DRG somata. Most cells were classified as medium-sized, while the proportion of cells classified as small and large soma DRG neurons were similar (Figure 4-9E).

To mimic inflammatory conditions, I used two mixtures of inflammatory mediators with different concentrations of bradykinin, histamine, and PGE_2 (Maingret et al., 2008). The low concentration IM consisted of 5 nM, 100 nM, and 50 nM and the high concentration IM of 50 nM, 1 µM, and 500 nM of bradykinin, histamine, and PGE_2, respectively. During calcium imaging, the DRG neurons were exposed to the sensitizing agents and finally to KCl, as a reactivity test for neurons. The detailed experiment protocol is presented in Table 3-1.

Qualitative analysis of the traces revealed that DRG neurons exhibit three distinct activity patterns recorded from somata when treated with IM: no activity (Figure 4-10A), a single activity peak (Figure 4-10B), or sustained activity throughout the treatment period (Figure 4-10C). The classification of the DRG neurons into these three categories is based on the number of calcium activity events observed in the treatment period.

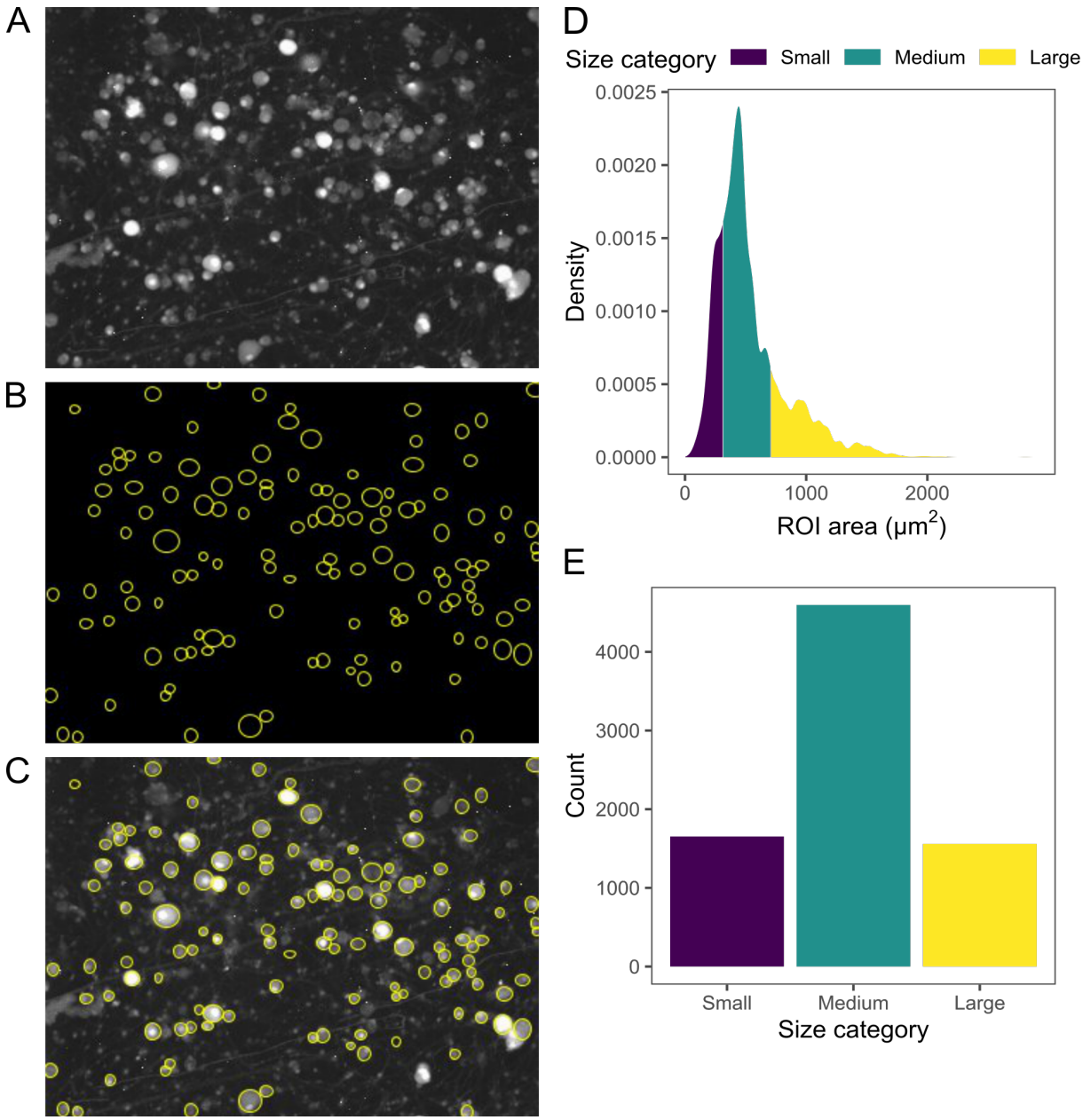

Figure 4-9 **Analysis of the area of somata of DRG neurons in calcium imaging.** Calcium imaging with low spatial resolution (10×, NA 0.3 objective, image: 1 pixel = 2.586 µm) was carried out with OGB-1 loaded DRG neurons (**A**). ROIs were placed on soma: (**B**) ROIs only, (**C**) overlay. Using ImageJ, the ROI area was measured and converted to µm^2. (**D**) Density plot showing the distribution of ROI area of all analyzed ROIs. (**E**) Bar plot indicating the distribution of discrete size categories based on the classification ranges reported in section 3.6.4.1. n = 8069. DRG, dorsal root ganglion; NA, numerical aperture; OGB-1, Oregon Green BAPTA 1-AM; ROI, region of interest.

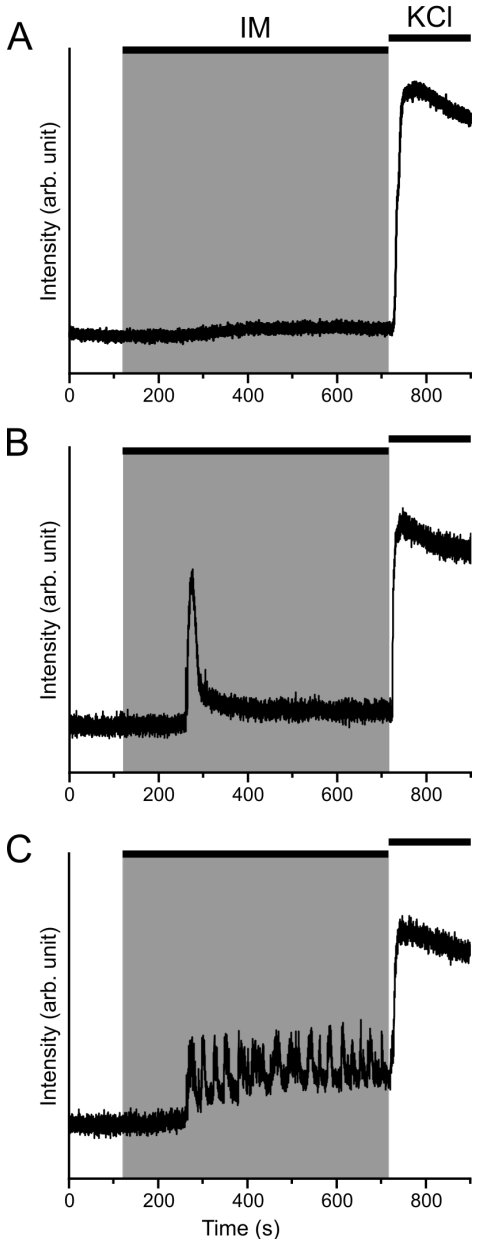

Figure 4-10: **WT DRG neurons respond to inflammatory mediators with distinct calcium signal patterns.** Calcium imaging with low spatial resolution (10×, NA 0.3 objective) was carried out with OGB-1 loaded DRG neurons. The neurons were exposed to two different mixtures of inflammatory mediators (IM, concentrations given in Table 2-9) or calcium imaging buffer (CIB, control). KCl was used to depolarize DRG neurons. Detailed information about the experimental protocol is given in Table 3-1. The observed responses to IM treatment could be grouped in three activity patterns: (**A**) no activity, (**B**) single peak or (**C**) sustained activity. The intensity of emitted fluorescence in arbitrary units is plotted against the time in seconds. Horizontal bars in plots indicate the periods in which DRG neurons were exposed to IM or KCl. The grey area emphasizes the period of IM exposition. Arb. unit, arbitrary units; CIB, calcium imaging buffer; DRG, dorsal root ganglion; IM, inflammatory mediator mixture; NA, numerical aperture; OGB-1, Oregon Green BAPTA 1-AM; WT, wildtype.

4.7 Analysis of calcium activity event counts recorded from DRG somata shows no difference between OxPAPC incubation and controls

To quantify the qualitative observations regarding DRG soma activity patterns, I used NA[3] to automate the count of calcium activity events of DRG neurons when treated with IM (low and high concentration) and FSK (10 µM). FSK exposition is used to investigate the involvement of the PKA pathway in neuronal responses.

Figure 4-11A and Figure 4-11B compare two SNR settings of different stringencies (1.75 and 2.25). At SNR 2.25 most analyzed cells showed no or a very low calcium activity (Figure 4-11A), while the number of signals detected with SNR set to 1.75 is shifted to higher values. This suggests that inflammatory mediators drive low stringency calcium activity events. Events detected with a low SNR were defined as signal-close-to-noise calcium activity (Prada et al., 2018). In the Bland-Altman plot (Figure 4-11B) almost all data points lie above the line of equality. Systematically more calcium activity events were detected when assessed with SNR 1.75. To avoid *zero inflation*, the SNR was set to 1.75 for further analyses.

The boxplots in Figure 4-12 show the calcium activity event frequencies detected by NA[3] of small- and medium-sized DRG neuronal somata under different experimentation protocols. Generally, all boxplots have very narrow IQR and medians just above zero calcium activity events per min, visualizing that most analyzed cells showed no or low signal frequencies (summarized in Table 4-1).

Figure 4-12A compares the treatment settings within the incubation methods (DMEM and OxPAPC) in small- and medium-sized DRG neurons. In both incubation settings, the highest count of cells with increased calcium activity event frequencies was observed in high concentration IM followed by low concentration IM, and FSK. The lowest number of calcium events was detected under control conditions (CIB). Most comparisons of treatments showed statistically significant differences, except for FSK vs. IM (low concentration) and IM (low concentration) vs. IM (high concentration) after OxPAPC incubation.

Figure 4-12B depicts the same data as Figure 4-12A but focuses on the comparison of incubation settings within treatment groups: neurons exposed to CIB or IM (low concentration) showed a significantly higher calcium activity event count per minute when incubated with OxPAPC. There was no difference in cells exposed to FSK or IM (high concentration).

In summary, calcium activity event counts detected after OxPAPC incubation are not conclusively different from controls.

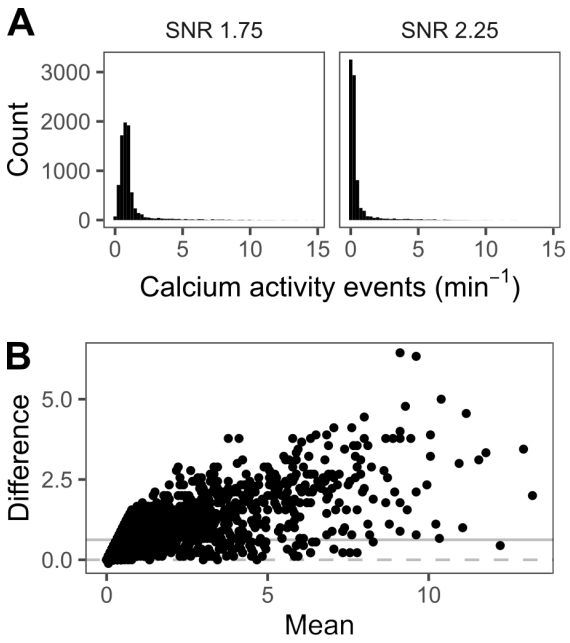

Figure 4-11: **Comparison of SNR settings in automated activity detection of DRG somata by NA^3.** DRG neurons were incubated with OxPAPC (10 µM) for 30 min. Then, calcium imaging was performed during treatment of the DRG neurons to calcium imaging buffer (CIB), forskolin (FSK, 10 µM), or inflammatory mediators (IM, low and high concentration, composition in Table 2-9). Calcium activity events in the treatment period were detected using NA^3 (SAT: 3.1, SNR: 1.75 and 2.25). (**A**) Histograms show the distribution of the detected calcium activity events per minute with SNR settings 1.75 or 2.25. (**B**) Bland-Altman plot (Bland and Altman, 1999) comparing SNR 1.75 and 2.25: the y-axis shows the difference in count between the two SNR settings, the x-axis shows the mean count of both settings combined. The grey dashed line shows the line of equality (difference = 0), the grey solid line shows the mean of differences. n = 8069. CIB, calcium imaging buffer; DMEM, Dulbecco's Modified Eagle Medium; DRG, dorsal root ganglion; FSK, forskolin; IM, inflammatory mediator mixture; NA^3, Neural Activity Cubic; OxPAPC, oxidized PAPC; SAT, signal average threshold; SNR, signal-to-noise ratio.

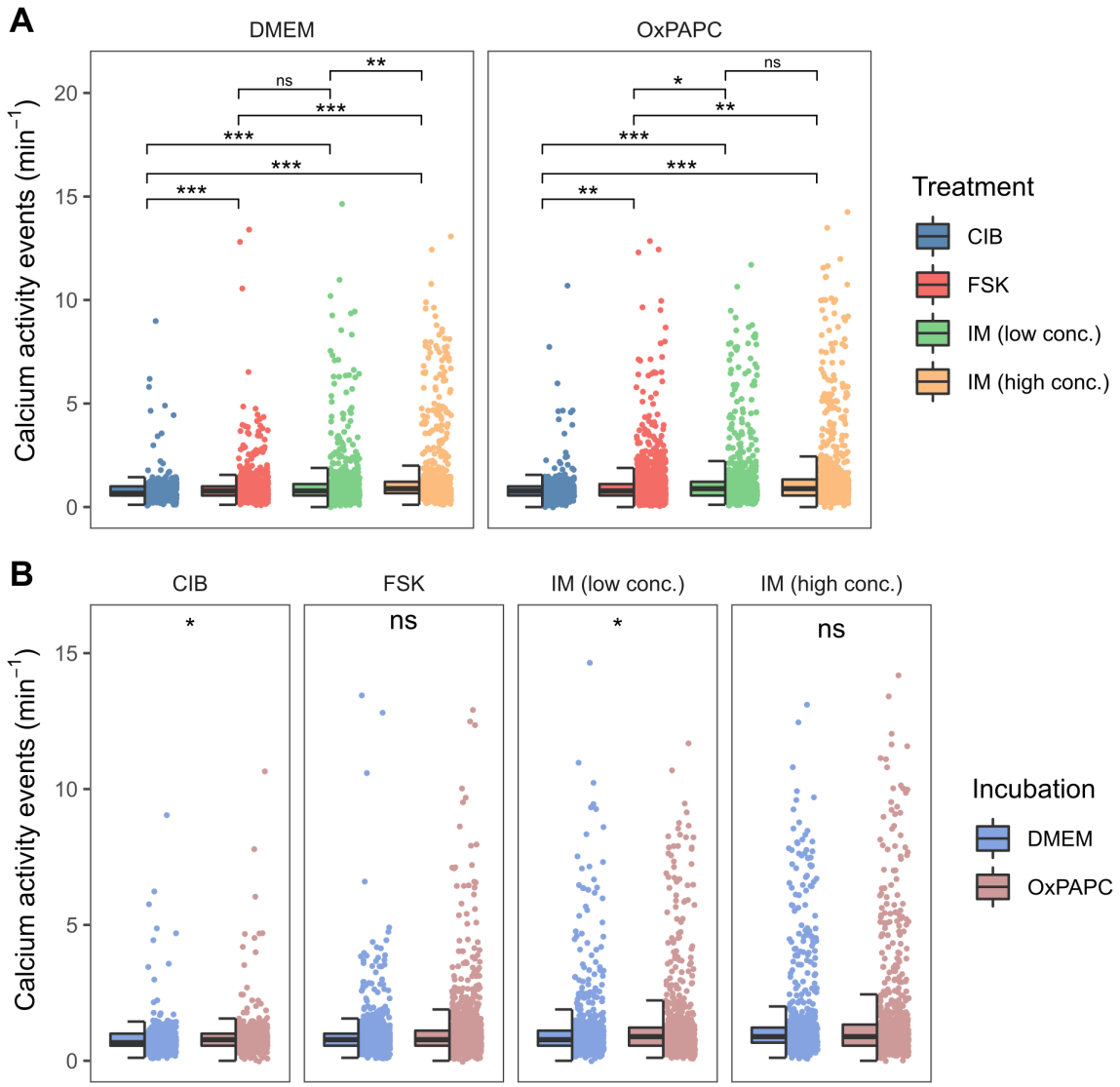

Figure 4-12: **Comparison of the activity count of DRG neurons after OxPAPC or DMEM incubation in response to mediator treatment.** DRG neurons were incubated in DMEM (control, ■) or DMEM medium with OxPAPC (10 µM, ■) for 30 min. Then, calcium imaging was performed during treatment of the DRG neurons with calcium imaging buffer (CIB, ■), forskolin (FSK, 10 µM, ■) or inflammatory mediators (IM, low ■ and high ■ concentration, composition in Table 2-9). Calcium activity event detection in the treatment period was performed using NA^3 (SAT: 3.1, SNR: 1.75). (**A, B**) Comparison of calcium activity event frequencies under indicated conditions. Data in both plots is the same, but plots visualize different comparisons. (**A**) Comparison of the influence of mediator treatment (CIB, FSK, or IM) on the calcium activity event count per minute of small- and medium-sized DRG neurons stratified by incubation (DMEM control or OxPAPC). (**B**) Comparison of the influence of incubation (DMEM control or OxPAPC) on calcium activity event count per minute of small- and medium-sized DRG neurons for each mediator treatment. n(DMEM, CIB) = 460, n(DMEM, FSK) = 938, n(DMEM, IM (low)) = 704, n(DMEM, IM (high)) = 771, n(OxPAPC, CIB) = 512, n(OxPAPC, FSK) = 1432, n(OxPAPC, IM (low)) = 747, n(OxPAPC, IM (high)) = 888. Boxplots in A and B show the count of calcium activity events per minute. The bold line indicates the median, the box indicates the IQR, and whiskers show the lowest/highest value within the 1.5-fold IQR. Original data points are shown to the right of the boxplot. Statistical hypothesis testing: (A) Kruskal-Wallis test and Dunn-Holm post hoc test; (B) Mann-Whitney U test. ns: $p > 0.05$, *: $p < 0.05$, **: $p < 0.01$, ***: $p < 0.001$. CIB, calcium imaging buffer; conc., concentration; DMEM, Dulbecco's Modified Eagle Medium; DRG, dorsal root ganglion; FSK, forskolin; IM, inflammatory mediator mixture; IQR, interquartile range; NA^3, Neural Activity Cubic; OxPAPC, oxidized PAPC; SAT, signal average threshold; SNR, signal-to-noise ratio.

Table 4-1: **Comparison of descriptive statistics on activity counts after DMEM or OxPAPC incubation in response to inflammatory mediator treatment.**

Incubation	Treatment	*n*	Median (min^{-1})	IQR (min^{-1})
DMEM	CIB	460	0.667	0.444
	FSK	938	0.778	0.444
	IM (low conc.)	704	0.778	0.556
	IM (high conc.)	771	0.889	0.556
OxPAPC	CIB	512	0.778	0.444
	FSK	1432	0.778	0.556
	IM (low conc.)	747	0.889	0.667
	IM (high conc.)	888	0.889	0.778

DRG neurons were incubated with OxPAPC (10 µM) or DMEM (control) for 30 min. Then, calcium imaging was performed during treatment of the DRG neurons with calcium imaging buffer (CIB), forskolin (FSK, 10 µM), or inflammatory mediators (IM, low and high concentration, composition in Table 2-9). Calcium activity event detection in the treatment period was automated using NA^3 (SAT: 3.1, SNR: 1.75). The table shows the number of analyzed neurons, median, and IQR of the activity counts per combination of mediator treatment and incubation. The data is visualized in Figure 4-12B and C. CIB, calcium imaging buffer; conc., concentration; DMEM, Dulbecco's Modified Eagle Medium; DRG, dorsal root ganglion; FSK, forskolin; IM, inflammatory mediator mixture; IQR, interquartile range; NA^3, Neural Activity Cubic; OxPAPC, oxidized PAPC; SAT, signal average threshold; SNR, signal-to-noise ratio.

4.8 The variance area of calcium imaging traces increases when DRG neurons are exposed to inflammatory mediators

Another biologically relevant parameter in calcium imaging data is the signal variance (Prada et al., 2018). The analysis tool NA^3 measures this parameter as variance area in a sliding window (Prada et al., 2018). To normalize variance areas measured from individual DRG neurons and allow comparison, I calculated the ratio of the variance area between baseline and treatment period (variance ratio).

Table 4-2 shows exemplary variance ratio values for the distinct calcium signal patterns presented in Figure 4-10. The variance ratio of the *sustained activity* pattern is higher than the variance ratio calculated from *no activity* or *single peak* activity patterns.

Figure 4-13 compares the variance ratio of DRG neurons incubated with DMEM or OxPAPC within the different treatments (CIB, FSK, IM low and high concentration). Most DRG neurons showed a variance ratio around 1.0, indicated by the narrow boxplots. Compared with CIB treatment, FSK treatment resulted in a higher spread of variance ratios above and below 1.0. Low and high concentration IM showed distributions of variance ratios shifted to values larger than 1.0. This effect was greater for high concentration IM compared to low concentration. Hypothesis testing did not reveal any significant differences when comparing cells incubated with DMEM or OxPAPC before calcium imaging in any of the four treatments. Table 4-3 summarizes the number of analyzed neurons, median, and IQR of the variance ratio measured in each experimental setup.

Next, I split the measurement period into 30 s timeframes and calculated the variance ratio relative to the baseline period for each timeframe resulting in 24 variance ratio data points per neuron (outlined in section 3.6.4.2). Figure 4-14A shows the variance ratio for all individual DRG neurons as time series for all different combinations of treatment and incubation settings. Treatment with CIB resulted in a stable low variance ratio throughout the experiment. Multiple neurons treated with FSK or IM (both concentrations) showed an increased variance ratio starting from time frame five. This behavior was similarly present in cells incubated with DMEM or OxPAPC. The median (black line in all graphs) was not affected by the raised relative variance area, indicating that most neurons did not show an increase in relative variance area.

To filter for neurons, which were responsive towards mediator treatment, I analyzed the variance ratio time series of each neuron. Figure 4-14B visualizes the variance ratio over time

for four DRG neurons with different levels of activity. If the variance area calculated for a timeframe was above the defined threshold, this was noted as *responsive* (indicated by ×). The threshold was set at the 1.5-fold IQR above the third quartile of the variance ratio of the control condition. For each neuron, I calculated the proportion of timeframes that showed a variance ratio above the threshold. This resulted in a metric describing the activity level of each individual neuron. E.g., in Figure 4-14B, the neuron represented by the solid line showed a variance ratio above the threshold in 15 out of 19 analyzed timeframes, resulting in a proportion of 0.79 timeframes above the threshold.

Figure 4-15 compares the proportion of *responsive* neurons (Figure 4-15A and C) and the proportion of *supra-threshold* timeframes (Figure 4-15B and D) between the different incubation-treatment conditions.

Figure 4-15A,B compare both metrics between treatment settings for neurons incubated with DMEM (control) only. Figure 4-15A shows that the proportion of responsive cells was increased when exposed to high concentration IM (22.8 %) compared to treatment with CIB (12.4 %), FSK (13.4 %), or low concentration IM (14.9 %). Treatment with CIB, FSK, or low concentration IM showed similar proportions of responsive neurons. Figure 4-15B shows that the median proportion of timeframes with a variance ratio above the threshold is similar between CIB and FSK treatment and between the two concentrations of IM treatment. The proportion of *supra-threshold* timeframes is significantly increased in the IM treatment experiments compared to CIB or FSK treatment.

Figure 4-15C,D compare DMEM and OxPAPC incubation before mediator treatment. Figure 4-15C shows that the proportions of responsive cells were similar between incubation settings for all four conditions. Figure 4-15D shows that in all treatment settings the median proportion of *supra-threshold* timeframes was similar between incubation settings. Comparing both metrics between incubation settings revealed no statistically significant difference.

In conclusion, incubation with OxPAPC compared to control incubation did not have a significant effect on the calculated variance metrics (variance ratio, the proportion of *responsive* cells, and the proportion of *supra-threshold* timeframes per cell). While only the high concentration IM solution increased the proportion of *responsive* neurons, both IM solutions increased the proportion of *supra-threshold* timeframes per cell.

Table 4-2: **Exemplary measurements of the variance area of distinct calcium signal patterns of DRG neurons.**

Activity pattern	Variance ratio	Label in Figure 4-10
No activity	1.03	A
Single peak	1.34	B
Sustained activity	2.98	C

Calcium imaging with low spatial resolution (10×, NA 0.3 objective) was carried out with OGB-1 loaded DRG neurons. The neurons were exposed to two different mixtures of inflammatory mediators (IM, concentrations given in Table 2-9). Responses observed while treatment with IM could be grouped in three activity patterns: no activity, single peak, or sustained activity. The measured variance area between 0 – 120 s (baseline period) and 150 – 690 s (treatment period) was used to calculate the variance ratio as described in 3.6.4.2. Labels in the last column reference the calcium signal patterns visualized in Figure 4-10. DRG, dorsal root ganglion; IM, inflammatory mediator mixture; NA, numerical aperture; OGB-1, Oregon Green BAPTA 1-AM.

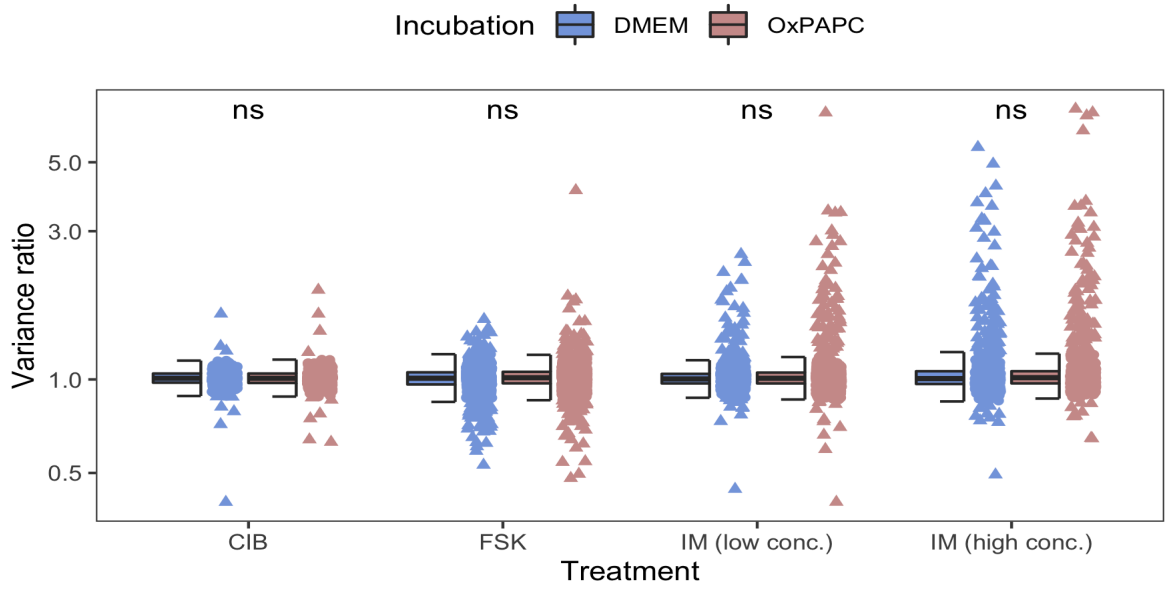

Figure 4-13: **The variance ratio is similar when comparing different treatment and incubation settings.** DRG neurons were incubated with DMEM (control, ■) or OxPAPC (10 µM, ■) for 30 min. Then, calcium imaging was performed during treatment of DRG neurons with calcium imaging buffer (CIB, control), forskolin (FSK, 10 µM), or inflammatory mediators (IM low and high concentration, composition in Table 2-9). The variance area was measured using NA^3 and used to calculate the variance ratio between baseline and treatment period. In this plot, data for small and medium soma DRG neurons is shown. n(DMEM, CIB) = 460, n(DMEM, FSK) = 938, n(DMEM, IM (low)) = 704, n(DMEM, IM (high)) = 771, n(OxPAPC, CIB) = 512, n(OxPAPC, FSK) = 1432, n(OxPAPC, IM (low)) = 747, n(OxPAPC, IM (high)) = 888. Y-axis in log scale. Boxplots show the count of calcium activity events per minute. The bold line indicates the median, the box indicates the IQR, and whiskers show the lowest/highest value within the 1.5-fold IQR. Original data points are shown to the right of the boxplot. Statistical hypothesis testing by Mann-Whitney-U test. ns: $p > 0.05$. CIB, calcium imaging buffer; DMEM, Dulbecco's Modified Eagle Medium; DRG, dorsal root ganglion; FSK, forskolin; IM, inflammatory mediator mixture; IQR, interquartile range; NA^3, Neural Activity Cubic; OxPAPC, oxidized PAPC.

Table 4-3: **Comparison of descriptive statistics on variance ratios calculated from calcium imaging traces in response to inflammatory mediator treatment.**

Incubation	Treatment	*n*	Median (min^{-1})	IQR (min^{-1})
DMEM	CIB	460	1.01	0.069
	FSK	938	1.01	0.091
	IM (low conc.)	704	1.00	0.071
	IM (high conc.)	771	1.01	0.096
OxPAPC	CIB	512	1.01	0.071
	FSK	1432	1.01	0.087
	IM (low conc.)	747	1.01	0.081
	IM (high conc.)	888	1.01	0.092

DRG neurons were incubated with OxPAPC (10 µM) or DMEM (control) for 30 min. Then, calcium imaging was performed during treatment of the DRG neurons with calcium imaging buffer (CIB), forskolin (FSK, 10 µM), or inflammatory mediators (IM, low and high concentration, composition in Table 2-9). The variance area was measured using NA^3 and used to calculate the variance ratio between baseline and treatment period. The table shows the number of analyzed neurons, median, and IQR of the activity counts per combination of mediator treatment and incubation. The data is visualized in Figure 4-13. CIB, calcium imaging buffer; conc., concentration; DMEM, Dulbecco's Modified Eagle Medium; DRG, dorsal root ganglion; FSK, forskolin; IM, inflammatory mediator mixture; IQR, interquartile range; NA^3, Neural Activity Cubic; OxPAPC, oxidized PAPC.

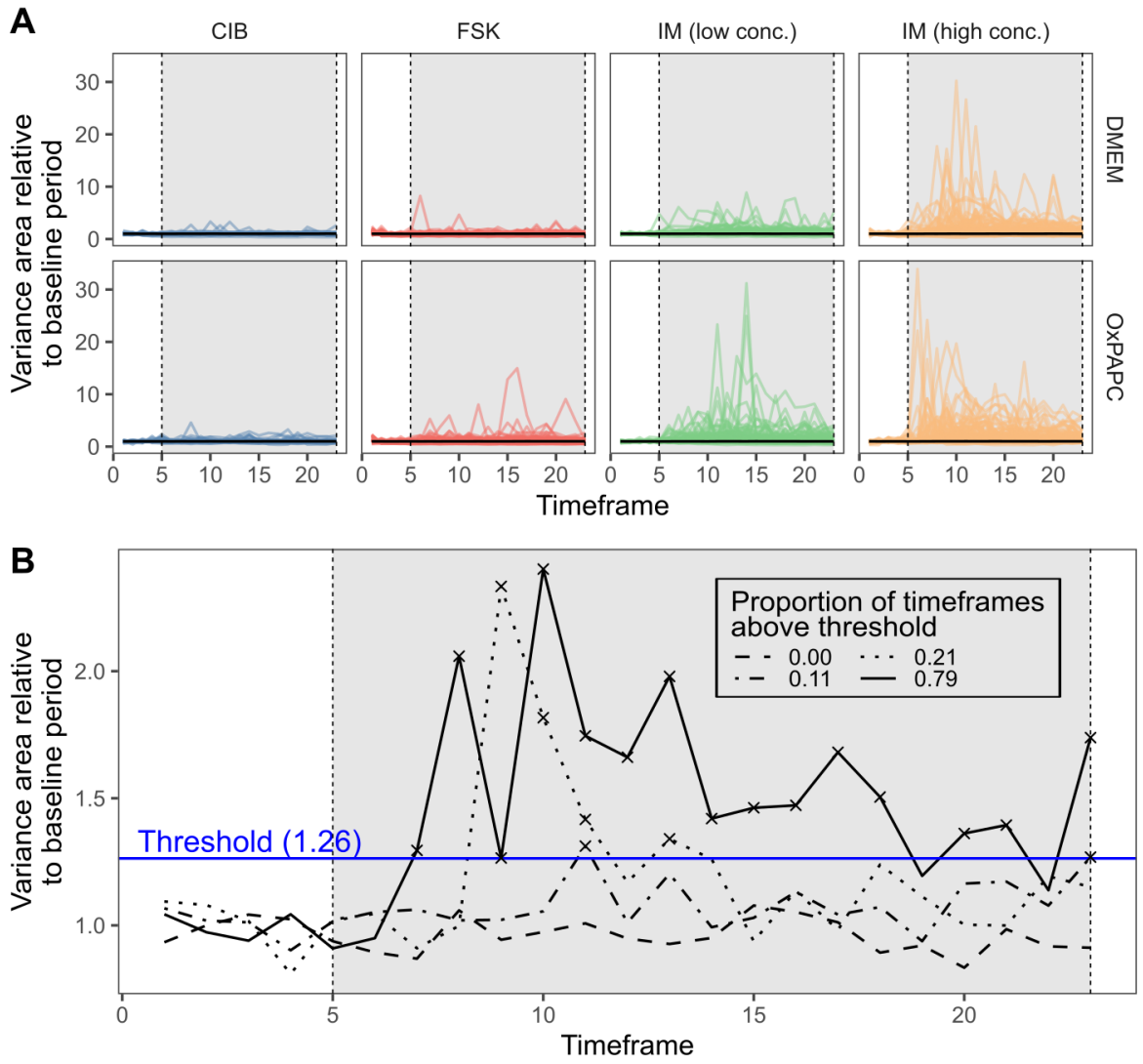

Figure 4-14: **Time series analysis of the variance ratio.** DRG neurons were incubated with OxPAPC (10 µM) or DMEM (Control) for 30 min. Then, calcium imaging was performed during treatment of the DRG neurons with calcium imaging buffer (CIB, ■), forskolin (FSK, 10 µM, ■) or inflammatory mediators (IM, low ■ and high ■ concentration, composition in Table 2-9). The variance area was calculated for each 30 s timeframe using NA[3]. For each timeframe, the variance area relative to baseline (variance ratio) was calculated. (**A**) The variance ratio is plotted against the timeframes of analysis for each incubation-treatment combination. The different incubation settings are shown in rows (DMEM and OxPAPC), the different treatments during calcium imaging are shown in columns (CIB, FSK, and IM (low and high concentration)). Black lines show the median of variance ratio values for each timeframe. The grey area indicates the mediator treatment period. (**B**) Visualization of the variance ratio over time for four selected DRG neurons. Measurements above the defined threshold (blue line) are indicated by ×. The grey area indicates the mediator treatment period. n(DMEM, CIB) = 460, n(DMEM, FSK) = 856, n(DMEM, IM (low)) = 704, n(DMEM, IM (high)) = 771, n(OxPAPC, CIB) = 512, n(OxPAPC, FSK) = 1311, n(OxPAPC, IM (low)) = 747, n(OxPAPC, IM (high)) = 888. CIB, calcium imaging buffer; DMEM, Dulbecco's Modified Eagle Medium; DRG, dorsal root ganglion; FSK, forskolin; IM, inflammatory mediator mixture; NA[3], Neural Activity Cubic; OxPAPC, oxidized PAPC.

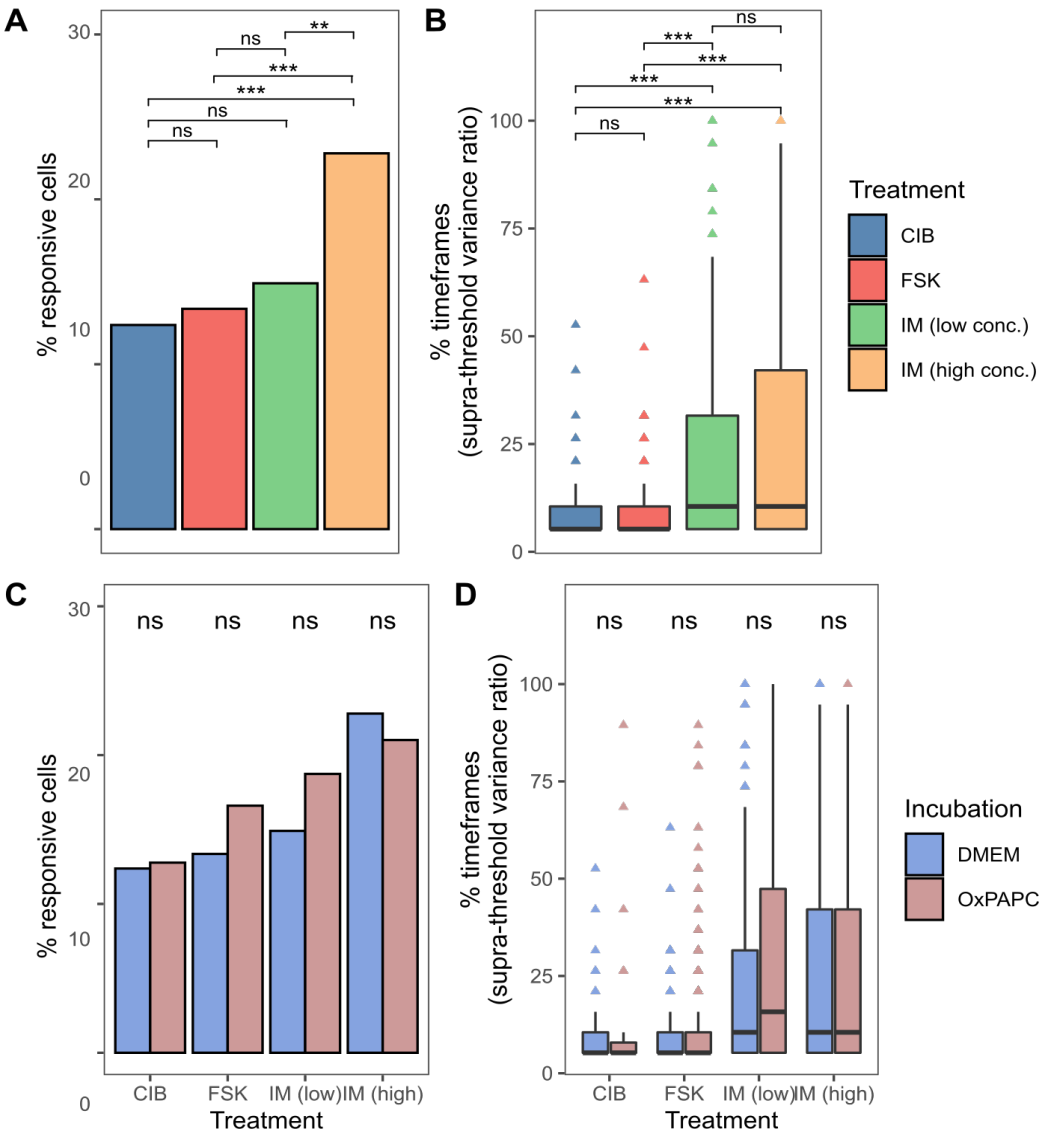

Figure 4-15: **Treatment of DRG neurons with inflammatory mediators results in increased variance ratios**. DRG neurons were incubated with DMEM (control, ■) or OxPAPC (10 µM, ■) for 30 min. Then, calcium imaging was performed during treatment of the DRG neurons with calcium imaging buffer (CIB, ■), forskolin (FSK, 10 µM, ■) or inflammatory mediators (IM, low ■ and high ■ concentration, composition in Table 2-9). The ratio of the variance area relative to baseline was calculated for each 30 s timeframe using NA[3]. Further, the proportion of responsive cells and the proportion of timeframes the variance ratio was above the defined threshold were calculated. In all plots, data of small- and medium-size soma DRG neurons is shown. (**A** and **B**) Plots show data on DRG neurons incubated with DMEM (control) before calcium imaging. (**A**) Compares the proportion of responsive cells. (**B**) shows the proportion of supra-threshold timeframes in responsive cells. (**C** and **D**) Both plots compare the effect of CIB, FSK, or IM (low and high concentration) treatments between the incubation conditions (DMEM or OxPAPC). (**C**) shows the proportion of responsive cells. (**D**) shows the proportion of supra-threshold timeframes in responsive cells. The bold line in boxplots indicates the median, the box indicates the IQR, and whiskers show the lowest/highest value within the 1.5-fold IQR. Outliers are shown as data points. Statistical hypothesis testing: (A and C) pairwise Pearson's χ^2 test and Holm post hoc test; (B) Kruskal-Wallis test and Dunn-Holm post hoc test; (D) Mann-Whitney-U test. ns: $p > 0.05$, *: $p < 0.05$. **: $p < 0.01$, ***: $p < 0.001$. n(DMEM, CIB) = 460, n(DMEM, FSK) = 856, n(DMEM, IM (low)) = 704, n(DMEM, IM (high)) = 771, n(OxPAPC, CIB) = 512, n(OxPAPC, FSK) = 1311, n(OxPAPC, IM (low)) = 747, n(OxPAPC, IM (high)) = 888. CIB, calcium imaging buffer; DMEM, Dulbecco's Modified Eagle Medium; DRG, dorsal root ganglion; FSK, forskolin; IM, inflammatory mediator mixture; NA[3], Neural Activity Cubic; OxPAPC, oxidized PAPC.

5 Discussion

Pain is a major symptom accompanying (chronic) inflammatory diseases (Basbaum and Jessell, 2013; Medzhitov, 2010). In a variety of pain conditions, an interplay of many inflammatory mediators causes peripheral sensitization of nociceptors. Nociceptor sensitization is characterized by lower thresholds for action potential generation and increased responsiveness of nociceptors (Gold and Gebhart, 2010; Loeser et al., 2011; Medzhitov, 2010). The VGSC $Na_V1.9$ is a key mediator of nociceptor sensitization in response to coincident inflammatory mediator signaling (Maingret et al., 2008; Martin et al., 2018). This ion channel can be activated at relatively negative membrane potentials, close to the resting membrane potential. Due to this unique property, $Na_V1.9$ regulates the excitability of DRG neurons (Bennett et al., 2019; Dib-Hajj et al., 2015). Recently, the OxPL mixture OxPAPC has been identified as an acute activator of TRPV1 and TRPA1 ion channel activity (Liu et al., 2016; Oehler et al., 2017). Notably, $Na_V1.9$ has been shown to potentiate acute, excitatory responses of nociceptors to OxPL, but this specific function was only observed under inflammatory conditions (Martin et al., 2018).

This thesis aimed to investigate the resting influence of $Na_V1.9$ on the excitability of DRG neurons. Additionally, this work aimed to determine whether OxPL alone are sufficient to induce inflammation-like states in DRG neurons. As patch clamp recording is not able to provide a spatiotemporal measure of neuronal excitability, a new approach to investigate nociceptor excitability was developed and experimentally validated. In this approach, calcium imaging with a high-affinity calcium indicator was used to identify signal-close-to-noise calcium activity in somata and neurites of cultured DRG neurons. As heuristic signal identification techniques are not applicable to analyze signal-close-to-noise calcium activity, objective signal calcium activity event identification was performed using NA^3, a computational activity inference tool that allows spatiotemporal calcium activity event identification (Prada et al., 2018).

In this study, I show that Nav1.9 has the potential to drive signal-close-to-noise calcium activity in axons of nociceptors, indicating that the channel is persistently active at the resting membrane potential. Furthermore, my work supplies evidence that OxPL do not induce inflammation-like states in DRG neurons, thus confirming the view that OxPL act primarily as acute excitants in nociception. Lastly, I propose an approach based on the variance ratio of raw calcium imaging signals as an unbiased strategy to assess neuronal excitability.

5.1 Automated calcium activity event detection correlates with manual activity analysis

In this thesis, NA^3 was applied for calcium activity detection. NA^3 is a tool that uses a hard-coded CWT algorithm (wavelet ridge walking) to identify calcium activity events (Prada et al., 2018). The approach avoids denoising of calcium traces but uses, instead, the raw calcium trace data for signal identification. This strategy leads to a rather high false-positive rate. As of yet, however, this approach is the only verified strategy for signal-close-to-noise calcium activity identification. It has been shown that strategies using denoising and signal demixing (Pnevmatikakis et al., 2016) or threshold-like methods (Romano et al., 2017) for signal identification fail to find homeostatic, signal-close-to-noise activity in neurons (Prada et al., 2018).

The comparison of manual and automated calcium activity detection by NA^3 revealed that both methods show a positive correlation in activity counts. Manual calcium imaging trace analysis depends on user-dependent judgments based on individually defined heuristics. This has been shown in other studies testing the variability in heuristic analysis of image features which results in high inter-rater variability between signal annotating experts (Segebarth et al., 2020). The use of automated activity detection algorithms replaces subjective interpretation with objective, reproducible decisions (Pnevmatikakis, 2019). In my analysis, NA^3 detected more activities than manual counting in most calcium imaging traces. This difference was more apparent in more active neurons. A Bland-Altman analysis (Bland and Altman, 1999) revealed that both methods correlate, but do not show high agreement.

A systematic difference in activity counts might be due to the high rate of false positive detections of NA^3, a high rate of false negatives in manual counting, or more sensitive detection by NA^3 (i.e., detection of signal-close-to-noise). Manual counting of many calcium imaging traces is likely to be imprecise, including a high false negative rate. NA^3 transforms the calcium traces via CWT based on the second derivative of the Gaussian function to detect peaks using the *wmtsa* R package (Constantine and Percival, 2017; Prada et al., 2018). CWT-based peak detection is established to analyze peaks in mass spectrometry (Du et al., 2006). Using this technique, peaks are not defined using an absolute threshold amplitude which enhances the SNR allowing the tool to detect small peaks with a low false-positive rate (Du et al., 2006). NA^3 has been verified using simultaneous patch clamp experiments and has been found to have a high sensitivity for signals-close-to-noise (Prada et al., 2018). However, some degree of uncertainty regarding the sensitivity of NA^3 remains: calcium signals-close-to-noise do not

necessarily depend on APs, which makes their presence hard to verify (Prada et al., 2018; Spitzer et al., 2000). Despite the advantages and limitations of the use of CWT-based activity detection in raw calcium imaging data, $Na_V1.9$ KO DRG neurons show a lower level of calcium activity than WT neurons. This verifies that NA^3 is able to statistically discriminate spatiotemporal biological differences of signal-close-to-noise calcium activity between different genetic or treatment conditions.

The most important tuning parameter of NA^3 is the SNR setting (Prada et al., 2018). In preparation for my experiments, I exploratively determined an SNR value within the recommended range (Prada et al., 2018), at which NA^3 did not detect activities in background ROIs. The results of the automated analysis strongly depend on the SNR setting. High SNR values can reliably detect large calcium events, which are in practice easy to detect. In striking contrast, signal-close-to-noise activity signals are per se signals with low SNR and should in theory be detectable at low stringency SNR settings above 1. Low SNR settings on the one hand result in high false-positive rates, but, on the other hand, allow the definition of biologically relevant excitability phenomena (Prada et al., 2018). To avoid arbitrary SNR settings selection further heuristics for suitable settings are needed.

5.2 Temporally and spatially highly resolved calcium imaging allows the characterization of spontaneous calcium activity events in DRG neurons

This study revealed new properties of spontaneous calcium activities in compartments of DRG neurons. Three qualitative features were most obvious: firstly, some neurons were spontaneously active while others were not. Secondly, these activities could occur temporally synchronous or asynchronous. Synchronous activities occurred simultaneously with other activities with equal kinetics in different areas of the same neuron. Asynchronous activities occurred independently of any further activities in this neuron. Thirdly, two major types of kinetics were observable: short spike-like and longer transient-like calcium activities.

Similar features have been observed in other kinds of neurons: synchronous (termed *global*) and asynchronous (*local*) calcium activities were originally described in embryonic neurons of Xenopus (Gu and Spitzer, 1995), and later identified in other types of neurons, including neuronal precursor cells (Ciccolini et al., 2003), neuronal postsynaptic processes and dendrites (Augustine et al., 2003) and murine motoneurons (Subramanian et al., 2012; Jablonka et al., 2007). Calcium spikes and waves (comparable to transient-like activities) were observed in developing spinal neurons, contributing to growth cone migration and differential gene

transcription (Spitzer et al., 2000; Berridge et al., 2003). Interestingly, similar kinetics of calcium activities (spike-like and transient-like activities) have been detected after PGPC stimulation (Martin et al., 2018). This indicates that the molecular origin of these calcium activities might be evolutionarily conserved.

To quantify the observed spontaneous calcium activity in DRG neurons, I conducted calcium imaging at high spatial resolution. Calcium activity was analyzed for different neuronal compartments (somata, axons, and axonal terminals). Hypothesis testing revealed no significant difference in calcium activity event counts per time in the compared structures, while median activity per minute was higher in somata (1.40 min^{-1}) compared to axons and axonal terminals (0.80 min^{-1} and 0.87 min^{-1}). To my knowledge, these results are the first demonstration of spontaneous calcium activity in distinct neuronal compartments of DRG neurons. In motoneurons, spontaneous calcium activity frequencies of 0.4 min^{-1} in somata and 0.7 min^{-1} in axons and axonal terminals have been observed (Subramanian et al., 2012), which are in the same order of magnitude as the frequencies observed in DRG neurons. Cultured small-diameter DRG neurons are a cellular model for investigating molecular-physiological properties of nociceptors. Therefore, it is important to note that *in vivo* DRG neurons might well show other spontaneous calcium activity frequencies, due to higher compartmentalization of the neuron itself and due to the embedding of the neuron in its natural tissue environment.

5.3 Spontaneous calcium activities serve as a measure for neuronal excitability

The analysis of calcium activity counts of $Na_V1.9$ KO DRG neurons revealed lower counts in somata, axons, and axonal terminals compared to WT neurons. The decrease in activity counts was statistically significant in axons and somata (decreased by 50 and 71 % respectively). This shows that the formation of spontaneous calcium activities is supported by $Na_V1.9$. Due to its unique electrophysiological characteristics, $Na_V1.9$ functions as a threshold channel in AP formation and is a determinant of neuronal excitability (Bennett et al., 2019; Dib-Hajj et al., 2015). This suggests that $Na_V1.9$ is an upstream trigger of spontaneous calcium activities, which are reduced in its absence. Similar results have been observed in murine motoneurons, where the number of calcium activity events in somata, distal axons, and axonal terminals was significantly lower in $Na_V1.9$ KO neurons compared to WT neurons (decrease by 75, 82, and 83 %; Subramanian et al., 2012). In the context of nociception, the absence of $Na_V1.9$ has been reported to decrease mechanical and thermal hyperalgesia (Amaya et al., 2006; Lolignier et al., 2011; Priest et al., 2005). In DRG neurons, the observed decrease in calcium

activity events in $Na_V1.9$ KO neurons can therefore be interpreted as an expression of lower neuronal excitability.

Despite the differences to WT neurons, the activity count in $Na_V1.9$ KO DRG is not reduced to zero. Nav1.9 seems to act as a trigger of excitability, a function that is stronger under inflammatory conditions (Martin et al., 2018; Maingret et al., 2008). Nav1.9 does not deterministically trigger AP generation but increases the probability for the generation of APs. This excitability concept is in line with a study showing that AP formation is not exclusively dependent on $Na_V1.9$ as nerve preparations of $Na_V1.9$ KO mice still exhibit APs (Hoffmann et al., 2017). Additionally, earlier studies described calcium activities (local, long-duration calcium waves) that are independent of APs (i.e., VGSC-independent; Spitzer et al., 2000). It can be hypothesized that calcium activities in $Na_V1.9$ KO neurons are made of a higher proportion of wave-like activities. Extended quantitative descriptions of the morphology and synchronicity of detected calcium activities could further explain the influence of $Na_V1.9$ on calcium activity dynamics in DRG neurons.

5.4 The excitability and inflammatory mediator response of DRG neurons is not influenced by OxPAPC incubation

Having found that fewer spontaneous calcium activity events in $Na_V1.9$ KO neurons express decreased excitability, I hypothesized to detect an increased rate of spontaneous calcium activity events in OxPAPC incubated DRG neurons as an expression of increased excitability. The analysis of spontaneous calcium activity of DRG neurons incubated with OxPAPC for 1 h before calcium imaging recordings, however, did not reveal any significant differences in counts per minute to DRG neurons incubated with control medium. OxPAPC is a transient, biochemically unstable mediator in inflammation (Domingues et al., 2013; Stemmer and Hermetter, 2012). It has been shown that fifteen minutes after local injection, OxPAPC components PGPC and POVPC are no longer detectable in the corresponding tissue, indicating that the substances underly rapid degradation in the tissue environment (Oehler et al., 2017). Despite this transient nature, long-lasting hyperalgesia was observed *in vivo* in rodents after OxPAPC injection into hind paws (Oehler et al., 2017). This led to the assumption that additionally to the direct activating effect of OxPAPC on TRPA1 (Liu et al., 2016; Oehler et al., 2017), OxPAPC contributes to long-lasting inflammatory pain via peripheral sensitization. My experiments in this cell-autonomous model could not deliver supporting evidence for this hypothesis as the excitability remained unchanged after OxPAPC exposition. This suggests that

the isolated nociceptive neuron might not be responsible for the long-lasting *in vivo* behavioral effects mediated by OxPL.

In contrast to my initial experimental setup, where DRG neurons were exclusively exposed to OxPAPC, inflammatory processes *in vivo* are characterized by the interplay of a multitude of inflammatory mediators (Medzhitov, 2010), which promote peripheral sensitization of nociceptors (Gold and Gebhart, 2010). In this milieu, OxPAPC may act as an intermediary mediatory to promote peripheral sensitization. To investigate this, cells incubated with OxPAPC for 1 h were exposed to a mixture of inflammatory mediators (bradykinin, histamine, and PGE_2) during calcium imaging.

Analysis of activity counts and variance ratios in response to FSK or IM treatment after 1 h of OxPAPC incubation did not reveal any conclusive statistically significant differences to preincubation with control medium. Non-parametric hypothesis testing on activity counts between OxPAPC and control incubation when DRG neurons were exposed to control treatment or low concentration IM resulted in significant p-values. However, the overlapping IQR of the data and the similar median activity counts suggest very low statistical power. The current analysis of these results suggests that the responsiveness of DRG neurons to inflammatory mediators is not increased by OxPAPC incubation before IM or FSK treatment. In striking contrast, Martin et al. showed that DRG neurons preincubated with inflammatory mediators (bradykinin, histamine, and PGE_2) exhibit increased AP firing and calcium spikes in response to stimulation with PGPC, a stable representative OxPL (Martin et al., 2018). This observation suggests that inflammatory conditions induce a resting, long-lasting, or even permanent activity of $Na_V1.9$ at rather stable resting membrane potential conditions. This implies that there must be a permanent $Na_V1.9$-mediated driving force for excitability events in structures of nociceptors predominantly expressing $Na_V1.9$ (i.e., somata and axons; Martin et al., 2018). In summary, the combined evidence suggests that OxPAPC alone cannot evoke increased excitability of DRG neurons, however, responses to PGPC are potentiated in inflammatory conditions. This shows that, on a cellular level, OxPL act as excitants and not as inflammatory mediators.

OxPAPC is a heterogeneous mixture of oxidation products from PAPC lipid peroxidation (Bretscher et al., 2015) eliciting a range of anti- and proinflammatory effects (Bochkov et al., 2010; Freigang, 2016; Oskolkova and Bochkov, 2020). *In vitro* and *in vivo* experiments verified TRPA1 as the preferred target of OxPAPC (Liu et al., 2016; Oehler et al., 2017). Experiments showed that alterations of the electrophilic binding site of TRPA1 diminish OxPAPC activation

(Oehler et al., 2017). However, the OxPL PGPC, a major component of OxPAPC, is a non-electrophilic acid but can anyhow acutely excite nociceptors via TRPA1 and TRPV1 (Martin et al., 2018). This suggests that the OxPAPC-dependent activation could depend on multiple mechanisms. Another hypothesis is based on the involvement of inflammation-dependent molecular switches such as $Na_V1.9$ that increase neuronal excitability and hereby potentiate OxPL stimuli (Martin et al., 2018).

Interference of OxPAPC components with the cell membrane has to be differentiated from receptor-dependent effects. Lipid peroxidation products may interfere with membrane protein function (Catala, 2009) and increase membrane rigidity (Borst et al., 2000). For example, POVPC is integrated into the cell membrane (Moumtzi et al., 2007). It has been hypothesized that due to the mechanosensitive properties of TRPA1 (Vilceanu and Stucky, 2010), membrane integration of OxPAPC components might trigger an indirect activation of TRPA1 via changes in membrane fluidity (Oehler et al., 2017). Such indirect activation does not influence intracellular pathways contributing to peripheral sensitization. Importantly, my experiments focused on long-lasting OxPAPC-derived effects, so that OxPAPC was not present during calcium indicator loading and calcium imaging. Therefore, directly activating effects, as outlined above, were not detectable in my setup.

My results showed no effect of OxPAPC incubation on the cellular responsiveness to stimuli of DRG neurons. Di Gioia et al. provide evidence suggesting that in macrophages 24 h OxPAPC pre-incubation does influence the cellular metabolism, shifting cells to a hyperactive, hypermetabolic state, augmenting proinflammatory IL-1-β production, and increasing responses to LPS stimuli (Di Gioia et al., 2020). While these insights are mainly relevant in the context of atherosclerosis research, they still provide evidence of OxPAPC as a driver of inflammation, with the potential to indirectly induce peripheral sensitization in nociceptors.

5.5 The variance ratio serves as an automated unbiased tool to assess neuronal excitability

I identified distinct morphological calcium signal patterns of DRG neurons in response to IM: *no activity*, a *single peak*, and *sustained activity*. Mohammed et al. observed similar responses of DRG neurons exposed to veratridine, an inhibitor of VGSC inactivation. Here, four different patterns were identified: *slow*, *intermediate*, and *rapid decay* and *oscillatory response* (Mohammed et al., 2017). The *decay* responses can be seen as a more fine-grained description of the *single peak* pattern observed in my experiments while *oscillatory responses*

can be equated with *sustained activity*. Interestingly, Mohammed et al. revealed that *oscillatory responses* can be attributed to nociceptors, while especially *slow decay* responses were characteristic of non-nociceptor neurons (Mohammed et al., 2017). In a more recent study, Mohammed et al. concluded that the proportions of neurons with *slow decay* and *oscillatory responses* serve as a readout for determining the excitability of DRG neurons and thereby assess potential effects of drugs on nociceptors (Mohammed et al., 2020). The authors call for an automated solution for assessing the excitability of sensory neurons.

NA^3 implements the calculation of the variance area of a calcium imaging trace, which is a measure for biological signal fluctuations (Prada et al., 2018). The variance area is the spread of the calcium signals around their mean calculated in a sliding window (here 30 frames). To facilitate comparisons of variance data between different measurements, I calculated the variance ratio, in which the variance area during the treatment period is standardized by the variance area in the baseline period. Hereby, calcium imaging data acquired using non-ratiometric dyes can be compared quantitatively.

I provided evidence that DRG neurons exhibiting *sustained activity*, yields higher variance ratios than neurons showing *no activity* or a *single peak*. My investigations did not statistically prove this relationship. However, the statistical concept of variance as a measure for the spread of a signal (Taboga, 2017) directly relates an increased variance to increased signal fluctuation, which is seen in *sustained activity* responses. Verification of the relationship between signal pattern and variance ratio could further improve interpretability.

To analyze the effect of FSK and IM treatment on the variance ratio, I calculated the variance ratio in windows of 30 s and plotted the values as time series. Neurons that showed a variance ratio above a threshold in at least one timeframe during mediator treatment were registered as *responsive.* The threshold was set at 1.5-fold IQR above the upper quartile of the control baseline variance ratio, similar to outlier detection methods. This approach allowed an unbiased, automated selection of neurons that showed fluctuations in the recorded calcium signal. Fluctuations in the calcium signal thereby serve as identification of neuronal activity. To be able to analyze the length of these signal fluctuations, I calculated the proportion of timeframes, where the variance ratio of *responsive* neurons was supra-threshold.

Comparing FSK (10 µM) with control settings did not show differences in the proportion of *responsive* neurons or the proportion of supra-threshold variance ratio. This is consistent with the mechanism of action of FSK: FSK is a direct activator of the adenyl cyclase elevating cyclic adenosine monophosphate (cAMP) concentration stimulating PKA pathways, without targeting

membrane receptors (Seamon et al., 1981). Sensitization of nociceptive receptors, such as TRPA1, by PKA, is evident but dependent on direct agonists of the receptor (Meents et al., 2017). Effects of FSK on spontaneous calcium signals in sensory neurons have also been seen at higher concentrations (50 µM) and later onset (approximately 10 min after the start of exposition; Gorbunova and Spitzer, 2002). Gorbunova and Spitzer here assume an interplay of calcium and cAMP in gene transcription (Gorbunova and Spitzer, 2002). This evidence conclusively explains the unaltered excitability state of DRG neurons during FSK treatment in my experiments.

The proportion of *responsive* DRG neurons was significantly higher in experiments with high concentration IM exposure compared to controls, while the proportion of *responsive* neurons exposed to low concentration IM was not significantly elevated. Higher concentrations of IM seem to recruit DRG neurons, which are unreactive at low IM concentrations. Evidence for the recruitment of previously unresponsive neurons has been demonstrated for PGE_2. PGE_2 exposition leads to an increase of cAMP and IP_3 (Smith et al., 1998), which sensitizes neurons for bradykinin (Smith et al., 2000) or histamine (Nicolson et al., 2007) stimuli. Additionally, it has been shown that the application of a combined mixture of inflammatory mediators potentiates the current of $Na_V1.9$ (Maingret et al., 2008). This was not the case when higher concentrations of the individual substances were applied (Maingret et al., 2008), indicating that coincident signaling of inflammatory mediators is needed to increase $Na_V1.9$ activity.

Irrespective of the concentration of IM applied, DRG neurons exhibited significantly more variance ratio measurements in the time series above the defined threshold, i.e., are active for a longer duration than controls. This suggests that the subpopulations of *responsive* neurons in both setups react with similar excitability levels towards inflammatory stimuli.

Combining the evidence of my experiments, it can be concluded that some DRG neurons show responses towards IM exposition (expressed by increased activity counts and variance ratios), while others do not. A different study identified 66 % of cultured DRG neurons as responsive to stimulation with capsaicin, ATP, and AITC suggesting their functional specialization as nociceptors (Mohammed et al., 2017). The proportion of *responsive* neurons towards high concentration IM in my experiments was only at 22.8 % (DMEM incubation). This is compatible with the notion of functional heterogeneity: potent stimulation with capsaicin, ATP, and AITC aimed to activate every single nociceptor, while exposition to IM most likely targeted only a subset of nociceptors responsive to the tested mediators. To which

extent this observation is a consequence of functional specialization of DRG neurons (Usoskin et al., 2015) has yet to be verified.

5.6 Zero-inflated models and Gaussian Mixed Models to enhance the conclusiveness of unbiased excitability assessments

I have demonstrated that the analysis of the variance ratio over time can serve as an unbiased estimator, applicable to non-ratiometric fast calcium imaging. As opposed to morphological analyses described by Mohammed et al. (Mohammed et al., 2020), the automated approach allows user-independent, efficient readout of a high number of DRG neurons. Additionally, in contrast to excitability analysis in patch and current clamp experiments, many cells can be included in the analysis at the same time, allowing to analyze the entire heterogeneous population of DRG neurons.

In this study, I conducted calcium imaging and automated activity detection in a large number of DRG neurons. Most neurons showed very low or no activity counts or a calculated variance ratio close to 1. This is a major challenge to data analysis, as the significant difference in activity count or variance ratio distributions in responsive neurons may be concealed by the large proportion of unresponsive neurons. Especially in my experiments recording calcium traces of a large number of neurons, hypothesis tests did not deliver conclusive results.

As discussed earlier, DRG neurons are heterogeneous and functionally specialized (Usoskin et al., 2015). This allows for the hypothesis that not all neurons will equally exhibit spontaneous signal-close-to-noise calcium activity and exhibit different levels of responsiveness to treatment with inflammatory mediators. The high number of zero activity counts (*zero inflation* (Tu and Liu, 2016)) or variance ratios close to 1 might be due to the inclusion of inactive neurons into the analysis, which do not show spontaneous activity, are unresponsive to inflammatory mediators, or do not contribute to peripheral sensitization in inflammation *in vivo*.

Several strategies were tested to overcome these problems: in single-cell measurements, I subjectively selected small-diameter DRG neurons, furthermore, I excluded neurons with somatic areas above 707 μm^2 from analysis in low spatial resolution measurement. Cell size has been shown to correlate with functional classification as nociceptive neurons (Usoskin et al., 2015) and has been used for nociceptor classification of cultured DRG neurons (Martin et al., 2018). Small-diameter neurons are known to be $Na_V1.9$-positive and belong to the nociceptor cell lineage (Cheng et al., 2021).

Hypothetically, the DRG neuron population consists of two groups: responsive and unresponsive neurons. Mixture models could overcome this biased selection process by modeling combinations of distributions. Discrete, non-negative *zero-inflated* activity count data could be modeled using a *zero-inflated* gamma mixture model. Recently, this approach was applied to activity counts from calcium imaging recordings from individual neurons and validated with various calcium imaging indicators (Wei et al., 2020). The continuous variance ratio data could be modeled by a Gaussian Mixed Model (GMM), which can be estimated by the unsupervised expectation-maximization algorithm (Murphy, 2012). By the use of such computational strategies, it would not be necessary to apply hard thresholding to distinguish *responsive* and *unresponsive* neurons. However, whether such an approach would work with our data, is not clear yet and would need detailed experimental validation.

Fitting the activity count or variance ratio data to mixture models and performing statistical hypothesis testing on the model parameters could reveal evidence of distributional differences, taking *unresponsive* neurons into account. The approach to model specific functional neuronal subpopulations is in line with the *population-coding* theory (Ma, 2012), which explains the formation of specific somatosensory sensations, such as pain, in terms of interactions of DRG neuron populations.

5.7 Limitations of this study

In my experiments, I performed cell culture, calcium imaging indicator loading, and mediator (OxPAPC and control) incubation at 37°C. Calcium imaging, however, was performed while the neurons were kept at 25°C using a temperature controller. Touska et al. investigated the electrophysiological characteristics of $Na_V1.9$ at 10, 20, and 30 °C temperature bath solutions. They reported that by increasing the temperature from 20 to 30 °C, $Na_V1.9$ (in-) activation kinetics sped up significantly, while conductance and peak current increased 4-fold (Touska et al., 2018). This reveals a significant gain-of-function of $Na_V1.9$ at increasing temperatures. In the context of my experiments, it could be hypothesized that this gain-of-function adaptation would further accentuate the differences in excitability of WT and $Na_V1.9$ KO neurons. Nevertheless, keeping experimental conditions as close as possible to physiology is desirable, meaning the potential impact of the surrounding temperature should be kept in mind.

In my analysis, I solely evaluated the qualitative features of the detected spontaneous calcium activities. To further evaluate the significance of synchronicity and the kinetics of

signal-close-to-noise calcium activities, unbiased metrics such as duration, full-width half-max (FWHM) and decay are of interest (Mackay et al., 2016). These metrics would provide additional information on the potential differences of these calcium activities between genotypes or mediator treatment.

To analyze the single-cell calcium imaging recordings, I used user-defined ROIs to determine calcium activity in neuronal compartments. This approach does, however, introduce bias concerning the selection of analyzed regions. NA^3 implements unbiased spatial analysis by separating the image into separately analyzed grid sections (Prada et al., 2018). Combining this functionality with automated image segmentation to label neuronal compartments, could further improve the unbiasedness of the analysis. However, models for unbiased image segmentation of calcium activity in DRG neurons are not developed or sufficiently validated yet. Manually annotated neuronal compartments in calcium imaging recordings, as demonstrated in this work, might be used in the future to train deep learning strategies for ROI annotation and segmentation. Alternatively, heuristic training data showing calcium-active ROIs could be leveraged to develop calcium activity annotation models.

5.8 Outlook

The methodological approach established in this study is based on fast calcium imaging of cultured DRG neurons and unbiased signal analysis of calcium signals and signal-close-to-noise activity, in a large number of neurons. The study shows for the first time that automated excitability assessment of neurons is possible by using the variance ratio of the calcium imaging signal. Thereby calcium imaging with high-affinity calcium indicators can be used to determine the excitability state of subregions of neurons with high temporal and spatial resolution or of a large number of neurons at low spatial resolution in a single readout. As a next analysis step, statistical analyses based on mixture models modeling the variance ratio and activity count data might allow for even more concise descriptions of excitability states of DRG neuron subpopulations.

This concept of unbiased activity detection has been validated by showing that signal-close-to-noise calcium activity, as analyzed here, is reduced in $Na_V1.9$ KO DRG neurons. As $Na_V1.9$ is known to be an excitability mediator, as well as known to drive calcium signals in axons, it is likely that signal-close-to-noise calcium activity is of biological origin. As this method can be used to read out the somatic calcium signal, it should also be suited to characterize the excitability state of neurons *in vivo*.

Applying the method to cultured DRG neurons, confirmed that typical inflammatory mediators, known to increase nociceptor excitability, increase the calcium signal variance ratio and calcium activity counts. Furthermore, the approach confirmed that OxPAPC, when given to cultured nociceptors, does not act as a sensitizing inflammatory mediator. Nevertheless, evidence exists for the development of hyperalgesia due to OxPAPC *in vivo* (Oehler et al., 2017). While OxPAPC has been shown to activate TRPA1 and TRPV1 (Liu et al., 2016; Oehler et al., 2017), the specific pathway in which OxPAPC mediates peripheral sensitization remains unclear. Due to the complex interplay of mediators and pathways in peripheral sensitization, there is a vast range of possible targets for further studies. Here, amongst others, interactions with other inflammatory mediators (Martin et al., 2018), influence on VGSCs $Na_V1.7$ and $Na_V1.8$, or recently demonstrated metabolic effects by OxPAPC exposition (Di Gioia et al., 2020) might be of interest. Due to the unstable nature of OxPAPC and its fast degradation, especially the resulting bioactive metabolites such as PGPC (Oehler et al., 2021) should be investigated in future research.

6 Conclusion

Here I developed an approach for unbiased excitability quantification of DRG neurons by analysis of the variance area of calcium imaging raw data. The approach might be used as a non-disruptive method for investigating neuronal excitability in different types of neurons.

Unbiased, objective activity analysis of fast calcium imaging recordings of $Na_V1.9$ KO DRG neurons showed a significantly lower count of signal-close-to-noise calcium activity compared to WT neurons. This confirms that signal-close-to-noise calcium activity is of biological origin.

The finding that signal-close-to-noise calcium activity reflects neuronal excitability allowed me to investigate whether OxPL act like inflammatory mediators in cultured DRG neurons. The data show that long-term OxPAPC exposition neither increases the excitability of DRG neurons nor sensitizes them for inflammatory mediators such as bradykinin, histamine, and PGE_2. This is in line with earlier studies by our group showing that OxPL are acting by inducing acute ion fluxes through ion channels.

In summary, this study proves that 'signal-close-to-noise' calcium activity reflects neuronal excitability. Thus, calcium imaging techniques are suited to investigate the spatiotemporal profile of neuronal excitability of nociceptors.

7 Abstract

Chronic pain conditions are a major reason for the utilization of the health care system. Inflammatory pain states can persist facilitated by peripheral sensitization of nociceptors. The voltage-gated sodium channel 1.9 ($Na_V1.9$) is an important regulator of neuronal excitability and is involved in inflammation-induced pain hypersensitivity. Recently, oxidized 1-palmitoyl-2-arachidonoyl-*sn*-glycerol-3-phosphatidylcholine (OxPAPC) was identified as a mediator of acute inflammatory pain and persistent hyperalgesia, suggesting an involvement in proalgesic cascades and peripheral sensitization. Peripheral sensitization implies an increase in neuronal excitability. This thesis aims to characterize spontaneous calcium activity in neuronal compartments as a proxy to investigate neuronal excitability, making use of the computational tool Neural Activity Cubic (NA^3). NA^3 allows automated calcium activity event detection of signal-close-to-noise calcium activity and evaluation of neuronal activity states. Additionally, the influence of OxPAPC and $Na_V1.9$ on the excitability of murine dorsal root ganglion (DRG) neurons and the effect of OxPAPC on the response of DRG neurons towards other inflammatory mediators (prostaglandin E_2, histamine, and bradykinin) is investigated. Using calcium imaging, the presence of spontaneous calcium activity in murine DRG neurons was established. NA^3 was used to quantify this spontaneous calcium activity, which revealed decreased activity counts in axons and somata of $Na_V1.9$ knockout (KO) neurons compared to wildtype (WT). Incubation of WT DRG neurons with OxPAPC before calcium imaging did not show altered activity counts compared to controls. OxPAPC incubation also did not modify the response of DRG neurons treated with inflammatory mediators. However, the variance ratio computed by NA^3 conclusively allowed to determine neuronal activity states. In conclusion, my findings indicate an important function of $Na_V1.9$ in determining the neuronal excitability of DRG neurons in resting states. OxPAPC exposition does not influence neuronal excitability nor sensitizes neurons for other inflammatory mediators. This evidence reduces the primary mechanism of OxPAPC-induced hyperalgesia to acute effects. Importantly, it was possible to establish an approach for unbiased excitability quantification of DRG neurons by calcium activity event detection and calcium trace variance analysis by NA^3. It was possible to show that signal-close-to-noise calcium activity reflects neuronal excitability states.

8 Zusammenfassung

Entzündliche Schmerzzustände können lange fortbestehen, was durch eine periphere Sensibilisierung von Nozizeptoren begünstigt wird. Der spannungsgesteuerte Natriumkanal 1.9 ($Na_V1.9$) ist ein wichtiger Regulator neuronaler Erregbarkeit und ist nachweislich an entzündungsbedingter Schmerzüberempfindlichkeit beteiligt. Kürzlich wurde oxidiertes 1-Palmitoyl-2-arachidonoyl-sn-glycerol-3-phosphatidylcholin (OxPAPC) als Mediator akuter Entzündungsschmerzen und anhaltender Hyperalgesie identifiziert, was auf eine Beteiligung an Mechanismen der peripheren Sensibilisierung hindeutet. Periphere Sensibilisierung setzt eine Erhöhung der neuronalen Erregbarkeit voraus. In dieser Arbeit soll neuronale spontane Kalziumaktivität charakterisiert werden, um Rückschlüsse auf die neuronale Erregbarkeit zu ziehen. Dazu wurde das Tool Neural Activity Cubic (NA^3) eingesetzt, welches die automatisierte Detektion von „signal-close-to-noise“ Kalziumaktivitätsereignissen und die Bewertung neuronaler Aktivitätszustände erlaubt. Mittels NA^3 wurde der Einfluss von OxPAPC und $Na_V1.9$ auf die Erregbarkeit von murinen Spinalganglion (DRG)-Neuronen untersucht. Zusätzlich wurde die Reaktion von DRG-Neuronen auf weitere Entzündungsmediatoren (Prostaglandin E_2, Histamin und Bradykinin) nach Inkubation mit OxPAPC beurteilt. Mittels Calcium-Imaging konnte spontane Kalziumaktivität in murinen DRG-Neuronen identifiziert werden. NA^3 wurde verwendet, um diese spontane Kalziumaktivität zu quantifizieren. $Na_V1.9$ Knockout-Neuronen (KO) zeigten signifikant Verringerte Kalziumaktivität im Vergleich Wildtyp (WT)-Neuronen. Die Inkubation von WT-Neuronen mit OxPAPC vor Calcium-Imaging resultierte in unveränderter Kalziumaktivität. Eine OxPAPC-Inkubation hatte ebenso keinen Einfluss auf die Reaktion von DRG-Neuronen, die mit einem Gemisch aus Entzündungsmediatoren stimuliert wurden. Die von NA^3 berechnete „variance ratio“ ermöglichte jedoch eine eindeutige Bestimmung der neuronalen Aktivitätszustände. Zusammenfassend weisen meine Ergebnisse auf eine wichtige Funktion von $Na_V1.9$ bei der Bestimmung der neuronalen Erregbarkeit von DRG-Neuronen im Ruhezustand hin. Eine Exposition mit OxPAPC beeinflusst allerdings weder die neuronale Erregbarkeit noch werden Neuronen für andere Entzündungsmediatoren sensibilisiert. Dies legt akute Effekte als primären Mechanismus der OxPAPC-induzierten Hyperalgesie nahe. Es war möglich, eine Methode für die unverzerrte Quantifizierung neuronaler Erregbarkeit von durch die Erkennung von Kalziumaktivitätsereignissen und die Varianzanalyse von Kalziumsignalen mit NA^3 zu etablieren. Es konnte gezeigt werden, dass die „signal-close-to-noise“ Kalziumaktivität den Zustand der neuronalen Erregbarkeit widerspiegelt.

9 Bibliography

Amaya, F. et al. (2006). The voltage-gated sodium channel NaV1.9 is an effector of peripheral inflammatory pain hypersensitivity. *J Neurosci*, **26(50)**, 12852-12860.

Amaya, F. et al. (2000). Diversity of Expression of the Sensory Neuron-Specific TTX-Resistant Voltage-Gated Sodium Ion Channels SNS and SNS2. *Molecular and Cellular Neuroscience*, **15(4)**, 331-342.

Amsalem, M. et al. (2018). Membrane cholesterol depletion as a trigger of NaV1.9 channel-mediated inflammatory pain. *EMBO J*, **37(8)**, e97349.

Augustine, G.J., Santamaria, F. & Tanaka, K. (2003). Local calcium signaling in neurons. *Neuron*, **40(2)**, 331-346.

Baker, M.D. et al. (2003). GTP-induced tetrodotoxin-resistant Na+ current regulates excitability in mouse and rat small diameter sensory neurones. *The Journal of Physiology*, **548(2)**, 373-382.

Baker, M.D. & Nassar, M.A. (2020). Painful and painless mutations of SCN9A and SCN11A voltage-gated sodium channels. *Pflugers Arch*, **472(7)**, 865-880.

Basbaum, A.I. et al. (2009). Cellular and molecular mechanisms of pain. *Cell*, **139(2)**, 267-284.

Basbaum, A.I. & Jessell, T.M. (2013) Pain. In Kandel, E.R. et al. (Eds.), *Principles of Neural Science, Fifth Edition,* (5th ed., pp. 530-555). McGraw Hill Professional.

Bautista, D.M., Pellegrino, M. & Tsunozaki, M. (2013). TRPA1: A gatekeeper for inflammation. *Annu Rev Physiol*, **75**, 181-200.

Bedi, S.S. et al. (2010). Chronic spontaneous activity generated in the somata of primary nociceptors is associated with pain-related behavior after spinal cord injury. *J Neurosci*, **30(44)**, 14870-14882.

Bennett, D.L. et al. (2019). The Role of Voltage-Gated Sodium Channels in Pain Signaling. *Physiol Rev*, **99(2)**, 1079-1151.

Berridge, M.J., Bootman, M.D. & Roderick, H.L. (2003). Calcium signalling: dynamics, homeostasis and remodelling. *Nat Rev Mol Cell Biol*, **4(7)**, 517-529.

Binder, C.J., Papac-Milicevic, N. & Witztum, J.L. (2016). Innate sensing of oxidation-specific epitopes in health and disease. *Nat Rev Immunol*, **16(8)**, 485-497.

Binshtok, A.M. et al. (2008). Nociceptors are interleukin-1beta sensors. *J Neurosci*, **28(52)**, 14062-14073.

Bland, J.M. & Altman, D.G. (1999). Measuring agreement in method comparison studies. *Stat Methods Med Res*, **8(2)**, 135-160.

Bochkov, V. et al. (2017). Pleiotropic effects of oxidized phospholipids. *Free Radic Biol Med*, **111**, 6-24.

Bochkov, V.N. et al. (2010). Generation and biological activities of oxidized phospholipids. *Antioxid Redox Signal*, **12(8)**, 1009-1059.

Borst, J.W. et al. (2000). Oxidation of unsaturated phospholipids in membrane bilayer mixtures is accompanied by membrane fluidity changes. *Biochim Biophys Acta*, **1487(1)**, 61-73.

Bretscher, P. et al. (2015). Phospholipid oxidation generates potent anti-inflammatory lipid mediators that mimic structurally related pro-resolving eicosanoids by activating Nrf2. *EMBO Mol Med*, **7(5)**, 593-607.

Brini, M. et al. (2014). Neuronal calcium signaling: function and dysfunction. *Cell Mol Life Sci*, **71(15)**, 2787-2814.

Carlin, D. et al. (2018). Deletion of Tsc2 in Nociceptors Reduces Target Innervation, Ion Channel Expression, and Sensitivity to Heat. *eNeuro*, **5(2)**, ENEURO.0436-17.2018.

Catala, A. (2009). Lipid peroxidation of membrane phospholipids generates hydroxy-alkenals and oxidized phospholipids active in physiological and/or pathological conditions. *Chem Phys Lipids*, **157(1)**, 1-11.
Caterina, M.J. et al. (1997). The capsaicin receptor: a heat-activated ion channel in the pain pathway. *Nature*, **389(6653)**, 816-824.
Chen, L., Yang, G. & Grosser, T. (2013). Prostanoids and inflammatory pain. *Prostaglandins Other Lipid Mediat*, **104-105**, 58-66.
Cheng, X. et al. (2021). Mini-review - Sodium channels and beyond in peripheral nerve disease: Modulation by cytokines and their effector protein kinases. *Neurosci Lett*, **741**, 135446.
Ciccolini, F. et al. (2003). Local and global spontaneous calcium events regulate neurite outgrowth and onset of GABAergic phenotype during neural precursor differentiation. *J Neurosci*, **23(1)**, 103-111.
Clapham, D.E. (2007). Calcium signaling. *Cell*, **131(6)**, 1047-1058.
Constantine, W. & Percival, D. (2017). wmtsa: Wavelet Methods for Time Series Analysis. R package version 2.0.3.
Cummins, T.R. et al. (1999). A novel persistent tetrodotoxin-resistant sodium current in SNS-null and wild-type small primary sensory neurons. *J Neurosci*, **19(24)**, RC43.
Debanne, D. (2009). Plasticity of neuronal excitability in vivo. *J Physiol*, **587(Pt 13)**, 3057-3058.
Di Gioia, M. et al. (2020). Endogenous oxidized phospholipids reprogram cellular metabolism and boost hyperinflammation. *Nat Immunol*, **21(1)**, 42-53.
Dib-Hajj, S.D., Black, J.A. & Waxman, S.G. (2015). NaV1.9: a sodium channel linked to human pain. *Nat Rev Neurosci*, **16(9)**, 511-519.
Dib-Hajj, S.D. et al. (2010). Sodium channels in normal and pathological pain. *Annu Rev Neurosci*, **33**, 325-347.
Dib-Hajj, S.D. & Waxman, S.G. (2019). Sodium Channels in Human Pain Disorders: Genetics and Pharmacogenomics. *Annu Rev Neurosci*, **42**, 87-106.
Djouhri, L. et al. (2006). Spontaneous pain, both neuropathic and inflammatory, is related to frequency of spontaneous firing in intact C-fiber nociceptors. *J Neurosci*, **26(4)**, 1281-1292.
Domingues, R.M. et al. (2013). Lipoxidation adducts with peptides and proteins: deleterious modifications or signaling mechanisms. *J Proteomics*, **92**, 110-131.
Du, P., Kibbe, W.A. & Lin, S.M. (2006). Improved peak detection in mass spectrum by incorporating continuous wavelet transform-based pattern matching. *Bioinformatics*, **22(17)**, 2059-2065.
Dubin, A.E. & Patapoutian, A. (2010). Nociceptors: the sensors of the pain pathway. *J Clin Invest*, **120(11)**, 3760-3772.
Freigang, S. (2016). The regulation of inflammation by oxidized phospholipids. *Eur J Immunol*, **46(8)**, 1818-1825.
Gangadharan, V. & Kuner, R. (2013). Pain hypersensitivity mechanisms at a glance. *Dis Model Mech*, **6(4)**, 889-895.
Gold, M.S. & Gebhart, G.F. (2010). Nociceptor sensitization in pain pathogenesis. *Nat Med*, **16(11)**, 1248-1257.
Goodwin, G. & McMahon, S.B. (2021). The physiological function of different voltage-gated sodium channels in pain. *Nat Rev Neurosci*, **22(5)**, 263-274.
Gorbunova, Y.V. & Spitzer, N.C. (2002). Dynamic interactions of cyclic AMP transients and spontaneous Ca2+ spikes. *Nature*, **418(6893)**, 93-96.
Grienberger, C. & Konnerth, A. (2012). Imaging calcium in neurons. *Neuron*, **73(5)**, 862-885.
Grobe, T.G., Steinmann, S. & Szecsenyi, J. (2021) *BARMER Arztreport 2021*.

Grosser, T., Smyth, E.M. & FitzGerald, G.A. (2017) Pharmacotherapy of Inammation, Fever, Pain, and Gout. In Bruton, L.L., Hilal-Dandan, R. & Knollmann, B. (Eds.), *Goodman and Gilman's: The Pharmacological Basis of Therapeutics,* (13th ed., pp. 685-709). McGraw-Hill Education.

Gu, X. & Spitzer, N.C. (1995). Distinct aspects of neuronal differentiation encoded by frequency of spontaneous Ca2+ transients. *Nature*, **375(6534)**, 784-787.

Hackel, D. et al. (2013). The connection of monocytes and reactive oxygen species in pain. *PLoS One*, **8(5)**, e63564.

Han, C. et al. (2015). The Domain II S4-S5 Linker in NaV1.9: A Missense Mutation Enhances Activation, Impairs Fast Inactivation, and Produces Human Painful Neuropathy. *Neuromolecular Med*, **17(2)**, 158-169.

Hoffmann, T. et al. (2017). Reduced excitability and impaired nociception in peripheral unmyelinated fibers from NaV1.9-null mice. *Pain*, **158(1)**, 58-67.

Hsieh, G.C. et al. (2010). H4 receptor antagonism exhibits anti-nociceptive effects in inflammatory and neuropathic pain models in rats. *Pharmacol Biochem Behav*, **95(1)**, 41-50.

Huang, J. et al. (2017). Sodium channel NaV1.9 mutations associated with insensitivity to pain dampen neuronal excitability. *J Clin Invest*, **127(7)**, 2805-2814.

Huang, J. et al. (2014). Gain-of-function mutations in sodium channel NaV1.9 in painful neuropathy. *Brain*, **137(Pt 6)**, 1627-1642.

Huang, J. et al. (2019). A Novel Gain-of-Function NaV1.9 Mutation in a Child With Episodic Pain. *Frontiers in Neuroscience*, **13**, 918.

Ibi, M. et al. (2008). Reactive oxygen species derived from NOX1/NADPH oxidase enhance inflammatory pain. *J Neurosci*, **28(38)**, 9486-9494.

Imai, Y. et al. (2008). Identification of oxidative stress and Toll-like receptor 4 signaling as a key pathway of acute lung injury. *Cell*, **133(2)**, 235-249.

Imaizumi, K. et al. (2018). Editorial: Spontaneous Activity in Sensory Systems. *Front Neural Circuits*, **12**, 27.

Jablonka, S. et al. (2007). Defective Ca2+ channel clustering in axon terminals disturbs excitability in motoneurons in spinal muscular atrophy. *J Cell Biol*, **179(1)**, 139-149.

Ji, R.R., Xu, Z.Z. & Gao, Y.J. (2014). Emerging targets in neuroinflammation-driven chronic pain. *Nat Rev Drug Discov*, **13(7)**, 533-548.

Johnson, I.D. & Spence, M.T.Z. (2010) *Molecular Probes Handbook, A guide to fluorescecent probes and labeling technologies*. ThemoFischer Scientific.

Julius, D. (2013). TRP channels and pain. *Annu Rev Cell Dev Biol*, **29**, 355-384.

Kawabata, A. (2011). Prostaglandin E2 and pain – an update. *Biol Pharm Bull*, **34(8)**, 1170-1173.

Keeble, J.E. et al. (2009). Hydrogen peroxide is a novel mediator of inflammatory hyperalgesia, acting via transient receptor potential vanilloid 1-dependent and independent mechanisms. *Pain*, **141(1-2)**, 135-142.

Koester, J. & Siegelbaum, S.A. (2013) Propagated Signaling: The Action Potential. In Kandel, E.R. et al. (Eds.), *Principles of Neural Science,* (5th ed., pp. 148-171). McGraw Hill Professional.

Kolaczkowska, E. & Kubes, P. (2013). Neutrophil recruitment and function in health and inflammation. *Nat Rev Immunol*, **13(3)**, 159-175.

Lee, S. et al. (2012). Role of phospholipid oxidation products in atherosclerosis. *Circ Res*, **111(6)**, 778-799.

Leipold, E. et al. (2015). Cold-aggravated pain in humans caused by a hyperactive NaV1.9 channel mutant. *Nat Commun*, **6**, 10049.

Leipold, E. et al. (2013). A de novo gain-of-function mutation in SCN11A causes loss of pain perception. *Nat Genet*, **45(11)**, 1399-1404.
Leng, X.R. et al. (2017). Gain-of-function mutation p.Arg225Cys in SCN11A causes familial episodic pain and contributes to essential tremor. *J Hum Genet*, **62(6)**, 641-646.
Lin, C.R. et al. (2006). Prostaglandin E2 receptor EP4 contributes to inflammatory pain hypersensitivity. *J Pharmacol Exp Ther*, **319(3)**, 1096-1103.
Liu, B. et al. (2016). Oxidized Phospholipid OxPAPC Activates TRPA1 and Contributes to Chronic Inflammatory Pain in Mice. *PLoS One*, **11**, e0165200.
Lodish, H. et al. (2016) Biomembrane Structure. In Lodish, H. et al. (Eds.), *Molecular Cell Biology,* (8th ed., pp. 271-299). W. H. Freeman and Company.
Loeser, J.D. et al. (2011) Pain Terms. A Current List with Definitions and Notes on Usage. In Merskey H, B.N. (Ed.), *Classification of Chronic Pain,* (2nd ed., pp. 209-214). IASP Press.
Lolignier, S. et al. (2011). NaV1.9 channel contributes to mechanical and heat pain hypersensitivity induced by subacute and chronic inflammation. *PLoS One*, **6(8)**, e23083.
Lopez, E.R. et al. (2020). Serotonin enhances depolarizing spontaneous fluctuations, excitability, and ongoing activity in isolated rat DRG neurons via 5-HT4 receptors and cAMP-dependent mechanisms. *Neuropharmacology*, **184**, 108408.
Ma, Q. (2012). Population coding of somatic sensations. *Neurosci Bull*, **28(2)**, 91-99.
Mackay, L. et al. (2016). Systematic Characterization of Dynamic Parameters of Intracellular Calcium Signals. *Front Physiol*, **7**, 525.
Maingret, F. et al. (2008). Inflammatory mediators increase NaV1.9 current and excitability in Nociceptors through a coincident detection mechanism. *Journal of General Physiology*, **131(3)**, 211-225.
Malin, S.A., Davis, B.M. & Molliver, D.C. (2007). Production of dissociated sensory neuron cultures and considerations for their use in studying neuronal function and plasticity. *Nat Protoc*, **2(1)**, 152-160.
Martin, C. et al. (2018). NaV1.9 Potentiates Oxidized Phospholipid-Induced TRP Responses Only under Inflammatory Conditions. *Front Mol Neurosci*, **11**, 7.
Medzhitov, R. (2010). Inflammation 2010: new adventures of an old flame. *Cell*, **140(6)**, 771-776.
Meents, J.E., Fischer, M.J. & McNaughton, P.A. (2017). Sensitization of TRPA1 by Protein Kinase A. *PLoS One*, **12(1)**, e0170097.
Melak, M., Plessner, M. & Grosse, R. (2017). Actin visualization at a glance. *J Cell Sci*, **130(3)**, 525-530.
Mittal, M. et al. (2014). Reactive oxygen species in inflammation and tissue injury. *Antioxid Redox Signal*, **20(7)**, 1126-1167.
Mohammadi, M. et al. (2018). Antinociception by the anti-oxidized phospholipid antibody E06. *Br J Pharmacol*, **175(14)**, 2940-2955.
Mohammed, Z.A. et al. (2017). Veratridine produces distinct calcium response profiles in mouse Dorsal Root Ganglia neurons. *Sci Rep*, **7**, 45221.
Mohammed, Z.A., Kaloyanova, K. & Nassar, M.A. (2020). An unbiased and efficient assessment of excitability of sensory neurons for analgesic drug discovery. *Pain*, **161(5)**, 1100-1108.
Moriyama, T. et al. (2005). Sensitization of TRPV1 by EP1 and IP reveals peripheral nociceptive mechanism of prostaglandins. *Mol Pain*, **1**, 3.
Moumtzi, A. et al. (2007). Import and fate of fluorescent analogs of oxidized phospholipids in vascular smooth muscle cells. *J Lipid Res*, **48(3)**, 565-582.
Murphy, K.P. (2012) *Machine learning: a probabilistic perspective*. MIT press.

Nicolson, T.A. et al. (2007). Prostaglandin E2 sensitizes primary sensory neurons to histamine. *Neuroscience*, **150(1)**, 22-30.
North, R.Y. et al. (2019). Electrophysiological and transcriptomic correlates of neuropathic pain in human dorsal root ganglion neurons. *Brain*, **142(5)**, 1215-1226.
Odem, M.A. et al. (2018). Isolated nociceptors reveal multiple specializations for generating irregular ongoing activity associated with ongoing pain. *Pain*, **159(11)**, 2347-2362.
Oehler, B. et al. (2017). Inflammatory pain control by blocking oxidized phospholipid-mediated TRP channel activation. *Sci Rep*, **7(1)**, 5447.
Oehler, B. et al. (2012). TRPA1 is functionally expressed in melanoma cells but is not critical for impaired proliferation caused by allyl isothiocyanate or cinnamaldehyde. *Naunyn Schmiedebergs Arch Pharmacol*, **385(6)**, 555-563.
Oehler, B. et al. (2021). Pain Control by Targeting Oxidized Phospholipids: Functions, Mechanisms, Perspectives. *Frontiers in Endocrinology*, **11**, 613868.
Okuda, H. et al. (2016). Infantile Pain Episodes Associated with Novel NaV1.9 Mutations in Familial Episodic Pain Syndrome in Japanese Families. *PLOS ONE*, **11(5)**, e0154827.
Oskolkova, O.V. & Bochkov, V.N. (2020). Gain of function mechanisms triggering biological effects of oxidized phospholipids. *Current Opinion in Toxicology*, **20-21**, 85-94.
Oskolkova, O.V. et al. (2010). Oxidized phospholipids are more potent antagonists of lipopolysaccharide than inducers of inflammation. *J Immunol*, **185(12)**, 7706-7712.
Ostman, J.A. et al. (2008). GTP up-regulated persistent Na+ current and enhanced nociceptor excitability require NaV1.9. *J Physiol*, **586(4)**, 1077-1087.
Paredes, R.M. et al. (2008). Chemical calcium indicators. *Methods*, **46(3)**, 143-151.
Patel, K.D. et al. (1991). Oxygen radicals induce human endothelial cells to express GMP-140 and bind neutrophils. *J Cell Biol*, **112(4)**, 749-759.
Ward, P.A. (2010) Acute and Chronic Inflammation. In Serhan, C.N., Ward, P.A. & Gilroy, D.W. (Eds.), *Fundamentals of inflammation,* ed., pp. 1-16). Cambridge University Press.
Petho, G. & Reeh, P.W. (2012). Sensory and signaling mechanisms of bradykinin, eicosanoids, platelet-activating factor, and nitric oxide in peripheral nociceptors. *Physiol. Rev.*, **92(4)**, 1699-1775.
Plantman, S. et al. (2008). Integrin-laminin interactions controlling neurite outgrowth from adult DRG neurons in vitro. *Mol Cell Neurosci*, **39(1)**, 50-62.
Pnevmatikakis, E.A. et al. (2016). Simultaneous Denoising, Deconvolution, and Demixing of Calcium Imaging Data. *Neuron*, **89(2)**, 285-299.
Pnevmatikakis, E.A. (2019). Analysis pipelines for calcium imaging data. *Current Opinion in Neurobiology*, **55**, 15-21.
Prada, J. et al. (2018). An open source tool for automatic spatiotemporal assessment of calcium transients and local 'signal-close-to-noise' activity in calcium imaging data. *PLoS Comput Biol*, **14(3)**, e1006054.
Priest, B.T. et al. (2005). Contribution of the tetrodotoxin-resistant voltage-gated sodium channel NaV1.9 to sensory transmission and nociceptive behavior. *Proc Natl Acad Sci U S A*, **102(26)**, 9382-9387.
Que, X. et al. (2018). Oxidized phospholipids are proinflammatory and proatherogenic in hypercholesterolaemic mice. *Nature*, **558(7709)**, 301-306.
R Core Team (2019). R: A language and environment for statistical computing. R Foundation for Statistical Computing, Vienna, Austria. https://www.R-project.org/.
Rao, R. (2008). Oxidative stress-induced disruption of epithelial and endothelial tight junctions. *Front Biosci*, **13**, 7210-7226.
Rathinam, V.A.K. & Chan, F.K. (2018). Inflammasome, Inflammation, and Tissue Homeostasis. *Trends Mol Med*, **24(3)**, 304-318.

Romano, S.A. et al. (2017). An integrated calcium imaging processing toolbox for the analysis of neuronal population dynamics. *PLOS Computational Biology*, **13(6)**, e1005526.
Rosa, A.C. & Fantozzi, R. (2013). The role of histamine in neurogenic inflammation. *Br J Pharmacol*, **170(1)**, 38-45.
Rudolf, R. et al. (2003). Looking forward to seeing calcium. *Nat Rev Mol Cell Biol*, **4(7)**, 579-586.
Rugiero, F. et al. (2003). Selective expression of a persistent tetrodotoxin-resistant Na+ current and NaV1.9 subunit in myenteric sensory neurons. *J Neurosci*, **23(7)**, 2715-2725.
Rush, A.M. & Waxman, S.G. (2004). PGE2 increases the tetrodotoxin-resistant NaV1.9 sodium current in mouse DRG neurons via G-proteins. *Brain Res*, **1023(2)**, 264-271.
Schneider, C.A., Rasband, W.S. & Eliceiri, K.W. (2012). NIH Image to ImageJ: 25 years of image analysis. *Nat Methods*, **9(7)**, 671-675.
Seamon, K.B., Padgett, W. & Daly, J.W. (1981). Forskolin: unique diterpene activator of adenylate cyclase in membranes and in intact cells. *Proc Natl Acad Sci U S A*, **78(6)**, 3363-3367.
Segebarth, D. et al. (2020). On the objectivity, reliability, and validity of deep learning enabled bioimage analyses. *Elife*, **9**,
Smith, J.A. et al. (1998). Characterization of prostanoid receptor-evoked responses in rat sensory neurones. *Br J Pharmacol*, **124(3)**, 513-523.
Smith, J.A., Davis, C.L. & Burgess, G.M. (2000). Prostaglandin E2-induced sensitization of bradykinin-evoked responses in rat dorsal root ganglion neurons is mediated by cAMP-dependent protein kinase A. *Eur J Neurosci*, **12(9)**, 3250-3258.
Spitzer, N.C. (2006). Electrical activity in early neuronal development. *Nature*, **444(7120)**, 707-712.
Spitzer, N.C. et al. (2000). Coding of neuronal differentiation by calcium transients. *Bioessays*, **22(9)**, 811-817.
Stemmer, U. & Hermetter, A. (2012). Protein modification by aldehydophospholipids and its functional consequences. *Biochim Biophys Acta*, **1818(10)**, 2436-2445.
Story, G.M. et al. (2003). ANKTM1, a TRP-like channel expressed in nociceptive neurons, is activated by cold temperatures. *Cell*, **112(6)**, 819-829.
Subramanian, N. et al. (2012). Role of NaV1.9 in activity-dependent axon growth in motoneurons. *Hum Mol Genet*, **21(16)**, 3655-3667.
Suzuki, H. et al. (2010). Characterization of sensory neurons in the dorsal root ganglia of Bax-deficient mice. *Brain Research*, **1362**, 23-31.
Taboga, M. (2017) Variance. Lectures on probability theory and mathematical statistics. Accessed on 31 Dec 2020. https://www.statlect.com/fundamentals-of-probability/variance
Thangam, E.B. et al. (2018). The Role of Histamine and Histamine Receptors in Mast Cell-Mediated Allergy and Inflammation: The Hunt for New Therapeutic Targets. *Front Immunol*, **9**, 1873.
Yaksh, T.L. (2010) Mediators and Mechanisms of Inflammatory Pain. In Serhan, C.N., Ward, P.A. & Gilroy, D.W. (Eds.), *Fundamentals of inflammation,* (1st ed., pp. 217-233). Cambridge University Press.
Touska, F. et al. (2018). Heat-resistant action potentials require TTX-resistant sodium channels NaV1.8 and NaV1.9. *J Gen Physiol*, **150(8)**, 1125-1144.
Treede, R.-D. et al. (2019). Chronic pain as a symptom or a disease. *PAIN*, **160(1)**, 19-27.
Tsien, R.Y. (1981). A non-disruptive technique for loading calcium buffers and indicators into cells. *Nature*, **290(5806)**, 527-528.

Tu, W. & Liu, H. (2016) Zero-Inflated Data. In Balakrishnan, N. et al. (Eds.), *Wiley StatsRef: Statistics Reference Online,* (online ed., pp. 1-7). John Wiley & Sons, Ltd.
Usoskin, D. et al. (2015). Unbiased classification of sensory neuron types by large-scale single-cell RNA sequencing. *Nat Neurosci*, **18(1)**, 145-153.
Usui, K. et al. (2009). Site-specific modification of Alzheimer's peptides by cholesterol oxidation products enhances aggregation energetics and neurotoxicity. *Proc Natl Acad Sci U S A*, **106(44)**, 18563-18568.
van der Valk, F.M. et al. (2016). Oxidized Phospholipids on Lipoprotein(a) Elicit Arterial Wall Inflammation and an Inflammatory Monocyte Response in Humans. *Circulation*, **134(8)**, 611-624.
Vilceanu, D. & Stucky, C.L. (2010). TRPA1 mediates mechanical currents in the plasma membrane of mouse sensory neurons. *PLoS One*, **5(8)**, e12177.
Vos, T. et al. (2017). Global, regional, and national incidence, prevalence, and years lived with disability for 328 diseases and injuries for 195 countries, 1990-2016: a systematic analysis for the Global Burden of Disease Study 2016. *Lancet*, **390(10100)**, 1211-1259.
Wang, H. et al. (2006). Bradykinin and peripheral sensitization. *Biological Chemistry*, **387(1)**, 11-14.
Wang, S. et al. (2008). Phospholipase C and protein kinase A mediate bradykinin sensitization of TRPA1: a molecular mechanism of inflammatory pain. *Brain*, **131(Pt 5)**, 1241-1251.
Waxman, S.G. & Zamponi, G.W. (2014). Regulating excitability of peripheral afferents: emerging ion channel targets. *Nat Neurosci*, **17(2)**, 153-163.
Wei, X.-X. et al. (2020). A zero-inflated gamma model for deconvolved calcium imaging traces. *arXivNeurons, Behavior, Data Analysis, and Theory, 2020*, 2006.03737v1.
Wetzel, A., Jablonka, S. & Blum, R. (2013). Cell-autonomous axon growth of young motoneurons is triggered by a voltage-gated sodium channel. *Channels (Austin)*, **7(1)**, 51-56.
Woods, C.G. et al. (2015). The phenotype of congenital insensitivity to pain due to the NaV1.9 variant p.L811P. *Eur J Hum Genet*, **23(5)**, 561-563.
Woolf, C.J. & Salter, M.W. (2000). Neuronal plasticity: increasing the gain in pain. *Science*, **288(5472)**, 1765-1769.
Woolf, C.J. & Ma, Q. (2007). Nociceptors – noxious stimulus detectors. *Neuron*, **55(3)**, 353-364.
Zhong, S. et al. (2019). An update on lipid oxidation and inflammation in cardiovascular diseases. *Free Radic Biol Med*, **144**, 266-278.

10 Appendix

10.1 List of abbreviations

Abbreviation	Definition
4-HNE	4-hydroxy-2-nonenal
AITC	Allyl isothiocyanate, mustard oil
AM	Acetoxymethyl
Arb. unit	Arbitrary units
ATP	Adenosine-5'-triphosphate
AVI	Audio Video Interleave
BAPTA	1,2-bis(o-aminophenoxy)ethane-N,N,N′,N′-tetraacetic acid
cAMP	Cyclic adenosine monophosphate
CCD	Charge-coupled Device
CGRP	Calcitonin gene-related peptide
CIB	Calcium imaging buffer
CNQX	6-cyano-7-nitroquinoxaline-2,3-dione
conc.	Concentration
COX	Cyclooxygenase
CSV	Comma separated values
CWT	Continuous wavelet transform
DMEM	Dulbecco's Modified Eagle Medium
DRG	Dorsal root ganglion
F-actin	Filamentous actin
fps	Frames per second
FSK	Forskolin
GPCR	G protein-coupled receptor
GTP	Guanosine-5'-triphosphate
GTPγS	Guanosine 5'-O-[gamma-thio]-triphosphate
H_2O_2	Hydrogen peroxide
IASP	International Association for the Study of Pain
IL	Interleukin
IM	Inflammatory mediator mixture
IQR	Interquartile Range
KO	Knockout
LPS	Lipopolysaccharide
MAP2	Microtubule-associated protein 2
NA	Numerical aperture

Abbreviation	Definition
NA^3	Neural Activity Cubic
$Na_V1.9$	Voltage-gated sodium channel 1.9
NFL	Neurofilament protein L
NFκB	Nuclear factor kappa-light-chain-enhancer of activated B cells
ns	Not significant
NSAID	Nonsteroidal anti-inflammatory drug
O_2^-	Superoxide anion
OGB-1	Oregon Green BAPTA 1-AM
OxPAPC	Oxidized PAPC
OxPL	Oxidized phospholipids
PAPC	1-palmitoyl-2-arachidonoyl-*sn*-glycerol-3-phosphatidylcholine
PBS	Dulbecco's Phosphate Buffered Saline
PECPC	1-palmitoyl-2-(5,6-epoxyisoprostaneA2)-*sn*-glycero-3-phosphocholine
PEIPC	1-palmitoyl-2-(5,6)-epoxyisoprostaneE2-*sn*-glycero-3-phosphocholine
PFA	Paraformaldehyde
PGE_2	Prostaglandin E_2
PGPC	1-palmitoyl-2-glutaryl-*sn*-glycero-3-phosphocholine
PKA	Protein kinase A
PKC	Protein kinase C
PORN	Poly-DL-ornithine hydrobromide
POVPC	1-palmitoyl-2-(5-oxovaleroyl)-*sn*-glycero-3-phosphocholine
ROI	Region of interest
ROS	Reactive oxygen species
SAT	Signal average threshold (NA^3 setting)
SNR	Signal-to-noise ratio
TH	Thermolysin high
TM	Thermolysin medium
TRP	Transient receptor potential
TRPA1	Transient receptor potential ankyrin 1
TRPV1	Transient receptor potential vanilloid 1
TTX	Tetrodotoxin
VGSC	Voltage-gated sodium channel
WT	Wildtype

10.2 List of tables

10.3 List of figures

10.4 Acknowledgements

The completion of this thesis would not have been possible without the continuous support of many people.

I would like to thank PD Dr. Robert Blum for his strong support during my time in his lab. He introduced me to the world of experimental lab research, gave helpful advice on data analysis, and was continuously supportive even beyond my time in his lab. He has been a truly committed supervisor.

I am very grateful to have received constant feedback on my project from Prof. Dr. Heike Rittner. From discussing my progress with her and the members of AG molecular pain research, I have learned to critically reflect on scientific work and develop suitable hypotheses.

Thanks to Dr. Beatrice Oehler, who introduced me to the topic of my thesis and was always interested to discuss the current challenges of my project.

I deeply appreciate the constant support of the members of AG Blum, especially Dr. Corinna Martin, Dr. Manju Sasi, Dr. Cora Rüdt von Collenberg, Caroline Stoffer, and Michi Kessler, who patiently answered any question I had regarding experimental lab work and enabled a cooperative atmosphere in the lab.

I wish to thank Prof. Dr. Carmen Villmann for being my third supervisor, Prof. Dr. Michael Sendtner for allowing me to conduct my experimental research in the Institute for Clinical Neurobiology, and Prof. Dr. Jens Volkmann for facilitating the completion of my thesis at the Department of Neurology.

I am very thankful for the financial and non-material support of the Graduate School of Life Sciences of the University of Würzburg and the Max Weber Program of the State of Bavaria throughout the work on this thesis.

Importantly, I would like to thank my parents for giving me the possibility to pursue my studies and work on this thesis. [redacted]

10.5 Curriculum vitae

10.6 Affidavit

I hereby confirm that my thesis entitled "'Signal-close-to-noise' calcium activity reflects neuronal excitability" is the result of my own work. I did not receive any help or support from commercial consultants. All sources and / or materials applied are listed and specified in the thesis.

Furthermore, I confirm that this thesis has not yet been submitted as part of another examination process neither in identical nor in similar form.

Place, Date Signature

Eidesstattliche Erklärung

Hiermit erkläre ich an Eides statt, die Dissertation „'Signal-close-to-noise' Kalziumaktivität als Ausdruck neuronaler Erregbarkeit" eigenständig, d.h. insbesondere selbstständig und ohne Hilfe eines kommerziellen Promotionsberaters, angefertigt und keine anderen als die von mir angegebenen Quellen und Hilfsmittel verwendet zu haben.

Ich erkläre außerdem, dass die Dissertation weder in gleicher noch in ähnlicher Form bereits in einem anderen Prüfungsverfahren vorgelegen hat.

Ort, Datum Unterschrift